POLITECNICO DI TORINO

Department of Environment, Land and Infrastructure Engineering

Master of Science in Petroleum and Mining Engineering

EXPERIMENTAL STUDY
OF CUTTING TRANSPORT BY NON-NEWTONIAN FLUID
IN HORIZONTAL ANNULUS
THROUGH PARTICLE IMAGE VELOCIMETRY (PIV)

PoliTo Supervisor: Prof. Guido Sassi (Polito)

TAMUQ Supervisor: Prof. Aziz Rahman (Texas A&M University at Qatar)

Student: Muhammad Yousuf Khan

July 2020

Thesis submitted in compliance with the requirements for the Master of Science degree

Preface

This written master's thesis is based on experimental studies on hole cleaning at the Texas University at Qatar in Advance Multiphase Flow Assurance Laboratory. This master thesis is weighted with 16 credits in the ECT system and has completed under the "Tesi su Proposta" Program from Politecnico Di Torino, Italy. Under this program, Prof. Guido Sassi from Politecnico Di Torino has supervised as the internal supervisor while Prof. Aziz Rahman from Texas A&M University at Qatar supervised as an external supervisor.

It has been an honor to work under remarkable professors and scientists in their fields and have written this thesis in their supervision. Besides the principal supervisors, I am also very thankful to my colleagues in Texas A&M University at Qatar specially Abinash Baroah (Ph.D. Student), Mojammel Haq (Ph.D. student) and Muhammad Usman Siddiqui (Master's student) for helping in generating quality data set for Particle Image Velocimetry (PIV) in hole cleaning. Their feedback, support, and knowledge have been very beneficial.

I want to express my most profound appreciation to Dr. Muhammad Saad Khan (Post-Doctoral researcher), for the time he dedicated to my work, for excellent assistance, for ideas on how to solve problems on the way, as well for his enthusiastic encouragement.

Finally, I would like to thank my family and friends, especially from Politecnico Di Torino, to provide extra confidence in me during this tenure.

Abstract

The research has conducted on the experimental studies performed on Advance Multi-Phase Flow Assurance Lab at Texas A&M University in Qatar. This thesis reports the analysis of uniform cutting transport through non-Newtonian hole cleaning fluid. Biopolymer Flowzan® is used in different concentrations to obtain non-Newtonian characteristics of the liquid. The focus of the study is to visualize the impact of fluid flow rate, fluid rheology, drill pipe rotation and eccentricity of drill pipe on cutting transport, transitional velocity profile, the effect of near-wall fluid turbulence and drag stress with and without the solid cutting bed to mimic best drilling conditions for horizontal wells in ex-situ conditions. The analysis has done using combine techniques of Laser induced Particle Image Velocimetry (PIV), Seeding/fluorescent tracers tracking, and Refractive Index Matching (RIM).

Experiments have performed on a plant scale multiphase flow loop. The pipe sections of the flow loop and investigation area were made up of acrylic glass to imagine fluid flow patterns better. For PIV analysis, seeding particles of a hollow glass material having a uniform diameter of 20 nm and fluorescent particles of size 20-30 µm have used to track and illuminate particles. A class IV LASER has used to illuminate the flow field inside the RIM box. The premixed seeding and fluorescent particles with the flow tracked to evaluate the velocity field for the respective interested area by the PIV system. High-speed CCD Phantom® v7.3 camera has utilized to capture flowing particles under the laser field. Both Laser and camera were placed in the normal position to capture PIV images. Refraction Matching Index (RIM) method has applied to calibrate the system by introducing the same fluid inside the RIM box to avoid the error of particle position in the annulus due to glass-liquid-glass refraction. To evaluate the statistics for the desired velocity field of the flow acquired, data has thoroughly investigated with DaVis 8.4 software. Additionally, the turbulent behavior of the slurry flow has also been identified with high preciseness, and the corresponding characteristics of the suspended particles have also observed at the same time.

The velocity field outcomes will suggest that at the bottom of the annulus section, the velocity at the near-wall region deviates from the bulk velocity of the fluid because of the solid accumulation tendency. However, a higher flow rate of the slurry may introduce more suspended solid particles, which can eventually result in a uniform velocity field for the whole annulus section. The fluid

flow patterns were altered due to drill pipe rotations and solid particles' helical motion. The rotation of the drill pipe resulted in the solid and tracer particles scattered more uniformly in the annular cross-section, which provided a constructive impression on the cutting transport. This technique provides better prediction of mass and momentum transfer and identification of velocity profiles and pressure drop gradient in multiphase flow on a large scale.

Contents

Chapter#1

1.1 Introduction

In a petroleum drilling and production, multiphase flow where gas-liquid-solid phases are co-existed through an interface that acted as a boundary between two phases (liquid/gas, liquid/liquid or liquid/solid). These phases are distinctly separated from each other. They do not intermingle due to the difference in their molecular environment (i.e., melting points of the solids and molecular kind of liquids). However, due to the high velocities of the fluids, the phases are intermingled together along the pipeline and cause severe flow assurance problems. The development of automated devices for technical inspection and process control and availability of high-performance computer hardware has created a solid technological basis to introduce numerical simulation methods into the industrial practice of petroleum pipeline analysis and operation. Drilling operation's cost mostly consumes on drilling and completion fluid program. To perform efficient drilling, it is necessary to provide effective cutting transport measures to avoid mechanical damage due to turbulent and drag forces by solid cuttings and results in proper hole cleaning..(Busahmin et al. 2017) These parameters include selecting appropriate rheology of fluid, fluid pump rate, rotation, and eccentricity of a drill string. Rheology of drilling and completion fluid is of paramount importance to lift, suspend, and transport drill cuttings. Newtonian and Non-Newtonian fluids are generally used for hole cleaning operations. This classification of drilling fluid is based on a correlation of shear stress and shear rate and Reynolds number. Hole cleaning problems in vertical wells are scrutinized by applying rheological models, whereas drilling cuttings embedded in horizontal, slanted, and extended reach wells are inevitable.(Girmaa and Belayneh 2013)

1.2 Background

Particle Image Velocimetry (PIV) technique has been developing for the last three decades. This technique has been used in various applications, particularly in aerodynamics, fluid mechanics, and even in the research for blood circulation and respiratory systems in the biomedical field.(Raffel et al. 2007) This is the non-invasive flow visualization practice that works on principles of illumination, tracking, and correlating the position of suspended particles allowed to flow in the fluid (gas or liquid) in each reference time frame.(Charogiannis, An, and Markides 2015)(Santiago et al. 1998) These particles mimic the flow pattern of fluid, and thus the movement of the particles is tracked as the movement of fluid to study its properties. The development in PIV results in a lot of different methods of particle tracking phenomenon such as Particle Tracking Velocimetry (PTV), stereoscopic PIV, Tomographic PIV, and Laser Speckle Velocimetry (LSV). Nowadays, it is becoming a more reliable technique to analyze fluid flow structures in micro scales. (Raffel et al. 2007)

1.3 Problem Statement

To perform a handy drilling program, it is necessary to have an efficient hole cleaning during drilling and after drilling. Inefficient cutting transportation can cause cost consuming operations, which is not desired. To avoid hole cleaning problems, especially in problematic formations, engineers preferred to drill vertical wells rather than horizontal or slanted wells. The reason is, when the angle of the well decreases concerning the horizontal, the drill cuttings start accumulating in the form of either stationary bed or as a moving cutting dune. It depends on the length of the excellent bore (Nazari, Hareland, and Azar 2010). Hole cleaning problems in vertical wells are scrutinized by the application of rheological models, whereas drill cuttings embedded in horizontal, slanted, and extended reach wells are inevitable. To tackle this problem, experimental investigations using different scientific techniques such as visualization method, resistivity, and conductivity analysis can define which parameters or approaches will be best to perform functional hole cleaning operations. In this thesis, I have analyzed the annular velocity profile, shear, rotation, and strain components of adaptive hole cleaning fluid in microscale to provide the best operative drilling parameters.

1.4 Aims and Objectives of Thesis

This study's objective was to retrieve an accurate and quantitative calculation of fluid velocity profile, turbulence due to shear and rotation profile, velocity vector profile, and strain field at a large number of points instantaneously. These parameters were calculated concerning the horizontal drilling parameters such as mud flow rate, drill pipe rotation, rheology of Non-Newtonian fluid, the concentration of uniform cuttings, and drill pipe eccentricity. The study also offered the relation of velocity profile with the particle removal from the moving bed to define good hole cleaning practices. The analytical technique applied is the tomographic laser-induced Particle Image Velocimetry (PIV). Using the LaVision ™'s DaVis® 8.4 software provided a good view of the velocity profile and other parameters under applied parameters.

1.5 Novelty

In this thesis, experiments have run on the Non-Newtonian fluid, which is prepared using a Flowzan® Biopolymer registered under Drilling Specialties Company – A division of Chevron Phillips Chemical Company LP. The concentration of the biopolymer to make Non-Newtonian fluid was 0.05% W/W. The PIV technique combined with Refractive Index Matching (RIM) is the novel technique to analyze the hole cleaning fluid in annular two-phase flow. The parameters under which the velocity vector profile, divergence in the vector field, shear, and rotation due to internal turbulence of fluid and strain components have analyzed with the operational drilling parameters.

1.6 Chapters distribution

This thesis is divided into six main sections (Chapters).

Chapter 1 (Introduction) is about relevant background theory, which provides an overview of this study, aims and objectives, and novel approaches for the hole cleaning experiments.

Chapter 2 (Literature review) contains the theory related to the PIV, its classification, different types of equipment and material used for its application, method of hole cleaning, and the effects of hole cleaning on drilling parameters.

Chapter 3 (Experimentation setup and working) describes the experimental procedure and setup used in this experimental study.

Chapter 4 (Methodology) explains the adaptive measures of image analysis mainly pre and post-image processing methods, and the Refractive Index Matching methodology has discussed in detail.

Chapter 5 (Results and discussions) In this section, the results from the study have discussed the graphs and images obtained from DaVis software.

Chapter 6 (Conclusion and recommendations) concludes the aim of the experimental study and the overall summary of the research along with the future directions to extend the investigation of hole cleaning by using PIV methodology.

Chapter #2

Literature Review

In this chapter, the theory behind our research and past studies related to PIV have been discussed. A brief review of the fundamentals of concepts and terminology have been defined. The understanding of fundamentals and terminologies is always helpful in understanding the research from introduction to conclusion.

2.1 Divergence:

It is the measurement of local alteration in the velocity vector field and is measured at a particular area by adding the components of adjacent vectors. The divergence corresponds to zero, positive, or negative. If contraction or inward-directed vector flux measured in the existing infinitesimal area, then it is termed as negative divergence whereas if the vector flux goes outward or expansion in local velocity field measured than it is termed as positive divergence. Zero divergence is called when there is no deviation in the velocity vector components from their origin. Translation, rotation, and shearing movements are illustrations of zero divergence due to balance in inward and outward velocity components.

Mathematically, the divergence of the vector field is derived as at any infinitesimal section the net outward flux of per volume as the volume about the point tends to zero:

$$div(\underline{A}) \triangleq \lim_{\Delta v \to 0} \frac{\oint_{s} \underline{A} \cdot d\underline{s}}{\Delta v} \qquad \text{---------------------- equation 1}$$

In fluid dynamics, the physical behavior of divergence is understood by considering the velocity field of liquid or gas flow. The flowing gas possesses velocity, and at each infinitesimal section, it is represented by the vector, and in bulk scale, it forms the vector field. Gaseous flow shows positive divergence if it is heated. The net movement of gas particles enclosed expands and results in an outward flux of the gas. On the contrary, negative divergence is obtained when gas is cooled. In the process of gas cooling, gas will contract, and particles of net flow of gas move inward in the close vessel. In the absence of the above conditions, gas velocity shows no divergence, and the field in which there is no or zero divergence is called the solenoidal field. (Sims, n.d.)

In the case of liquid flow in the cylindrical vessel or tube, the fluid will show outward velocity with the introduction of any thermodynamic conditions. Thus, the fluid particles will push outward in all directions obeying the Archimedes principle. In this condition, positive divergence will be observed. In the case of Laminar flow in isothermal conditions, divergence in the velocity field will be zero. In the case of multiphase flow, divergence in the velocity field will be rigorous due to turbulence. (Webpage, n.d.)

2.2 Shear rate:

Shear rate referred to as a rate of relative motion between layers of moving fluid. It is calculated by considering the velocity of relative motions of flowing liquid layers and is represented by γ and is expressed as (1/s or sec^{-1}). For liquid flow in a pipe, the velocity of the fluid at the pipe wall is zero. Velocity increases towards the center of the pipe. Shear stress is also present due to adjacent layers of liquid moving with relative velocities to each other.

$$\gamma = \frac{u}{y}$$

Where $\frac{u}{y}$ is the velocity gradient

The behavior of shear is different in different types of liquids. For Newtonian fluids, shear stress is the linear function of the shear rate due to dynamic viscosity, which is constant for such fluids. For Non-Newtonian fluids, shear is a complex function of velocity gradient or shear rate which is described by:

$$\tau = A + B\left(\frac{du}{dy}\right)^n$$

Where

A B and n are constants. For Newtonian fluids, A=0, B=μ, and n=1.

Laminar flow ideally obtains in pipe flow with a fluid having deficient Reynolds number as well as smooth inner pipe surfaces. Usually, we find turbulent flow in industrial applications. The main feature of turbulent flow is the velocity of the fluid, which varies substantially and unevenly with both position and time. Consequently, unsteady vortices occur, and shearing behavior of fluid can be best illustrated with statistical methods. The energy dissipation rate can be used to estimate the level of intensity of the turbulence.

2.3 Axial Strain

In an axial strain, the mean flow is strained in its flow path. In a wall-bounded flow, an axial strain can be simply produced by the change in the cross-sectional area of the flow field. This variation in the cross-sectional area can either be a locally continuous decrease (contraction) or increase (diffuser) or decrease, followed by an increase (constriction).

Following are the two characteristics that will impact the strain in practice:
• The wall friction effects locally the strain field.
• The way the cross-sectional area varies with axial position.

In turbulent flow, it is crucial to identify the effects of strain. How an axial strain affects a turbulent flow depends on the magnitude of the strain. The strain rate S can be interpreted as the inverse of a time scale. So higher the strain rate, the smaller its time scale. If the straining time scale is smaller than the turbulent time scale, the strain is considered to be rapid. This implies during the straining phenomenon the geometry of the turbulence is deformed, but the turbulence does not have time to react on the deformation. On the other hand, when the straining time scale is less than the deformation, and the reaction to this deformation will take place simultaneously. (Messio et al. 2008)

2.4 Swirling strength

Swirling strength is measured by the speed of local fluid rotation in the investigation region. Areas of flow with the more substantial value of swirling strength are seen as vortices. (CHAKRABORTY, PINAKI, S. BALACHANDAR 2005) Mathematically swirling strength is the imaginary part of complex eigenvalues for the velocity gradient tensor and describes a good indication of the vortex in wall turbulence under strong mean shear values. Vortices dominate turbulent flows in pipes by providing wall turbulence. Wall turbulence and vortex extraction measurement by 2D PIV from velocity fields sometimes may not purely two dimensional. Therefore, recent studies in characterizing 3D or volumetric PIV made it possible to visualize vortices from a 3D perspective. (Gao, q., c. Ortiz-dueñas 2011) (carlier, Johan 2005). Vortex identification and characterization is the necessary step to calculate swirling strength analytically. Swirling strength from velocity fields is denoted by $1/s^2$.

Flowzan

Flowzan is a biopolymer commonly known as Xanthan gum. This polymer is commonly used in the drilling industry for hole cleaning operations. For the experiments, Flowzan was provided by Chevron Phillips Chemical Company LP, Texas, USA. The polymer shows the shear-thinning property at an optimal flow rate, reduces formation damage, reduces pressure loss, and makes the hole cleaning effective.

Physical and chemical characteristics	Properties
Form	Powder
Colour	Cream to light yellow
Odor	Slight
Relative density	From 1.4 to 1.6
Specific Gravity	0.995
pH	From 5.5 to 8.5

Table 1 Physical and Chemical Properties of Flowzan.

2.5 Particle Image Velocimetry

The PIV is an optical fluid flow visualization technique first practiced in the 1960s. The method initially used for research and educational purpose to track particles in the flowing fluid. Later, this non-intrusive technique has developed with time and now applying widely in all related fluid mechanics fields. This method allows us to determine the velocities of micro and nano seeding particles flowing in both liquid and gas flows in 2D and 3D views (Raffel et al. 2007) (Adrian 2005).

PIV setup consists of the following components 1. An illumination system, i.e., Dual pulsed class IV Laser 2. High quality and fast Image capturing system, i.e., Phantom® v7.3 CCD cameras and image processing tools such as MATLAB or LaVision's DaVis software. The schematic view of the PIV system is shown in figure 1

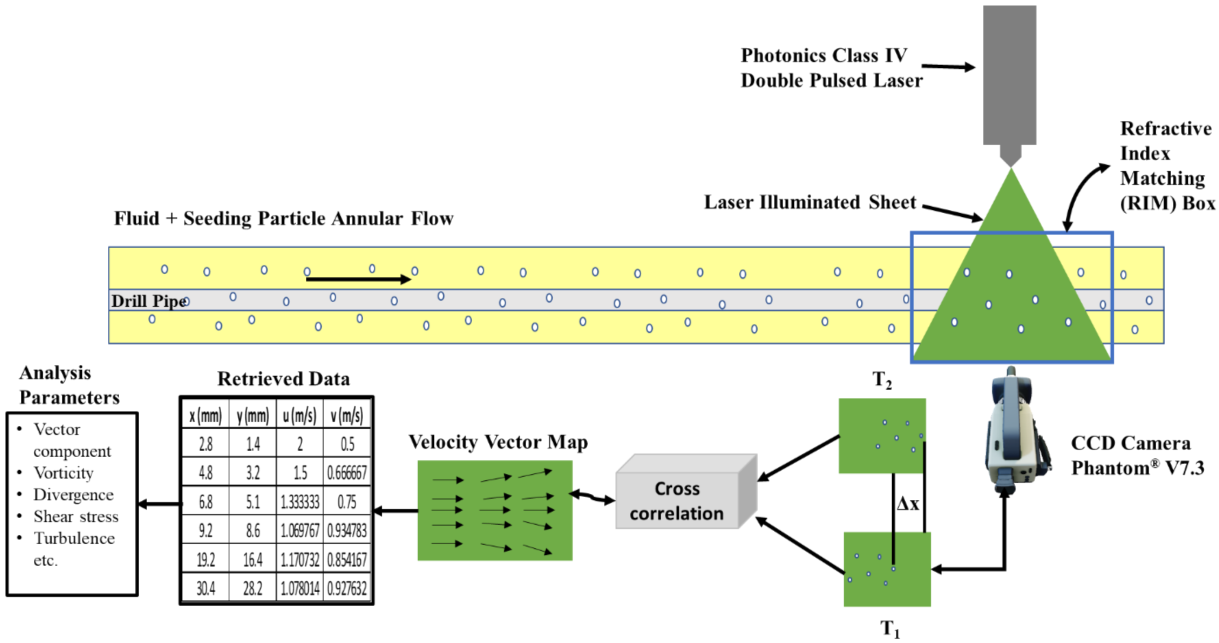

Figure 1PIV setup on Multiphase flow loop in TAMUQ 259I Lab

In this method, micro/nano seeding particles and fluorescent particles are introduced in the flowing fluid. These small particles are tiny enough to follow the flow dynamics; therefore, this technique describes the best flow behavior of the fluid. The intense pulse laser is then incident on the flow in the form of a light sheet that illuminates the flowing particles. The high-speed CCD camera captures the images of flowing illuminated particles. Later, the images are processed to retrieve desired optimal results.

2.5.1 Principle of PIV

Assessment of the captured image is an essential tool that is based on the fundamental equations in which distance articulates shift tracer particles in the fluid at a particular time. Hence, the actual anticipated position of particles required accurately. It is mandatory to make sure that that the position of particles may not change during the incident of the light source. Thus, in our case, we have implemented the Refractive Index Matching technique to reduce the error of shifting tracer particles from its original position while taking images. It is also needed to keep in mind that the wavelength of the laser light should be small (for our case 527 nm) so that continuous laser light sheets would incident on the investigation region. Since the type of Laser is Class IV double pulsed Laser, therefore it is necessary to record two images for the position of particles also for cross-correlation.

The first recorded set of images shows the preliminary position of particles, and the second set provides the final position. The quality and requirement of the recorded data set depend on the exposure methods, which are termed as single or individual exposure method and dual exposure method.

In a **single exposure method**, every entry position of the particle in the image plane is displayed in one frame. The first image acquired referred to the initial position of particles, while the second image referred to the final position. Presently, this method becomes significant than the dual exposure method.

In the **dual exposure method**, both first and final acquired positions of particles are achieved by a single exposure shot. In this method, it is impossible to identify the initial and final positions of particles. Currently, the CCD camera is used to capture images. Before the photographic film is used from which digital image postprocessing was not allowed in that case where CCD camera allows to process the digital data using different software. (RATKOVSKÁ 2014)

2.5.2 Evaluation of PIV Images

The analysis of recorded images is made by allocating the grids of square shape in the images. These square shape grids contain the particle data that is used in scrutinizing the average displacement of particles in each square grid. (Brossard et al. 2015)

2.5.3 Correlation

Correlation is the algorithmic analysis of PIV images that defines the relationship between two processes. The result of correlation after assessing PIV images is the average of change of displacement of particles in the investigation window. For single exposure, this relation is termed as a cross-correlation method. In contrast, for double exposure, it is simply termed as correlation because, in double exposure, we do not have initial and final positions of particles. There is another option of autocorrelation, but it's different from cross-correlation and does not define the direction of particle displacement. Therefore, advanced dual exposure is usually used for PIV image evaluation that does not requires single exposure in which the cross-correlation technique could be applied. (Ratkovská 2014)

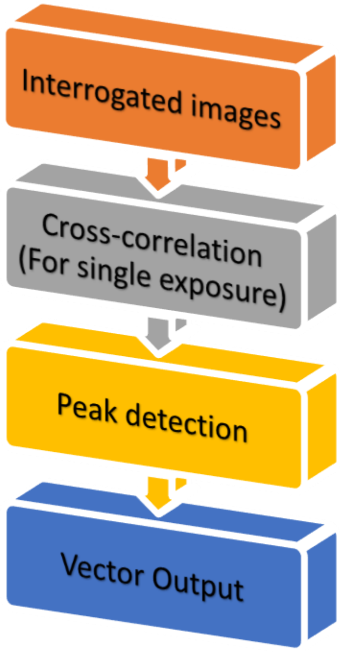

Figure 2 PIV image evaluation process

2.5.4 Mathematical Background

Background of PIV measurements contains the statistical evaluation of images based on the cross-correlation technique proposed by (Adrian 2005; Santiago et al. 1998), but the development of PIV now based on digital PIV which is based on proper mathematical algorithms (Lindken et al. 2009). In this section, I have described the simple mathematical algorithms for statistical evaluation of PIV images that have widely used and cited for PIV correlation and cross-correlation.

2.5.5 Fourier Transformation

Fourier transformation is the underlying mathematical model implies for 1D and 2D PIV measurements. It is used to define time relative signals by using harmonic sine and cosine functions. Practically, Fourier transformation is used to interpret the signal from the time domain to the frequency domain. One dimensional PIV measurement is represented as the sum of complex exponential trigonometric, i.e., sine and cosine referred to Euler's theorem.

Euler's theorem

$$e^{i\varphi}=cos\varphi+i.\ sin\varphi$$

1D Fourier transform equation:

$$F(\omega) = \int_{-\infty}^{\infty} \mathrm{f(t)}e^{-\mathrm{i\omega t}}dt$$

1D inverse Fourier transform equation

$$f(\omega) = \frac{1}{2\pi}\int_{-\infty}^{\infty} \mathrm{f(t)}e^{-\mathrm{i\omega t}}d\omega$$

Two-dimensional Fourier transformation is also based on Euler's equation, but for the 2D Fourier transform, it is interpreted as a function of two variables. 2D transformation does not provide a digital image that has taken from the PIV camera. (RATKOVSKÁ 2014; Raffel et al. 2007; Brossard et al. 2015)

2D Fourier Transform equation

$$F(u,\, v)\text{=}\int\int_{-\infty}^{\infty} \mathrm{f(x,y)}e^{-\mathrm{i}(xu,yv)}dxdy$$

2D Inverse Transform equation

$$F(x,y) = \frac{1}{4\pi 2}\int\int_{-\infty}^{\infty} \mathrm{f(x,y)}e^{-\mathrm{i}(xu,yv)}dxdy$$

2.5.6 Discrete Fourier Transformation

Discrete Fourier transformation is the numerical expression use to express the solution of the problem to find the range of sampled signals or signals from the sampled spectrum. This requires mathematical knowledge of signals or spectrums of finite interval. The following are the mathematical equations of discrete Fourier and inverse discrete Fourier transformation. (RATKOVSKÁ 2014)

Fourier Discrete equation

$$F(k) = \sum_{n=0}^{N-1}\left(F(n)e\frac{-2\pi ikn}{N}\right)$$

Fourier Inverse discrete equation

$$f(n) = \frac{1}{\mathrm{N}}\sum_{n=0}^{N-1}\left(F(k)e\frac{-2\pi ikn}{N}\right)$$

2.5.7 Wienerova - Khinchin theorem

Wienerova – Khinchin is another mathematical theorem that is numerically involved in PIV image evaluation. This theorem plays a vital part in measuring cross-correlation and autocorrelation by relating Fourier transform to autocorrelation. Recorded signal first undergoes Fourier transform, then the power spectrum is determined by the absolute root of complex function and correlation function generated by using a discrete Fourier transform. (RATKOVSKÁ 2014)

2.5.8 Fast Fourier Transform

Fast Fourier Transform (FFT) is the newly developed and effective mathematical algorithm used to manipulate Fourier and inverse Fourier transform. It provides rapid and high-speed calculations. The basic principle of FFT is to eradicate the correlation noise, especially at the edges of the image assessment range, and used the window as a filter function in the frequency domain. (Ref: R. Balamurugan, and B. Jeeva) provided a new optical measurement method of Particle Image velocimetry by interrogating seeding particles under laser light and captured images through double frame single exposure method. The images were then cross-correlated and evaluated by Fast Fourier Transform.

Cross-correlation has performed using equation 1 and detailed derivation and explanation can be cited from(Balamurugan and Jeeva 2019)

$$R(s,t) = \frac{1}{N2} \sum_{i=0}^{N-1} \sum_{j=0}^{N-1} F'I, J(i,j)(F''I.J(i+s, j+t))$$

Where, R is the recurrent cross-correlation among sub-windows I, J in the first image of the image pair (F') and the next image of the image pair (F"), i, j is the pixel location within sub-window *I, J* and *s, t* are the 2-D cyclic lag for that cross-correlation computing is mentioned in the equation (1).

R is usually calculated in the spectral domain, so the equation is referred to as:

$$R(s,t) = F - 1[F * \{F'I, J(i,j)\}F\{F'I, J(i+s, j+t\}]$$

where and are the Fourier and Inverse Fourier Transform operators, and the star denotes the complex conjugate.

2.5.9 Main features of PIV data processing

In the book Particle Image Velocimetry- A Practical Guide (Raffel et al. 2007; Adrian 2005) has reported almost all basic and modern features associated with Particle Image Velocimetry. These features stated all the evaluation and evolution of PIV data processing found until then.

Non-invasive velocity acquisition technique.

PIV is the non-intrusive visual approach applicable in highspeed flows for both liquid and gases in boundary layers near to the wall where the flow can be disturbed.

Implicit velocity measurement.

It measures the velocity of the flow indirectly. Measuring velocity indirectly means that this technique measures the velocity of nano and microparticles that are allowed to flow in the fluid. These seeding or tracer particle mimics the flow pattern and the velocity of the fluid to provide the velocity profile of the flowing system. This is somehow related to the Laser Doppler Velocimetry (LDV) technique.

Whole field technique.

PIV can measure velocity and other parameters in the whole flow field rather than measure at a single point. It permits to record images of sizeable flow fields and provides excellent spatial resolution and relatively limited temporal resolution due to some technological limitations. Even in unsteady and turbulent flow, Instantaneous image recording and high spatial resolution help in the detection of spatial structures.

Velocity delay.

This function requires to check whether the tracer particles are correctly following the flow pattern of fluid or not, at least for the desired investigation objectives. The smaller size of particles, the better would be the resulted motion and fluid parameters visualized.

Time of Laser's pulses

The duration of the laser pulse should be small so that the particle's motion can be easily detected and stored during the pulse exposure. By considering this parameter image would be sharp in terms of particle illumination and would avoid blurred image.

Time delay of Laser's pulses.

In contrary to the duration of illumination pulses, the time delay between Laser's pulses should be high enough to capture the displacement between the recorded images having seeding/tracer particles with appropriate resolution and also low enough to calculate velocity components of detected particles in the captured flow field.

Proper dispersal of seeding/tracer particles

For PIV measurement, qualitative as well as quantitative flow visualization is the paramount consideration. Proper distribution of seeding/tracer particles in the flow should be visible enough and should mark a specific investigation area such as in our case, we have Refractive Index Matching (RIM) box where we have marked the scale of measurement as well as tracked the seeding particles by illuminating them under laser sheet. For PIV, homogeneous dispersal of desired density for high-definition recording to obtain an excellent PIV evaluation.

Vector components of the velocity field

Since the laser sheet illuminates the investigation flow field in planer components, therefore, the velocity components resulted have also been in standard two components (i.e., horizontal and vertical). This is also called 2C-PIV. PIV can also be resolve in three components system, but the methods are slightly different, especially in terms of their equipment. For 3C-PIV, two recording cameras are needed to be placed at an optimal angle in order to correlate/cross-correlate images in planer domains of the flow field to get three components velocity field.

2.5.10 Source of Illumination (Lasers)

Lasers are the main illumination source used in particle tracking techniques. The reason behind using Laser as a light source is its wavelength, which is close to the green light spectrum and sensitive to CCD camera. Generally, the functioning of Laser is based on the involvement of three different phenomena between atoms and electromagnetism, i.e., absorption, spontaneous emission, and stimulated emission. Particularly, atoms in their ground state get photon of specific energy to reach their excited state. After residing there at a very very short period, they go back to their ground level after releasing out energy packets in terms of photons.

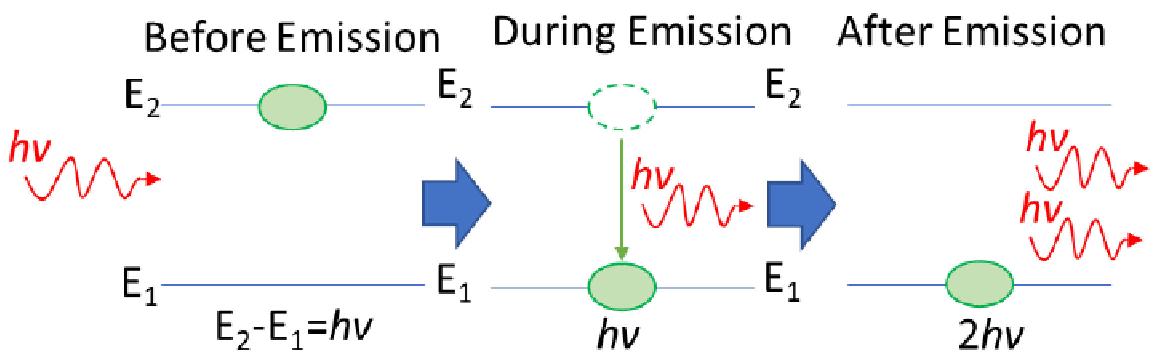

Figure 3 Physical phenomenon of Laser

Where:

E2 is the excited energy state, E1 is the ground energy state, and *hv* is the energy provided to the atoms and released with the emission. (Taso 2018)

Figure 4 Photonics Laser and controller

For the PIV experiments, Photonics dual-head DM 30-527-DH laser has been used, as shown in the figure. This Laser produces a maximum of 30 mJ energy/pulse. The laser light produce has a wavelength of 527 nm and has excellent energy stabilization and decrease noise. By using sheet optics, the laser beam can be transformed into a light sheet to perform PIV operations. This Laser delivers optimized PIV results by providing the best correlation. This Laser can be triggered simultaneously as well as independently. The photonics laser controller controls the Laser. This provides the Laser to be operated by the DaVis 8.4 software in the form of a remote controller. A chiller is also installed in the laser system to maintain the laser temperature and overall safe operations.

2.5.11 Light Sheet Optics

Light-sheet optics is the specific lens or combination of lenses whose primary function is to transform the Laser into the light sheet. The arrangement and selection of the lenses in the light sheet optics may be different according to the use of the specific purpose. In the PIV setup, the LaVision's VZ17-0862 sheet optics has used that contains two telescope lenses and two cylindrical divergence lenses that make laser beam into a light sheet. The focal length of the diverging lenses determines the aperture of the light sheet. Usually, a light sheet is produced by a cylindrical lens. Still, if the laser beam has a bigger diameter, the cylindrical divergence lens is required to combine with the two telescope lenses to produce a sharp light sheet. The aperture and height of the laser sheet depend on the focal length of the cylindrical lens.

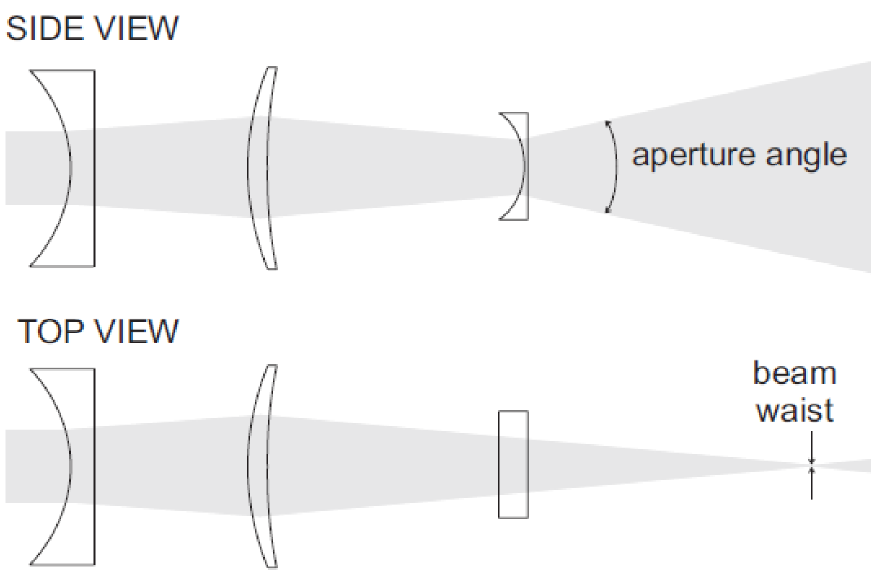

Figure 5 Schematic of Sheet optics (LaVision; Manual)

Figure 6 Schematic of Sheet optics (LaVision; Manual)

2.5.12 Image Acquisition Cameras

Since PIV is an optical visualization method, therefore image sensing devices are required to capture images. For PIV imaging, Charge-Coupled Device (CCD) camera or Complementary Metal Oxides Semiconductor (CMOS) devices are used. For my experiment, Phantom v7.3 CCD camera has used. The primary function of the CCD camera is to convert light into an electric charge. These charges then transformed into potential difference levels and finally generated an analog signal. The signal then amplified and converted into digital form.

Phantom® v7.3 Camera Specification	
Resolution	800 x 600
Rate	6688 Hz
Min. interframe time	3.5 µsec
Pixel size	22 µm
Sensor format	17.6 x 13.2 mm
Dynamic Range A/D	8/10/12/14bit
Memory	32 GB
Lens mount	F-mount, C-mount, M 42 (optional)

Table 2 Camera specifications (Imaging, Focus on Phantom v7.3, v9.1)

Figure 7 Phantom v7.3 camera (Imaging, Focus O N Phantom v7.3, v9.1, n.d.)

2.5.13 Seeding and fluorescent Particles

Particle Image Velocimetry technique provides the particle flow rate in the fluid rather than the flow rate of the fluid. Therefore, the particles induced in the flow known as seeding particles have the paramount importance in the accuracy of result analysis. Hence, it is required to have proper seeding particles size in the appropriate fluid (gas or liquid) so that these particles can easily be illuminated, tracked, and imaged accurately. Also, follow the same behavior of the fluid stream. The seeding particle size should be uniform in size so that they provide uniform speeds for the same particles. (Raffel et al. 2007)(Jahanmiri 2011) (Boiten 2016)

As we have discussed that seeding particles determine the flow behavior of the fluid. So, an appropriate type of seeding particles must be selected for liquids or gases flow to scatter laser light sheets for the acquisition of successful and accurate experimental data sets. Mostly in liquid flows, seeding particles are the suspended solids nanoparticles of different physical characteristics that allowed to be mixed in the liquid to achieve a homogenous distribution of suspended particles. Similarly, for gas flows, mostly solid seeding particles are used, but liquid seeding sprays may also use depending on the properties of gas flow.

Below are the tables of seeding particles available at LaVision® that are currently available and used for PIV, flow visualization, and LDA techniques.

Fluid	Material	Particle size	Particle density g/cm³	Nature of seeding material
Liquid	Polyamide particles	20-100 µm	1.03-1.2	Solid particles
	Borosilicate glass particles	10 µm	1.1	Solid particles
	Polystyrene	0.3-20.0 µm	1.05	Solid particles
	Polymethyl methacrylate (PMMA)	1.0-50.0 µm	1.19	Solid particles
	Melamine resin	10 µm	1.51	Solid particles
Flames	Aerosil	12 nm	0.05	Solid particles
	Titanium dioxide	> 250 nm	3.9 – 4.2	Solid particles
	Graphite	3.5 µm	2.2	Solid particles
Gas	Helium-filled soap bubbles (HFSB) soap fluid	-	-	Liquid soap
	Di-Ethyl-Hexyl-Sebacat (DEHS)	1 µm	0.91	Liquid
	Fog fluid	-	1.05	Liquid droplets

Table 3 Seeding particles by LaVision (LaVision GmbH, n.d.; Raffel et al. 2007)

Fluid	Seeding Material	Mean diameter in µm	Nature of seeding material
Liquid	Aluminum flakes	2 – 7	Solid
	Granules for synthetic coatings	10 – 500	Solid
	Different oils	50 – 500	Liquid
	Oxygen bubbles	50 – 1000	Gas
Gas	Alumina Al2O3	0.2 – 5	Solid
	Glass micro-spheres	0.2 – 3	Solid
	Glass micro-balloons	30 – 100	Solid
	Granules for synthetic coatings	10 – 50	Solid
	Dioctyl phthalate	1 – 10	Solid
	Smoke	< 1	Solid
	Different oils	0.5 – 10	Liquid

Table 4 other available seeding particles (Raffel et al. 2007)

Figure 8 Fluorescent particles and hollow glass spheres (LaVision GmbH, n.d.)

2.5.13 Types of PIV techniques

2.5.13. 1 Stereoscopic PIV

Stereoscopic PIV is one of the effective methods to perform PIV analysis because it needs two cameras to capture images placed at either in an angular direction or parallel to each other for viewing two directions of particle flow. This type of PIV is best for measuring the 3-dimensional flow field and vector field. This method is so impressive that it removes the perception of error, which means proper velocity vectors can be found from two concurrent views, which is not expected to have in standard PIV. (Taso 2018)

2.5.13.2 Tomographic PIV

The tomographic PIV method uses a single image sensing device. Thus, it provides an accurate result of PIV in the 2D plane. There is also the possibility to provide particle velocity in 3D-planar volume since the mathematical algorithm has been developed enough to provide satisfactory results and overcomes the use of stereoscopic PIV due to the high cost of additional camera and software. But there is still some limitation, and compromise between results of stereoscopic and tomographic PIV, such as tomographic PIV, requires high power approximately five times greater than stereo PIV and requires more considerable time to evaluate the recordings ultimately needs more significant storage to store data. (Taso 2018)

2.6 State of the art (PIV in multiphase flow)

Particle Image Velocimetry (PIV) technique is to investigate complex flow streams. PIV system uses a whole flow field approach providing instantaneous velocity vector measurements throughout the cross-section of flow. Prediction methods for two-phase annular flow require accurate knowledge of the velocity profile within the liquid film flowing at its perimeter as the gradients within this film influence to a large extent the overall transport processes within the entire channel. This film, however, is quite thin, and variable and traditional velocimetry methods have met with only minimal success in providing velocity data. The present work describes the application of Particle Image Velocimetry (PIV) to the measurement of velocity fields in the annular liquid flow (Ashwood et al. 2015). Because the liquid is constrained to distances on the order of a millimeter or less, the technique employed here borrows strategies from micro-PIV. Nonetheless, micro-PIV studies do not typically encounter the challenges presented by annular flow, including substantial velocity gradients, a free surface that varies in position from moment to moment, the presence of droplet impacts, and the passage of waves that can be ten times the average thickness of the base film. This technique combines the seeding and imaging typical to micro-PIV with a unique lighting and image processing approach to deal with the challenges of a continuously varying liquid film thickness and interface. Mean velocity data are presented for air-water in two-phase co-current upward flow in a rectangular duct, which are the first detailed velocity profiles obtained within the liquid film of upward vertical annular flow. The velocity data presented here do not distinguish between data from waves and data from the base film. The resulting velocity profiles are compared with the classical law of the wall turbulent boundary layer model and found to require a decreased turbulent diffusivity for the model to predict well. These results agree with the hypotheses previously presented in the literature. (Shi, Wei, and Pang 2015)

(Wu, Ye, and Meng 2013) used laser-induced PIV practice to determine the 2D flow field of liquid flow to analyze tangential and radial velocity and Reynold's number in a vortex gripper. Vortex gripper consists of the vortex cup, and a small opening served as a gas film. From the PIV study, they found trends of tangential velocity and radial velocity as the gas film gap gradually increase and found radial velocity is approximately half of tangential velocity in the air film gap. From the analysis of Reynold's number, the fluid flow becomes laminar to turbulent as the gas film gap increases, but due to some limitations in the experimental setup transition state between laminar and turbulent flow could not be attained.

(Corredor, Bizhani, and Kuru 2013) the used polymer to reduce drag forces in the annular space of the horizontal pipe by using Laser-induced PIV. They used Partially Hydrolyzed Polyacrylamide (PHPA) polymer as a drag-reducing agent ranging from 0.07 to 0.12 V/V concentration. They observed that drag reduction is improved with the enrichment of polymer concentration, and after an optimum concentration, it started to decrease. The best concentration of polymer PHPA was suggested 0.1 V/V. Selected Reynold's number of values was acquired for the solvent to observe the drag-reducing percentage versus increasing Reynold's number. The velocity of thoroughly turbulent flow was the aim of the study and measured mean axial velocity close to the numerical model, i.e., universal wall law and effect of Reynold's shear stress, which was decreasing with an increase in PHPA concentration. The relationship between the velocity of fluid near the inner pipe wall region shows inversely proportion to drag reduction, which meant that at optimum PHPA concentration velocity near the pipe wall region was the least in comparison with acquired maximum drag reduction.

(Rodriguez-Corredor et al. 2014) investigated horizontal concentric annulus having highly turbulent water flow. They compared axial mean velocity contour with universal law and found axial velocity profiles obeys the law near the pipe wall and follows logarithmic law far from the wall. The turbulence of water flow was ranged from 17700 to 66900 Reynold's number. RMS values of velocity, vorticity, and shear terms were also investigated.

(Rodriguez Corredor, Bizhani, and Kuru 2015) studied similar parameters on the same flow loop and PIV method by using drag-reducing fluids to find stats like Reynold's stresses, axial and radial velocity trends, and turbulent kinetic profile.

(Kopplin 2003) studied axial and radial velocities in two-phase flow (i.e., liquid and gas) using tri-color LED strobe lights to track small bubbles that are naturally present alongside pipes during liquid flow. He tracked these bubbles and provided the contrast with his data and the past studies annular two-phase horizontal flow data. Formation of ripples and waves in the annular flow impacted indigenous liquid film velocity, but they are arbitrarily scattered. According to his research, his data did not follow any liquid distribution theory and previously studied data, but his mechanism might be significant if studied further.

(Allahvirdizadeh, Kuru, and Parlaktuna 2016) studied experimentally cutting transport of non-uniform marble cuttings in the horizontal concentric annulus by using PHPA polymer dissolved in water with different concentrations to study the mechanism of cutting transport, drag reduction percentage, friction factors at different fluid velocities and percentage of pressure drop, percentage of cutting area in comparison with ROP and polymer concentrations by visualization technique. He found up to 38% of drag reduction at 0.07% W/W PHPA concentration, which leads to better cutting transport of solids. He suggested from his study that increasing fluid viscosity is not a valid measure for better cutting transportation at more high flow rates.

(Goharzadeh and Rodgers 2009) studied comparative visualization techniques for cutting transport by slug flow in a small-scale horizontal pipe through high-speed photography and Particle Image Velocimetry (PIV). Digital imaging was made to analyze solid cutting transport, and the velocity field of slug flow was obtained by Particle Image velocimetry (PIV). The study visualized the physical behavior of uniform solid particles movement due to slurry flow. Velocity profile inside the pipe varied and shown major descent in variation over the solid particles dune that causes the critical velocity of solid particles for cutting transportation was increased.

(Messio et al. 2008) observed velocity and vorticity fields of inertial waves created from the rotating disk in a small cylindrical tank filled with water by PIV.

(Chang and Lee 2010) investigated swirling turbulent flow in annular geometry by using 2D Ar-Ion Laser-induced PIV technique on the fluid containing smoke and liquid dye at Reynold's number 60K to 80K to analyze axial turbulence velocity and intensity and swirl angle.

(Rodriguez-Corredor et al. 2014) investigated horizontal concentric annulus having highly turbulent water flow. They compared axial mean velocity contour with universal law and found axial velocity profiles obeys the law near the pipe wall and follows logarithmic law far from the wall. The turbulence of water flow was ranged from 17700 to 66900 Reynold's number. RMS values of velocity, vorticity, and shear terms were also investigated.

(Bizhani, Kuru, and Ghaemi 2016) studied how particle remove from solid cutting beds in horizontal well upon hole cleaning operations. Previous studies of Majid Bizhani and Ergun Kuru were based on multiphase flow in the horizontal pipe, concentric annulus, and varied turbulence characteristics of water and drag-reducing fluids through 2D PIV methodology. In this study, they observed instantaneous velocity profile and near-wall turbulence intensities for the removal of solid particles from cutting dunes in a horizontal well. In the presence of solid dune, the parameters such as Reynold stress, radial, and axial velocity profiles were shown unfavorable effects for hole cleaning ideology. Also, larger solid cuttings provided a minor increase in turbulence.

Chapter#3

Experimental setup and working

3.1 Flow loop

The flow system consists of a 6.4 cm * 11.4cm (2½ *4½ in.) and 6.16 m long annulus, thus giving an annulus flow area of 70.9 cm2 (Figure 2). The annulus is made up of an outer acrylic pipe and an inner PVC pipe. The outer pipe consists of four 1m sections made of transparent acrylic material forease of observation and 1m of metal pipe. All pieces have an internal diameter of 11.43 cm (4.5-in). Theinner pipe is made of five 1 m PVC pipes with an outer diameter of 6.35 cm (2.5-in). The inner pipe can berotated and placed concentrically or eccentrically. The whole unit is set up on a frame capable of providing inclination from horizontal to about 15°, to study the effects of inclination. Thesystem includes a flow tank of 1.0 m^3 capacity (265 gals) equipped with an agitator. A high-speed camera has placed to record a solid transportation phenomenon. Specially designed fasteners are used to secure the frame in position and also allow the system to move inone axis to position it manually eccentric or concentric. A rotor can rotate the inner tube between 0-150rpm. The system will be operated with maximum pressure in the annulus of 1.0 barg (15psig) when havingair-liquid (two-phase) flowing in the annulus and 2.0 barg (30 psig) when having only liquid flow.

Other multiphase research facilities are also installed in the flow loop system such as a pressure differential measurement system, Electrical Resistivity Tomography (ERT) system, visualization system, and Particle Image Velocimetry (PIV) system. Each system has installed to retrieve specific results for the multiphase annular flow. For this thesis, my work was focused on PIV.

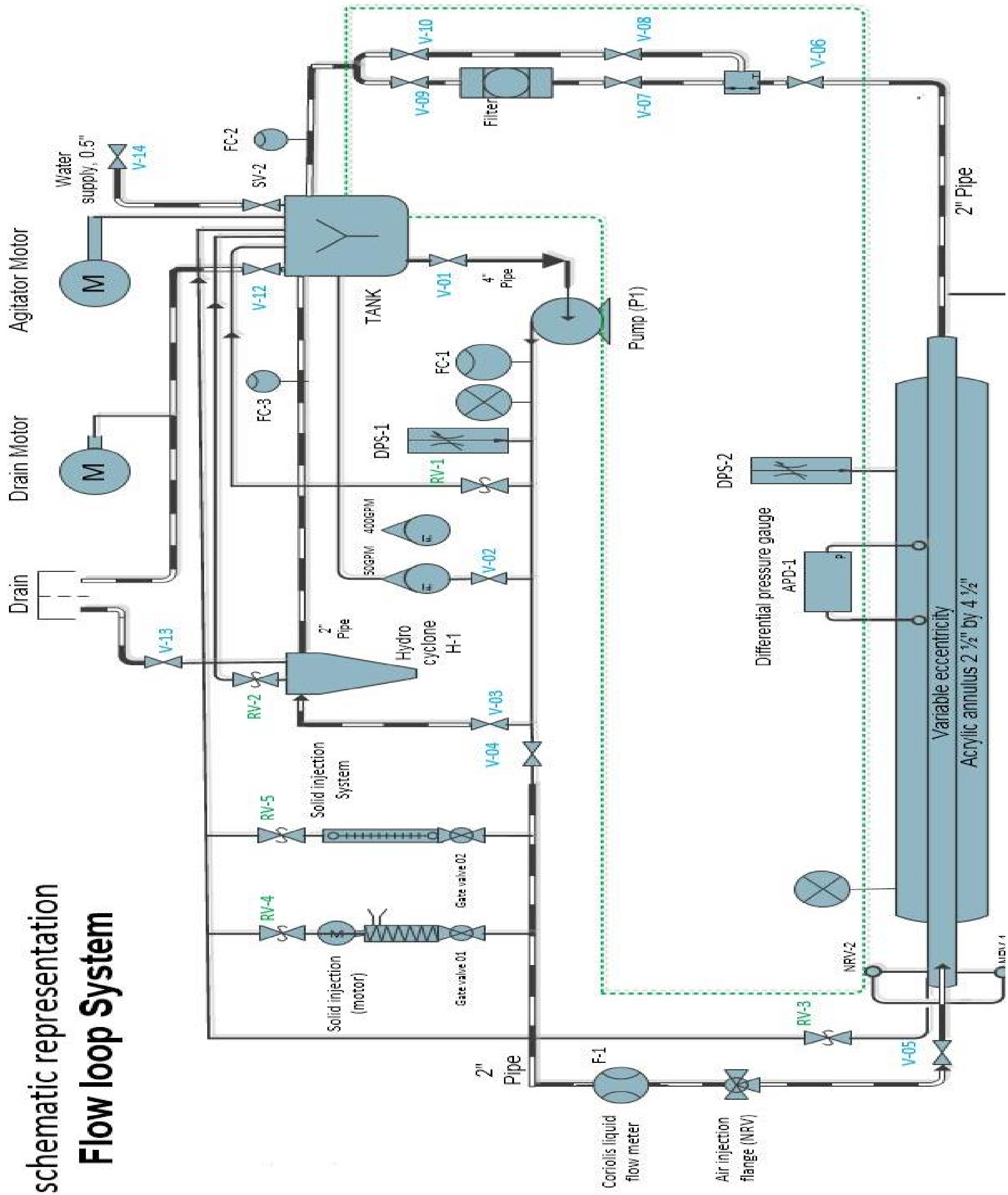

Figure 9 Schematic of multiphase flow loop in Lab 259I TAMUQ

3.2 PIV Setup

PIV setup in Advance Multiphase Flow Assurance Lab (AMFAL) consists of the class IV Photonics DM 30 527 Laser has been installed to perform the PIV analysis. The Particle Image Velocimetry (PIV) requires the Laser to illuminate the flow field inside the RIM box. Then the premixed seeding particles with the flow are being tracked by the PIV system to evaluate the velocity field for the respective interested area. The LASER can produce a maximum of 30 mJ of energy per pulse. The wavelength of the radiation is 527 nm. The diode current range is 16-30 amp. A controller is also set to control the laser parameters. The chiller is filled with a mixture of distilled water and the OptiShield Plus (around 10%) solution. The chiller pump outlet hose is connected to the laser-head IN hose connector, and the chiller inlet hose is connected to the Laser-head OUT hose connector.

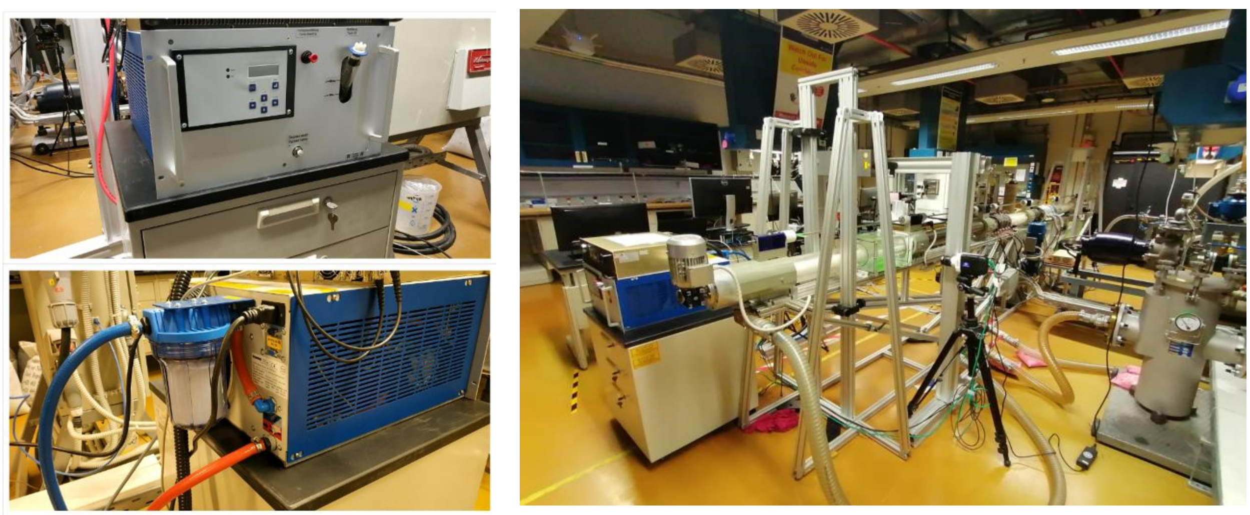

Figure 10 PIV setup in the lab 259I.

Chapter # 4

Methodology

4.1 Refractive index matching

Inflow visualization, an unusual calculation discrepancy encountered. To remove that discrepancy, an optical diagnostic technique applied to fluid dynamics studies such as flow visualization with a high-speed camera and particle image velocimetry have practiced. This error arises when the refraction of light passing through transparent investigation pipe walls. Refraction through a cylindrical pipe wall generates the phenomenon of multiple images and wrong estimation of the position of substances flowing inside it. For instance, if you place a pencil inside a half-filled glass of water, you will notice that the image position of pencil that can be seen through the water in the glass is apart from the real object. This discrepancy must be removed to take effective measurements through visualization. The method that removes this error usually termed as Refractive Index Matching. The type and the equipment used for RIM may be different according to the system, fluid dynamics, and total internal reflection phenomenon.

For the flow loop system, to eradicate the refraction phenomenon inside the multiphase flow, RIM has achieved by placing a RIM box, as shown in figures (11, 12). The box is made up of flat walls having the same acrylic material and thickness with that of cylindrical pipe walls, in the volume created between RIM box and the outer walls of the pipe, the same fluid that has been flowing in the pipe filled with viewing the least refraction error.

The refractive index of the acrylic glass medium is 1.49, whereas the refractive index of Non-Newtonian fluid (Flowzan® at 0.05% W/W) is near to water approximately 1.35. The alternate acrylic glass and the fluid provide no angular refraction and total internal reflections. However, the final image is 95% - 98% accurate, and the position of particles the is needed to focus has just shifted their position in parallel direction rather than angular, which is intolerable for velocity measurement. Through this technique, we can measure the displacement and velocity of particles accurately.

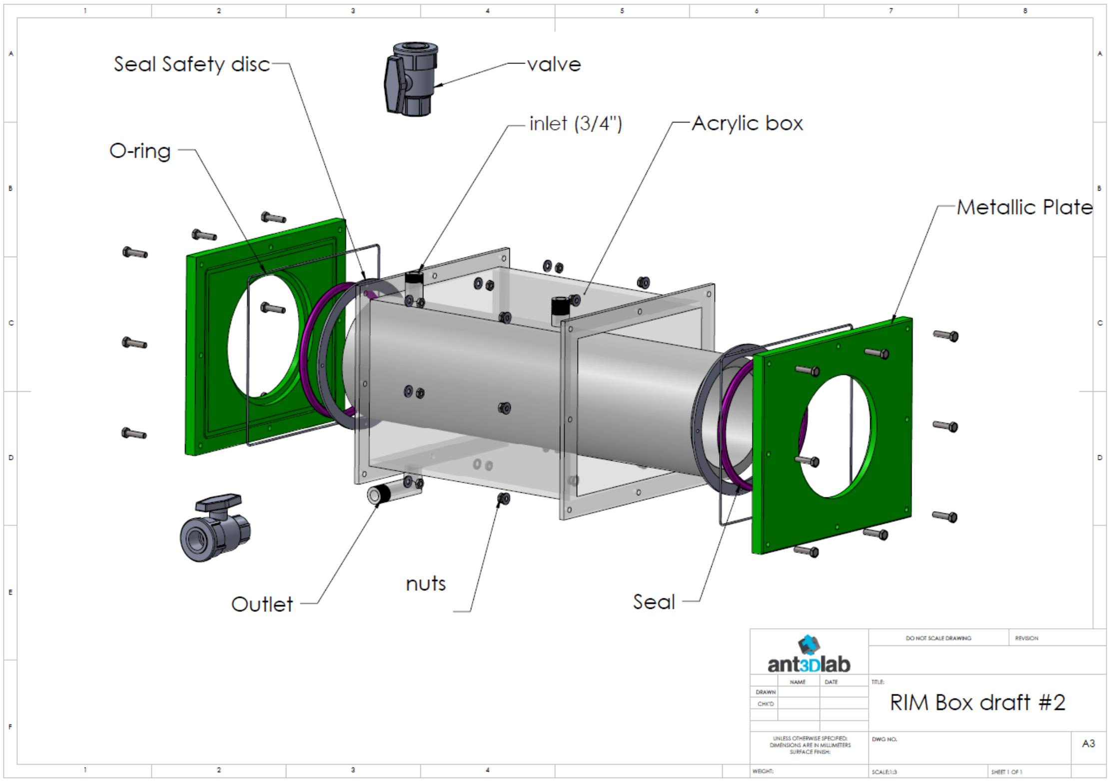

Figure 11 Engineering drawing of the RIM box.

Figure 12 RIM Placement in the multiphase flow loop

4.2 Working of the flow loop

The large-scale multiphase flow loop system has a wide range of advanced equipment dedicated to different research findings and calculations. PIV is one of the advanced flow visualization facilities equipped on the flow loop. In this section, I have provided a detailed experimental procedure that starts from how fluid prepares, solid injected, and multiphase flow visualizes in the RIM box.

The conducting experiments in flow loop aim to exhibit the hole cleaning procedure in a real case scenario during drilling processes, where cuttings solid beds initiate to develop on the bottom of the annulus.

1. Fill the tank with 300 liters of water and then start adding Flowzan powder in the tank gradually with constant agitation so that the Flowzan solution becomes a homogeneous solution. For our practice, agitation was provided for 1 hour with the help of a built-in agitator in the tank.
2. To achieve 0.05% w/w concentration of Flowzan solution, 150 g of Flowzan powder was added in water, then the circulation of the solution made ready at our desired flow rate.
3. A small amount of seeding and fluorescent particles was also added so that particles can be illuminated by Laser and captured by image acquisition camera for PIV calculations.
4. 12 Kg of solid glass beads is added to the solid injection system.
5. From the control panel of the flow loop, pump flow rate, agitation, and drill pipe rotation have been controlled.
6. Solid was injected from a solid injection system along with the liquid flow. The solid dunes were allowed to travel the whole flow loop, and at the last section where the RIM box was mounted, we analyzed the fluid behavior during the passing of dune from the investigation box.
7. By considering all safety measures, Images were taken by applying a laser sheet on the flow.
8. The eccentric condition of the drill pipe was achieved by adjusting the rotating sleeve dedicated to providing eccentricity in the annulus.
9. Solid was collected at the solid filtration system to reinject in a solid injection system to carry another set of experiments.
10. The annulus needs to be cleaned carefully after the experiments.

4.3 PIV measurement steps

1. Calibrate the high-speed camera and make sure it focuses the RIM box

2. Scaling of the imaging area is set to on default since it covers the RIM box.

3. Calibrate the inner pipe area through PIV – Davis 8.4 software.

4. Setting the Laser's diode Current to 20 Ampere and turn it to on "On" mode.

5. Make sure, Cycle rate and Cycling Image rate is set to 1 Hz and 1 kHz.

6. Set the number of images to 200 images.

7. Record the images when solid glass beads enter the RIM box area.

4.4 Scaling

The term scaling refers to the calibration process. Doing a calibration is important because the results should be shown in scaled units representing the true (world) dimensions. So the image scale pixel/mm should be determined.

4.5 Calibration

Calibration is important for all processing because:

- The results should be shown in scaled units representing the true (world) dimensions. So the image scale pixel/mm should be determined.
- For oblique viewing setups or views through curved glass windows, the images show some image distortions due to perspective projection (and possibly inherent camera lens distortions). This can be corrected via the appropriate calibration.
- For stereo measurements, an internal representation for the geometrical setup of both cameras relative to the sample is needed.

There are some suppositions for the calibration:

- Knowledge to operate the hardware to collect the calibration images must be available.
- If the camera(s) are focused on the sample surface, it is a simple task to move the calibration plate into the focal plane - and when it is removed, you are immediately ready to start acquiring images. If the calibration is done first without being careful about the plate position, the system might be unfocussed on the sample, necessitating refocusing and recalibration.

- Calibration can be performed after the sample images have been acquired (providing the camera system has not been altered).

4.6 Image processing

Image preprocessing allows manipulating the particle image before vector calculation is performed. Often this helps to improve the quality of the results, especially if we have to work with high or locally changing background intensities.

4.7 Vector field calculation

The PIV project offers two Groups for Vector calculation in the DaVis Processing dialog. These are Vector calculation - double frames and Vector calculation - time series of single frames.
Basic operation:

- Adjust the layout using the window manager.
- Open the “Vector calculation” parameter and “Vector postprocessing” dialogue box.
- Adjust the evaluation parameters.
- Take an image with activated Processing after Take/Grab checkbox.
- Check the vector field quality.

Chapter # 5

Results and discussion

In this chapter, the results obtained from the pre-defined experimental matrix will be presented. These results include average velocity profiles, strain rate, shear, divergence from the velocity field, and swirling strength at different drilling parameters from PIV. Necessary figures and graphs will be presented, while complete sets of profiles can be viewed at the end.

5.1 Rheological properties of Flowzan (0.05% W/W)

The water-based non-Newtonian fluid was prepared by adding Flowzan (Xanthan gum) a biopolymer was used in the experiments. The rheological properties were necessary to discover to know about the behavior of the fluid. The rheological properties were tested by using a rheometer. The plot between shear stress and share rate has schemed, as shown in the graph. The fluid shows pseudoplastic behavior according to Power-law having values of consistency index (K) 0,005434403 Pa.s, flow behavior index (n) 0,878228013 Precision adjustment (R^2) 0,996749007 and Tensile strength (T_o) 0,228688761.

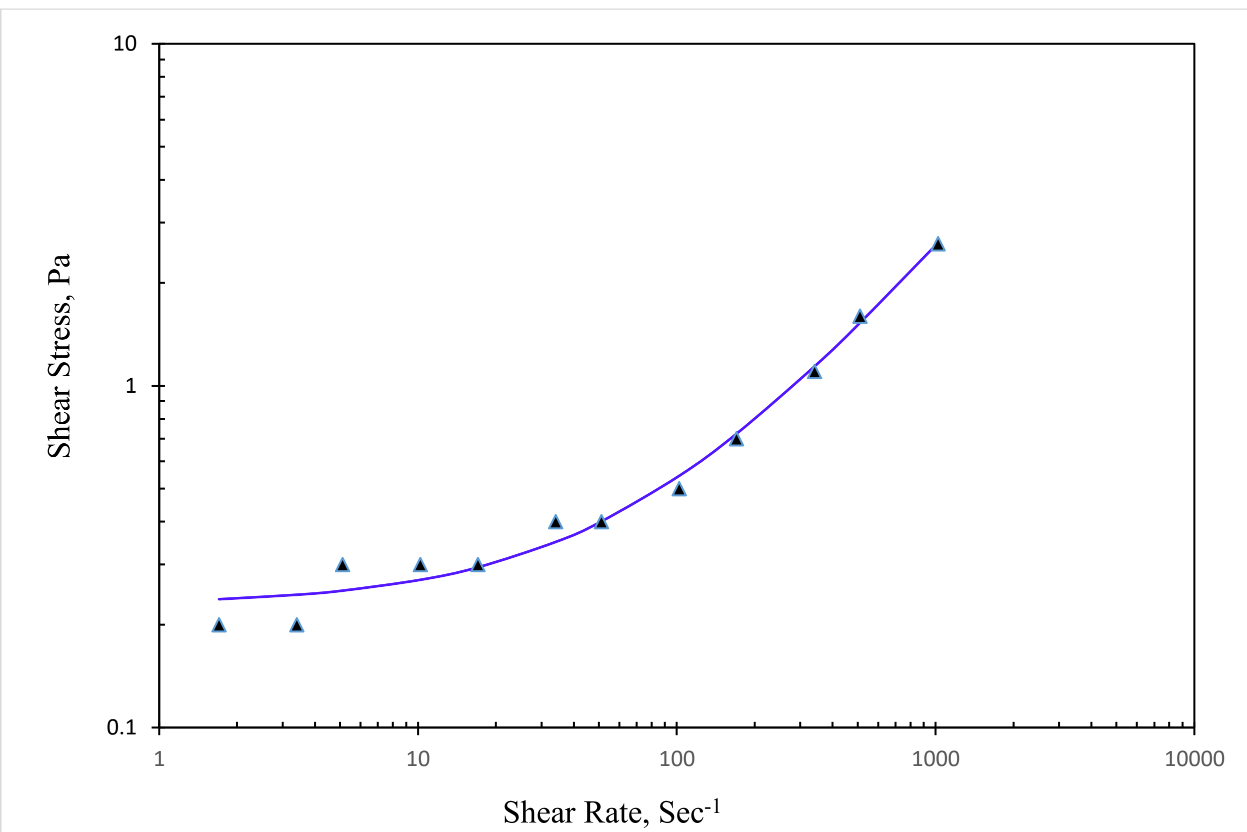

5.2 Velocity Vector Images

To obtain the velocity vector field, it is necessary to acquire raw images having flowing seeding + tracer particles as shown in Figure 13. Once the raw images had captured, from DaVis 8.40 velocity vector field have been generated.

Figure 13 Typical PIV image captured during the test without a solid flow

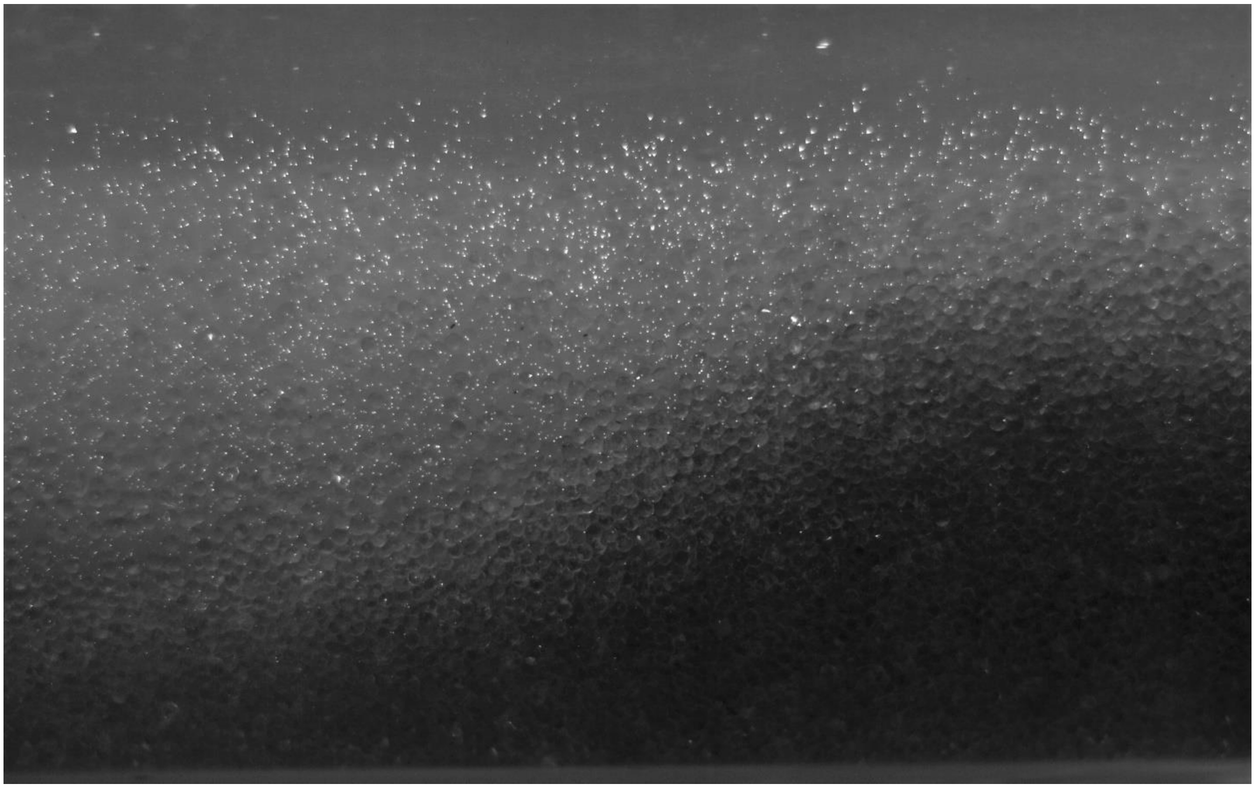

Figure 14 Typical PIV image captured during the test with solid bed formation

In the study, from raw images following velocity vector field was generated by Particle Image Velocimetry technique through DaVis 8.4 software under different sets of parameters as shown in figures.

5.2.1 Mass flow rate 205 Kg/min @ Flowzan 0.05% w/w

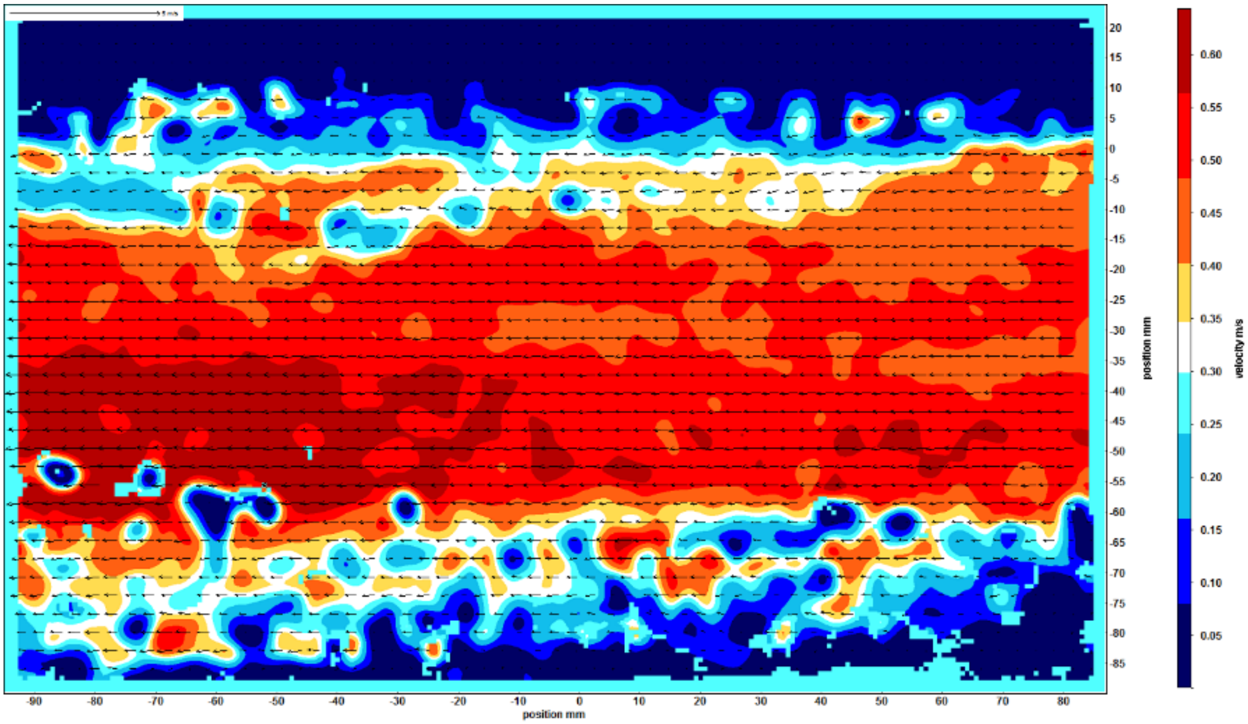

Figure 15 Without solid and drill pipe rotation

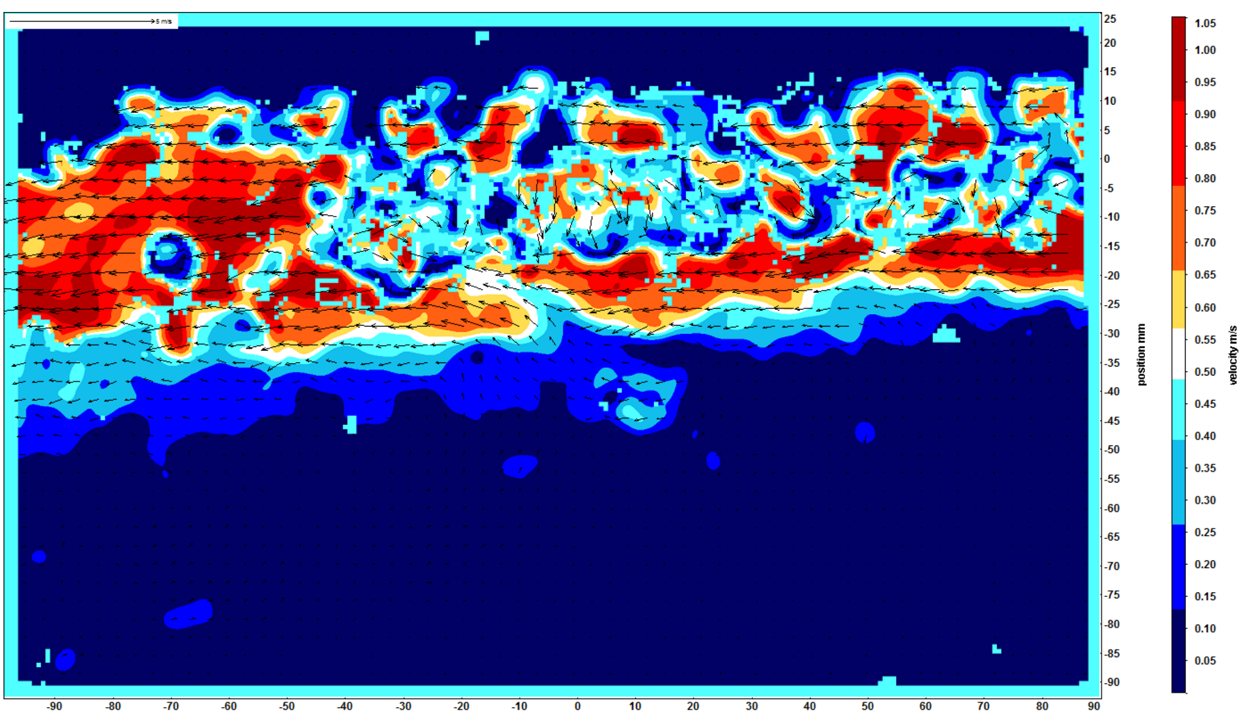

Figure 16 With solids and without drill pipe rotation

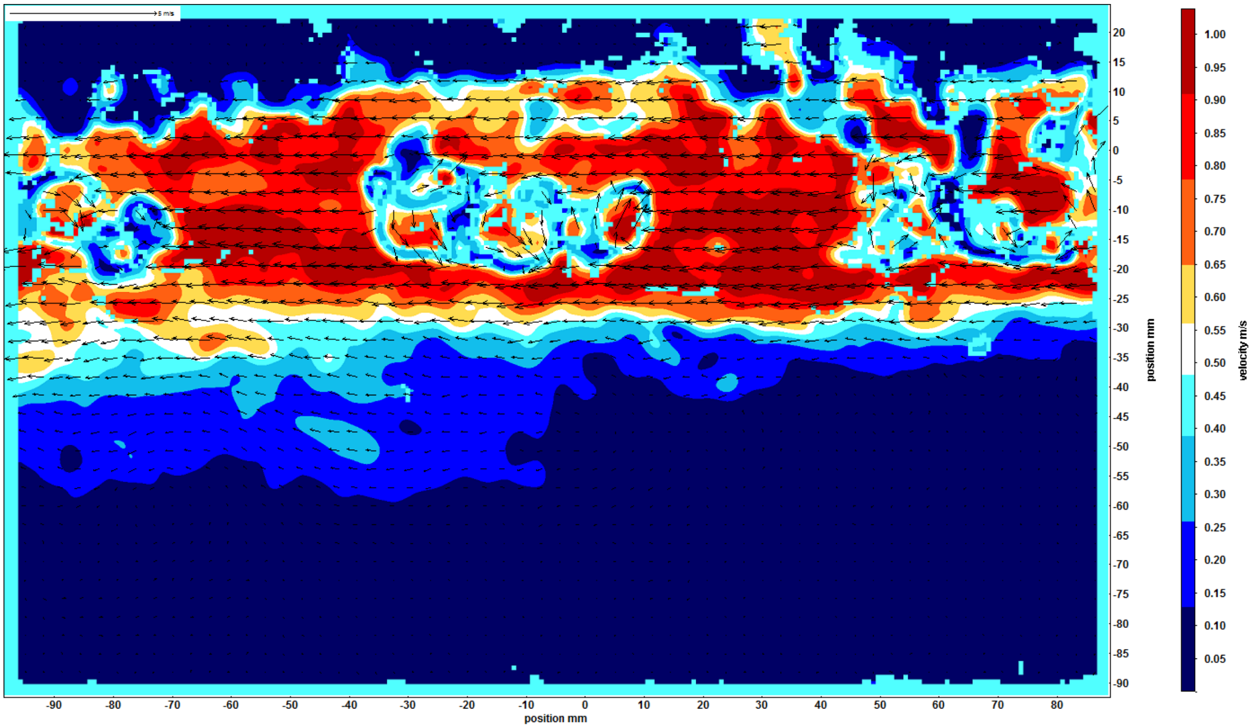

Figure 17 With solids and drill pipe rotation of 40 RPM

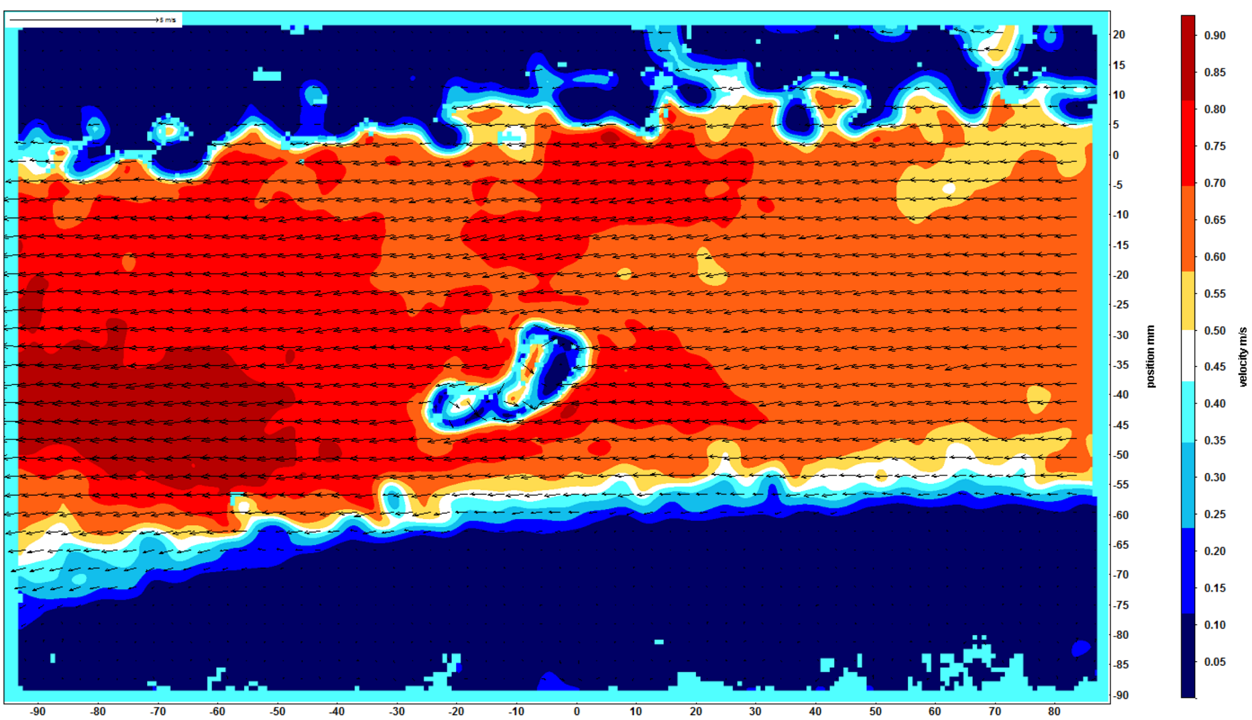

Figure 18 With solids and drill pipe rotation of 80 RPM

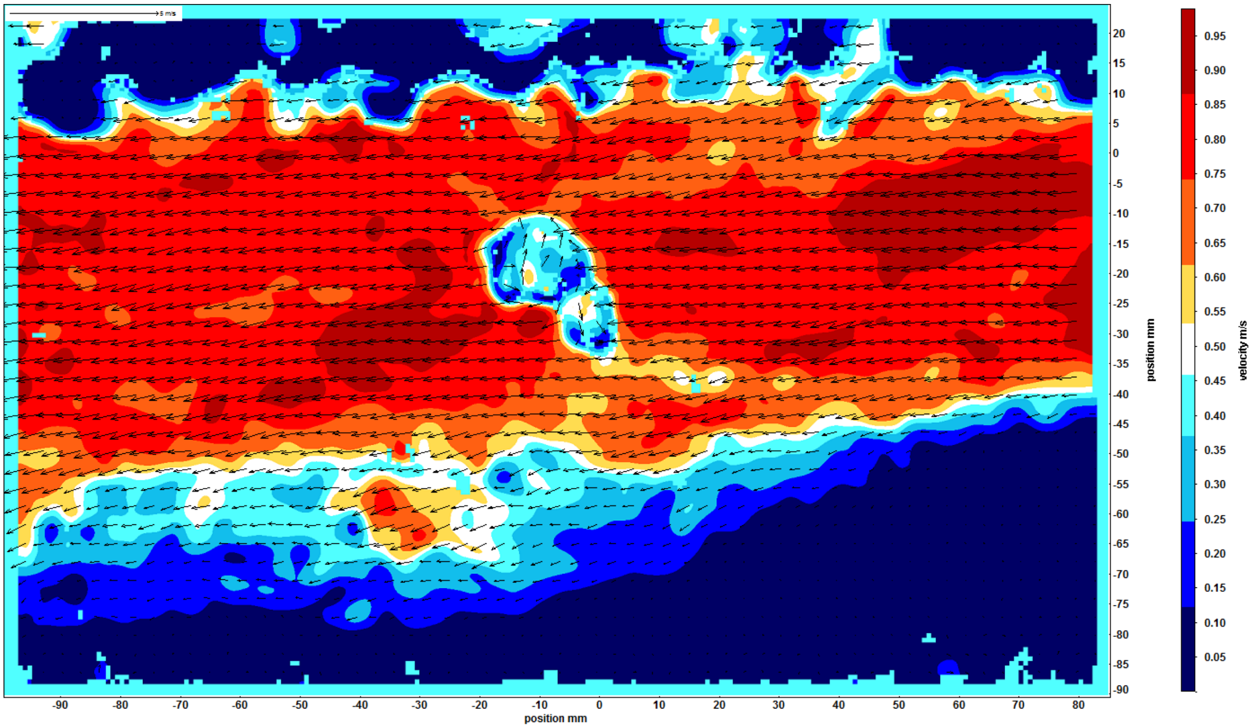

Figure 19 With solids and drill pipe rotation of 80 RPM

5.2.2 Mass flow rate 225 Kg/min @ Flowzan 0.05% w/w

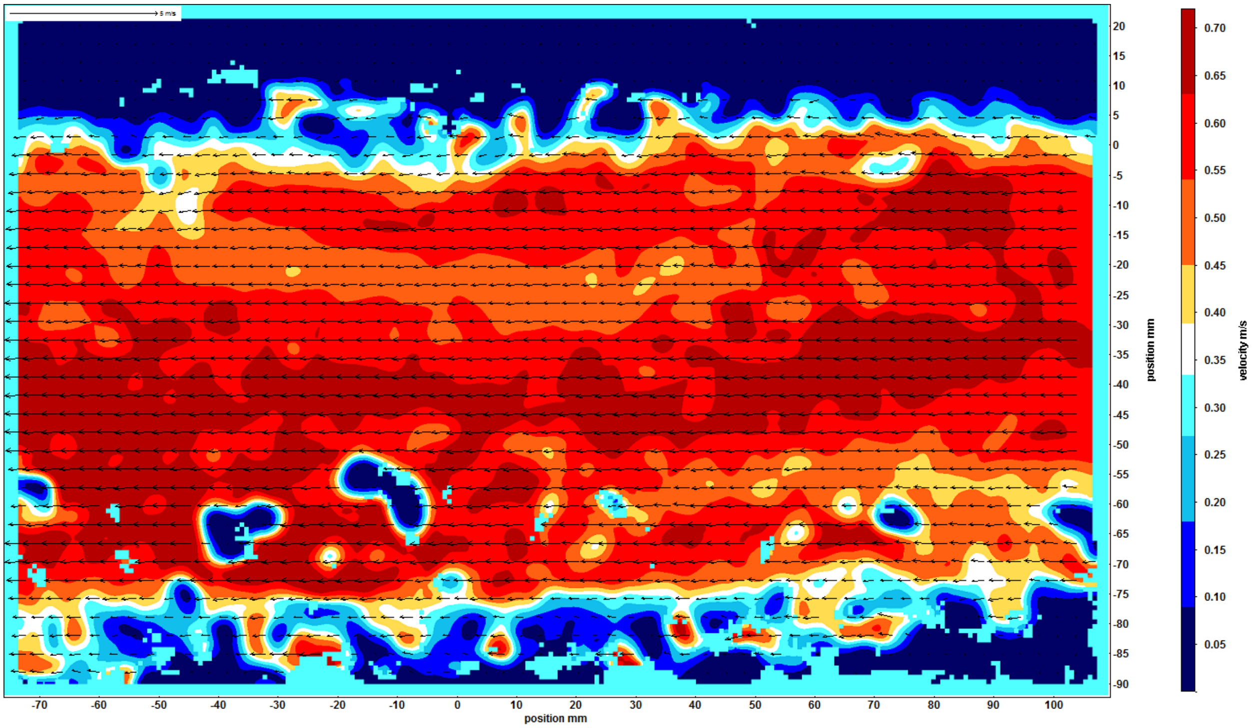

Figure 20 Without solid and drill pipe rotation

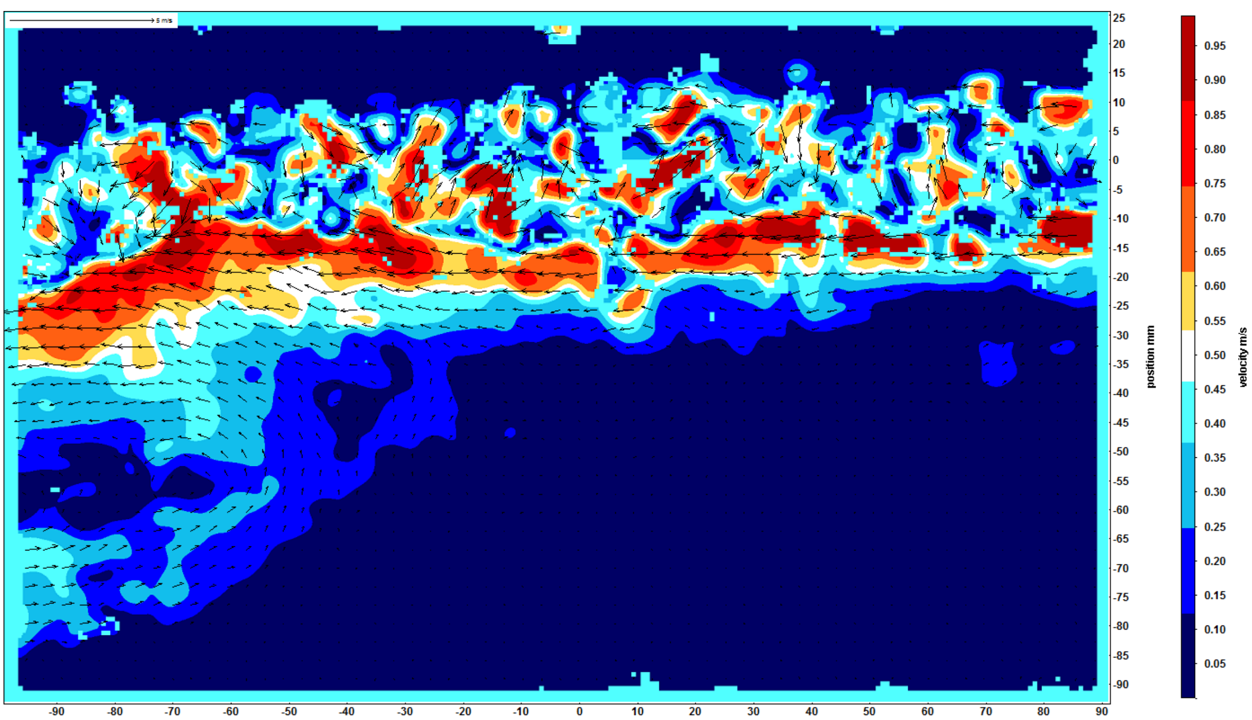

Figure 21 With solid and without drill pipe rotation

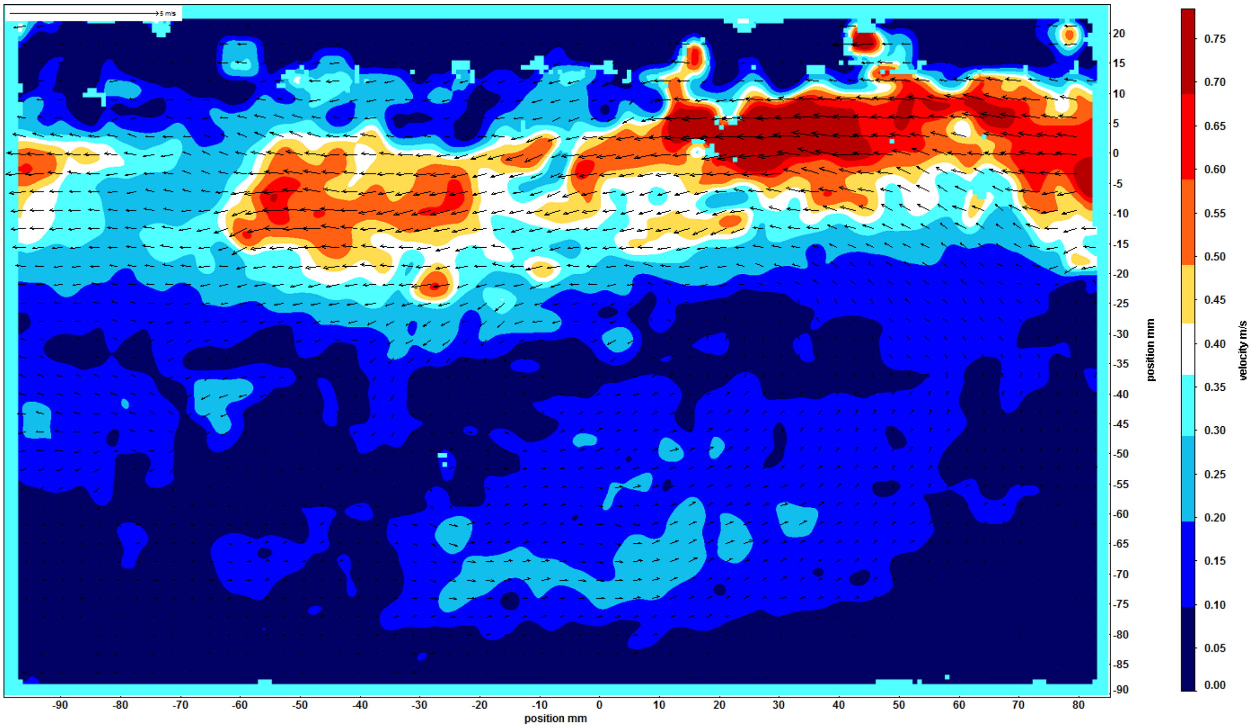

Figure 22 With solid, without drill pipe rotation and 0.5 eccentric condition of drill pipe

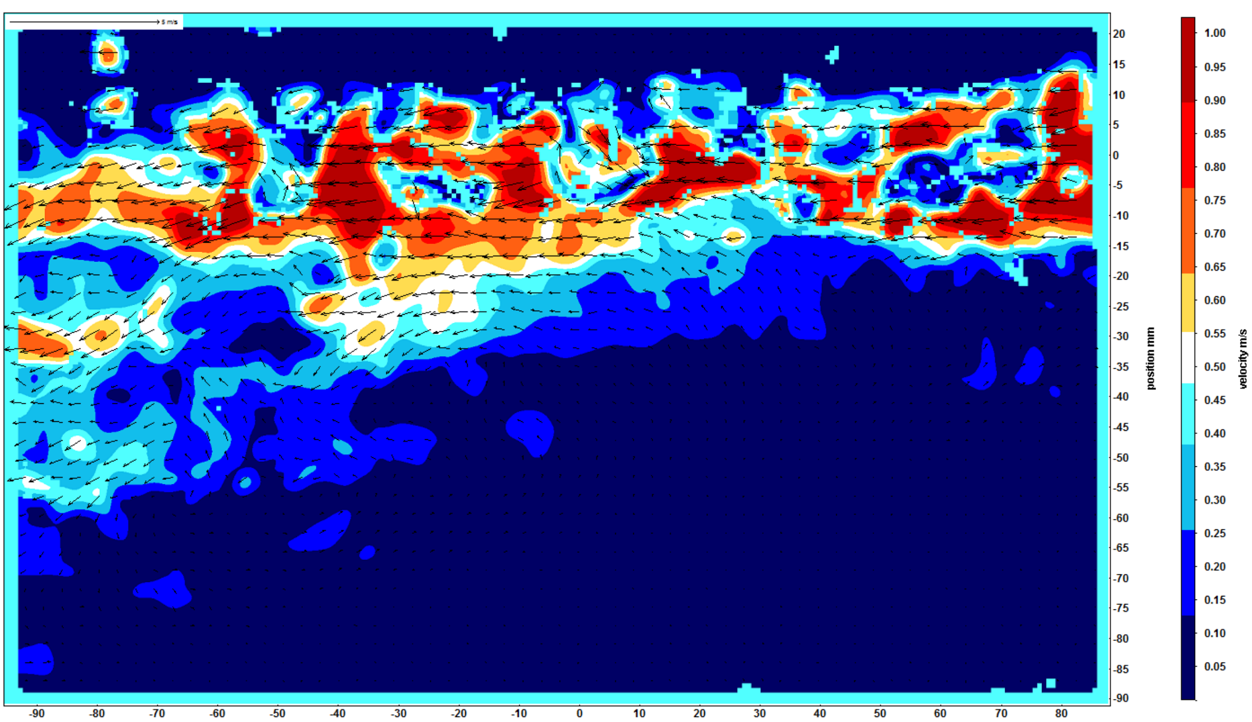

Figure 23 With solid and drill pipe rotation of 40 RPM

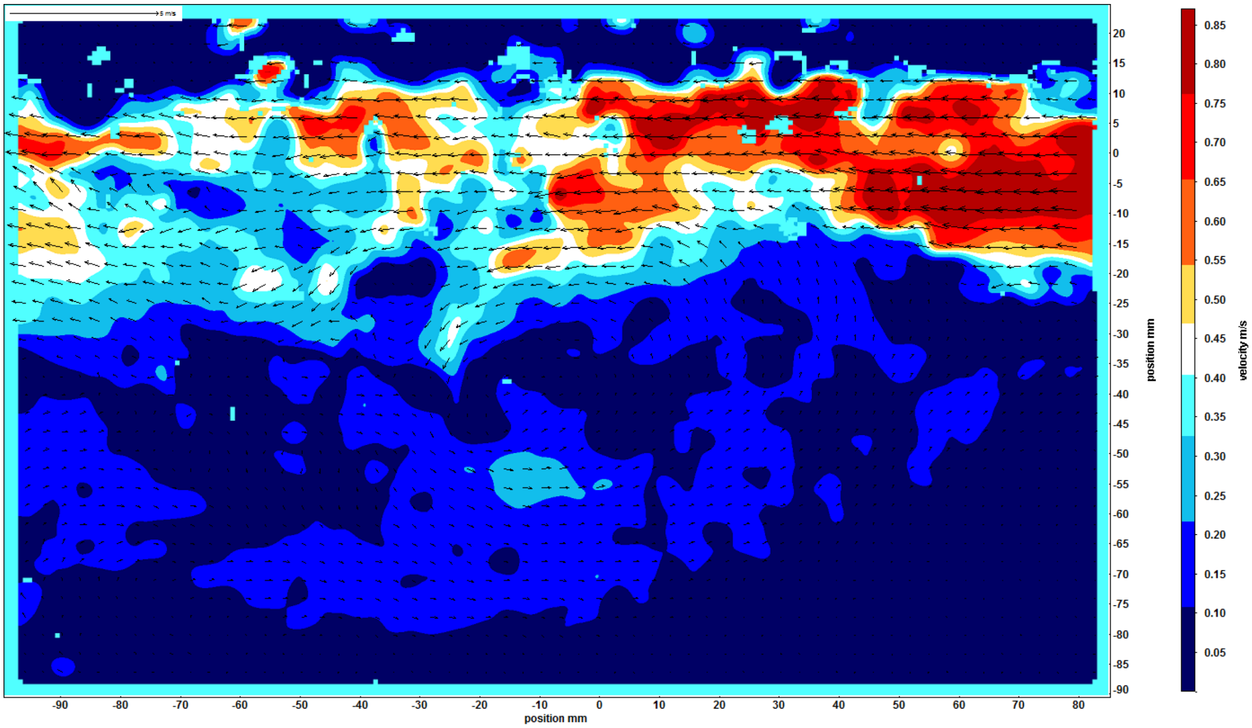

Figure 24 With solid, drill pipe rotation of 40 RPM and 0.5 eccentric condition of drill pipe

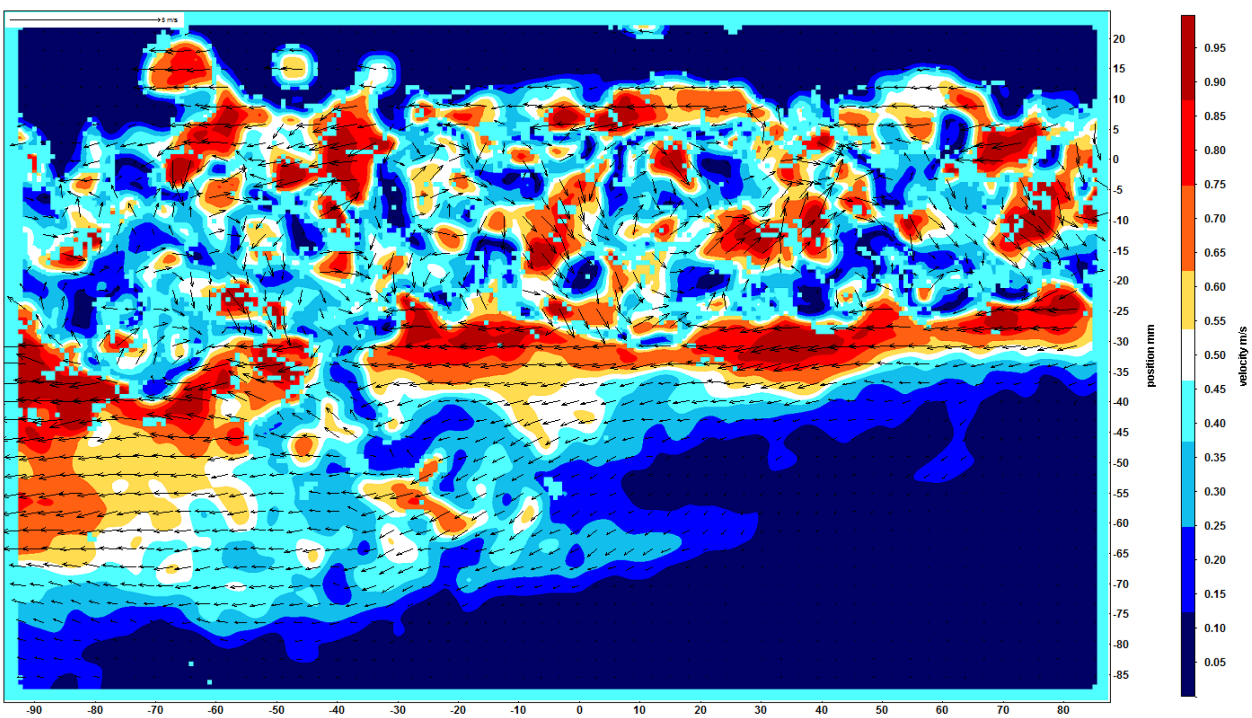

Figure 25 With solid and drill pipe rotation of 80 RPM

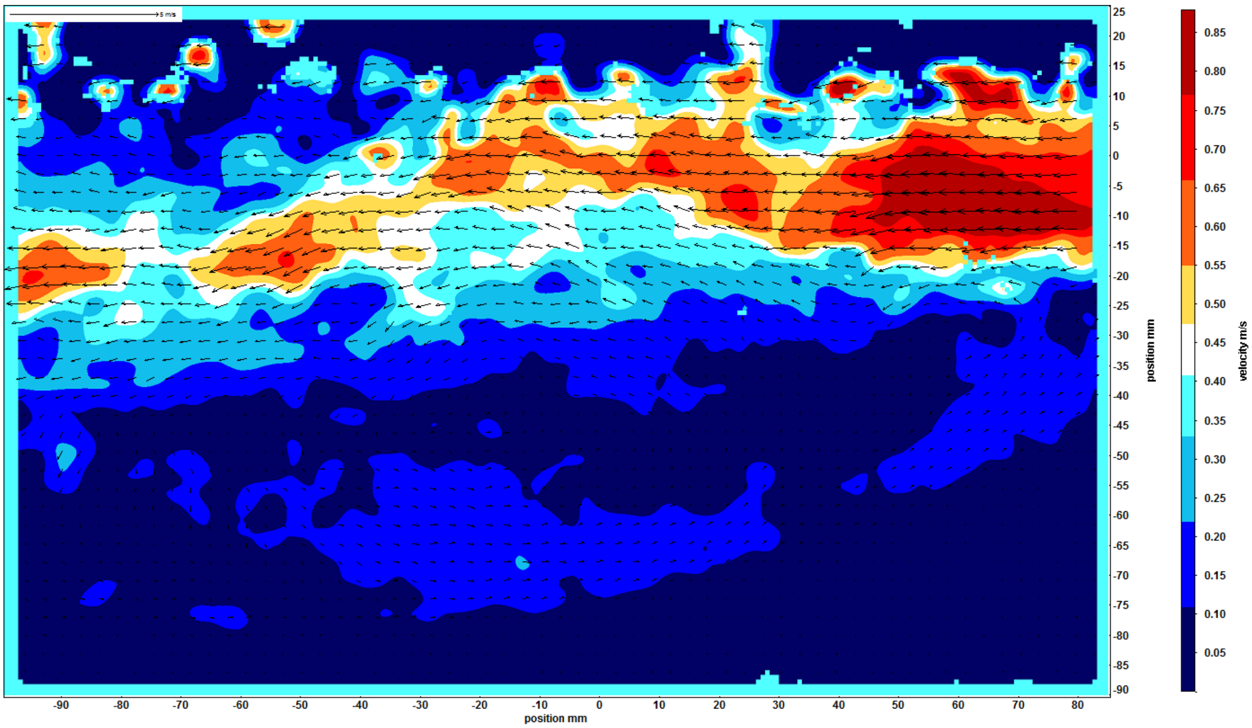

Figure 26 With solid, drill pipe rotation of 80 RPM and 0.5 eccentric condition of drill pipe

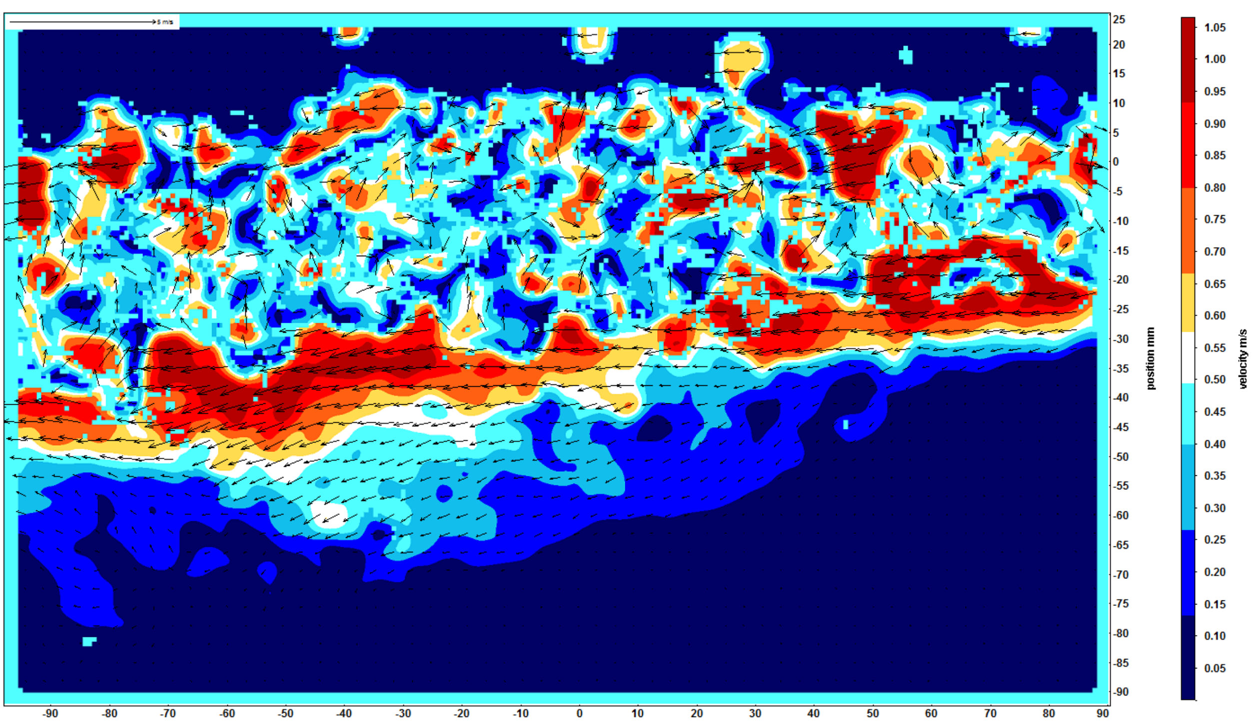

Figure 27 With solid and drill pipe rotation of 120 RPM

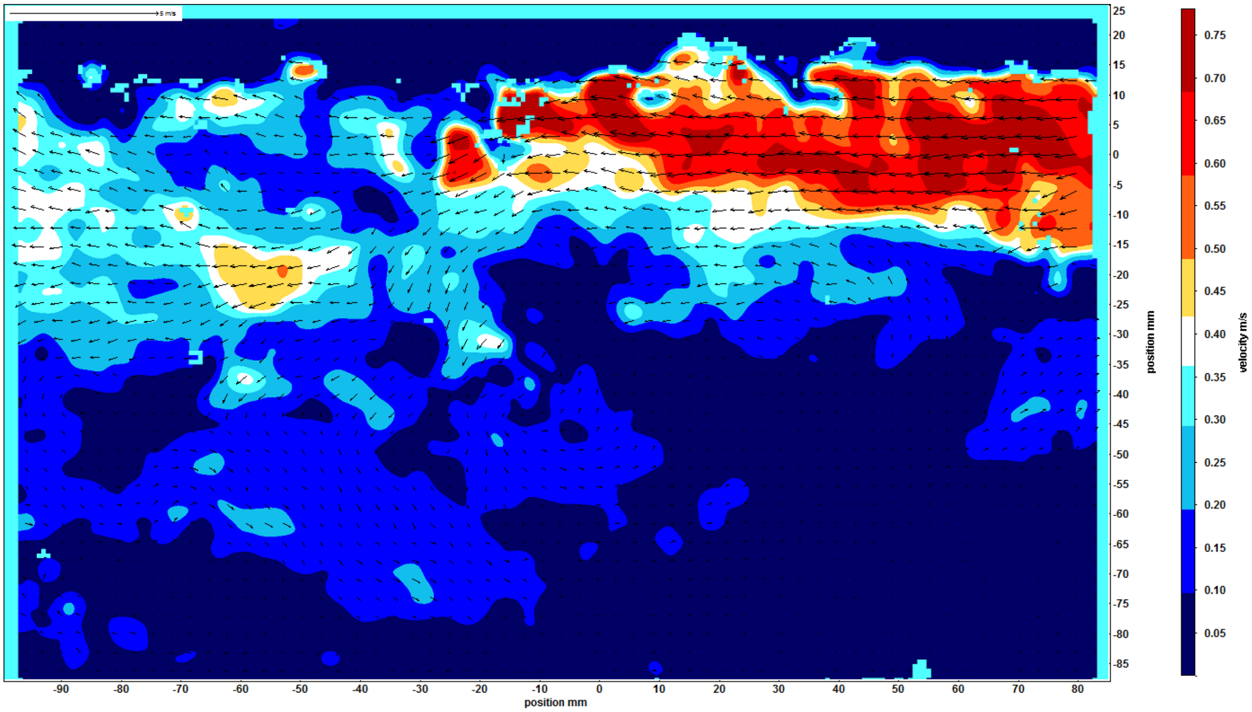

Figure 28 With solid, drill pipe rotation of 80 RPM and 0.5 eccentric condition of drill pipe

5.2.3 Mass flow rate 265 Kg/min @ Flowzan 0.05% w/w

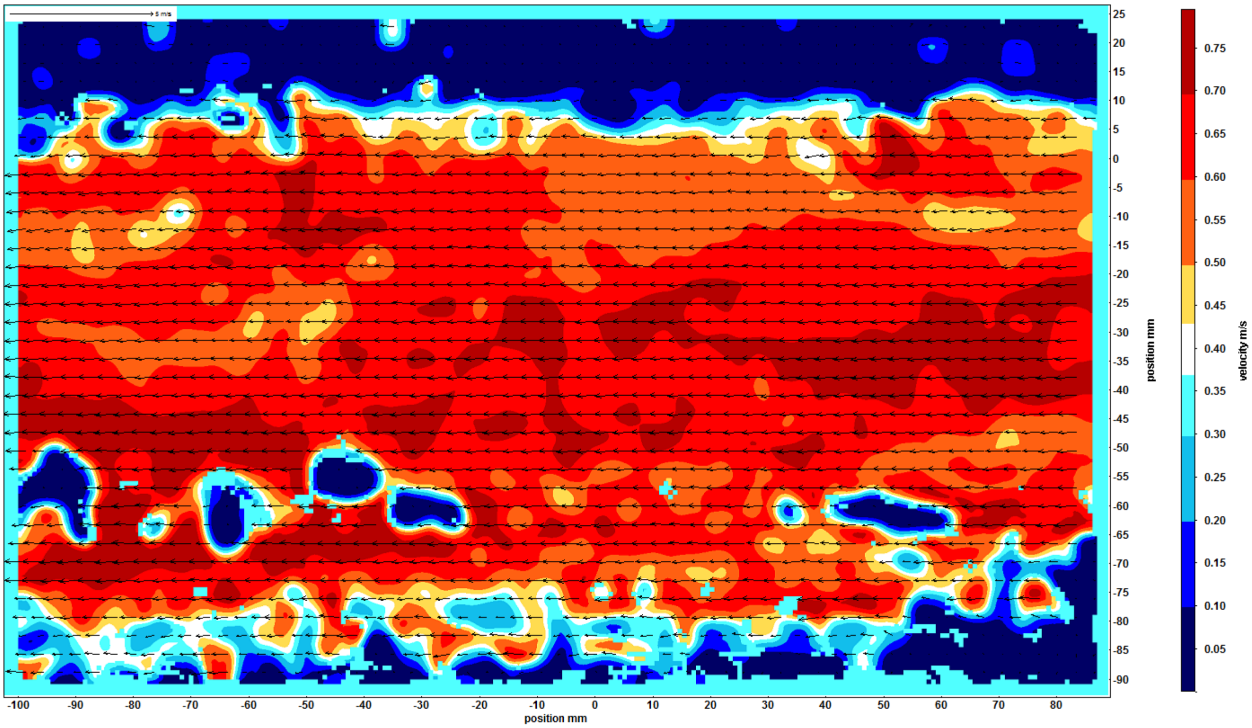

Figure 29 Without solid and drill pipe rotation

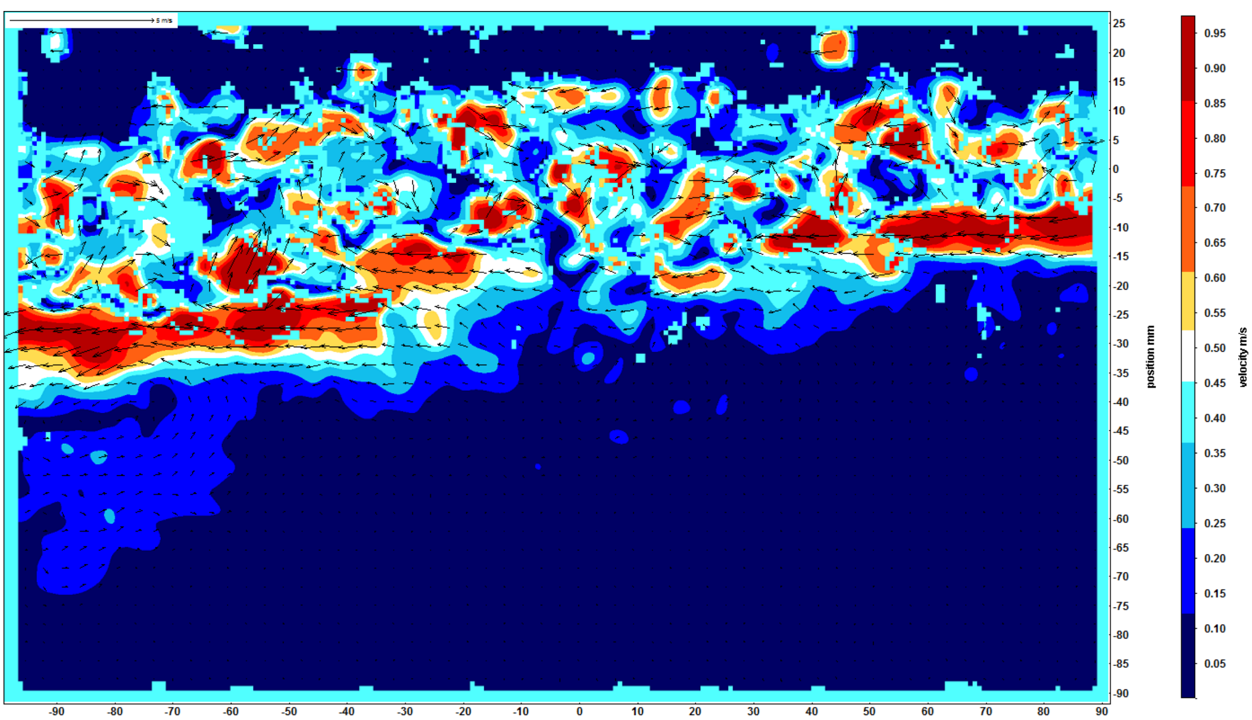

Figure 30 With solid and without drill pipe rotation

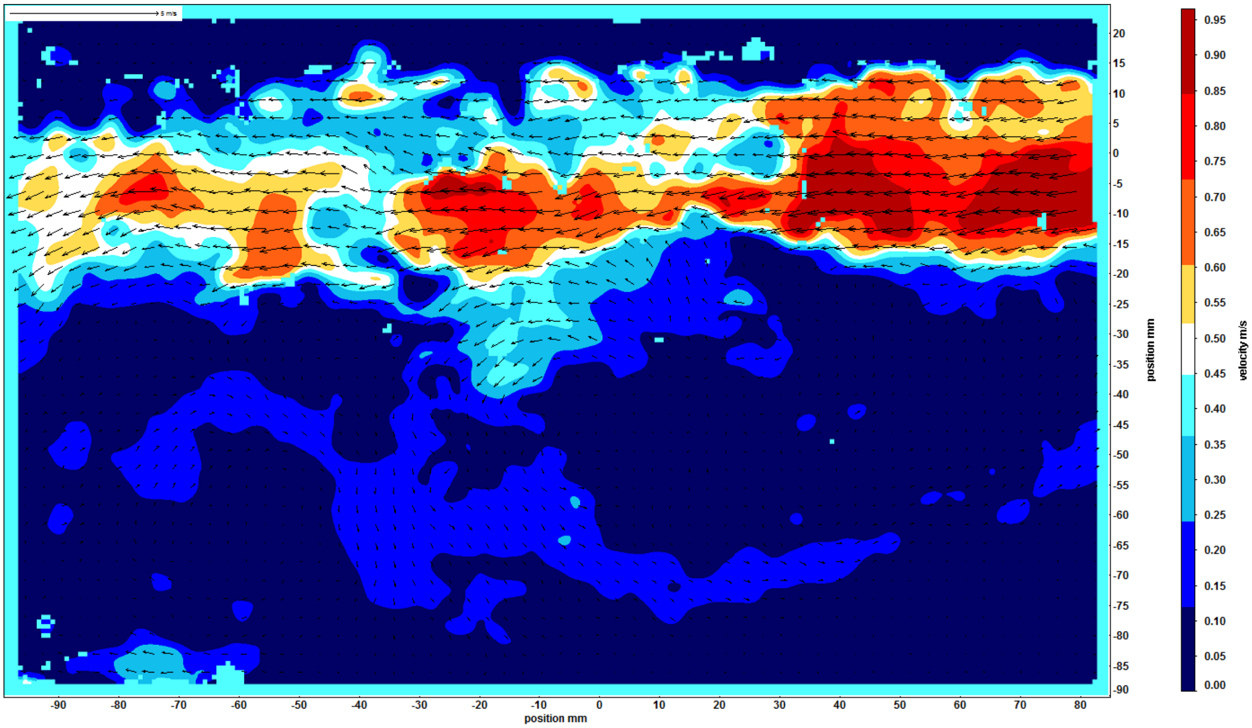

Figure 31 With solid, without drill pipe rotation and 0.5 eccentric condition of drill pipe

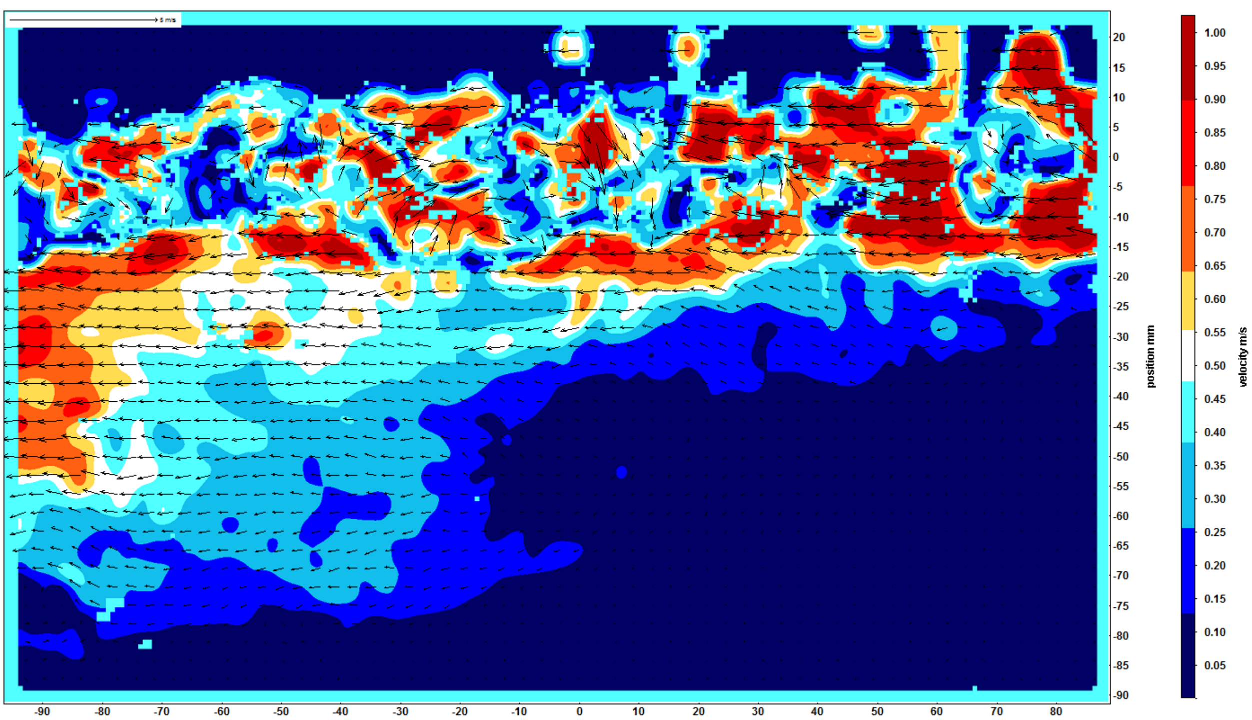

Figure 32 With solid and drill pipe rotation of 40 RPM

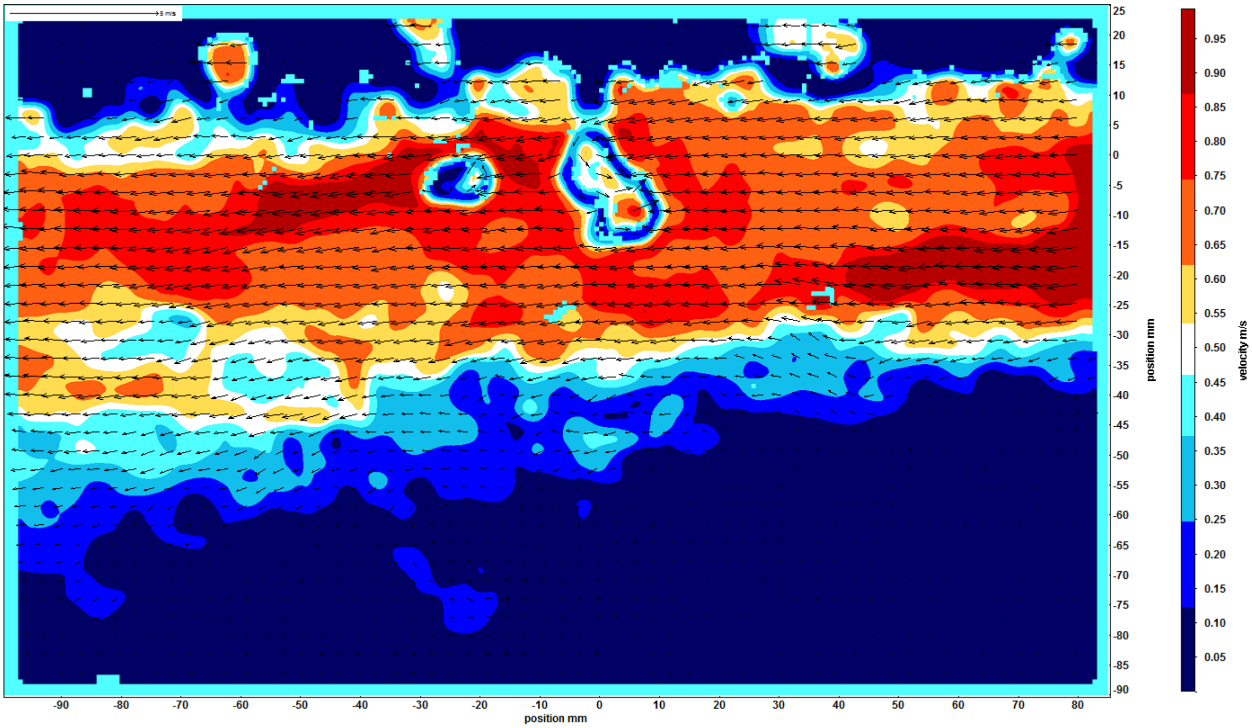

Figure 33 With solid, drill pipe rotation of 40 RPM and 0.5 eccentric condition of drill pipe

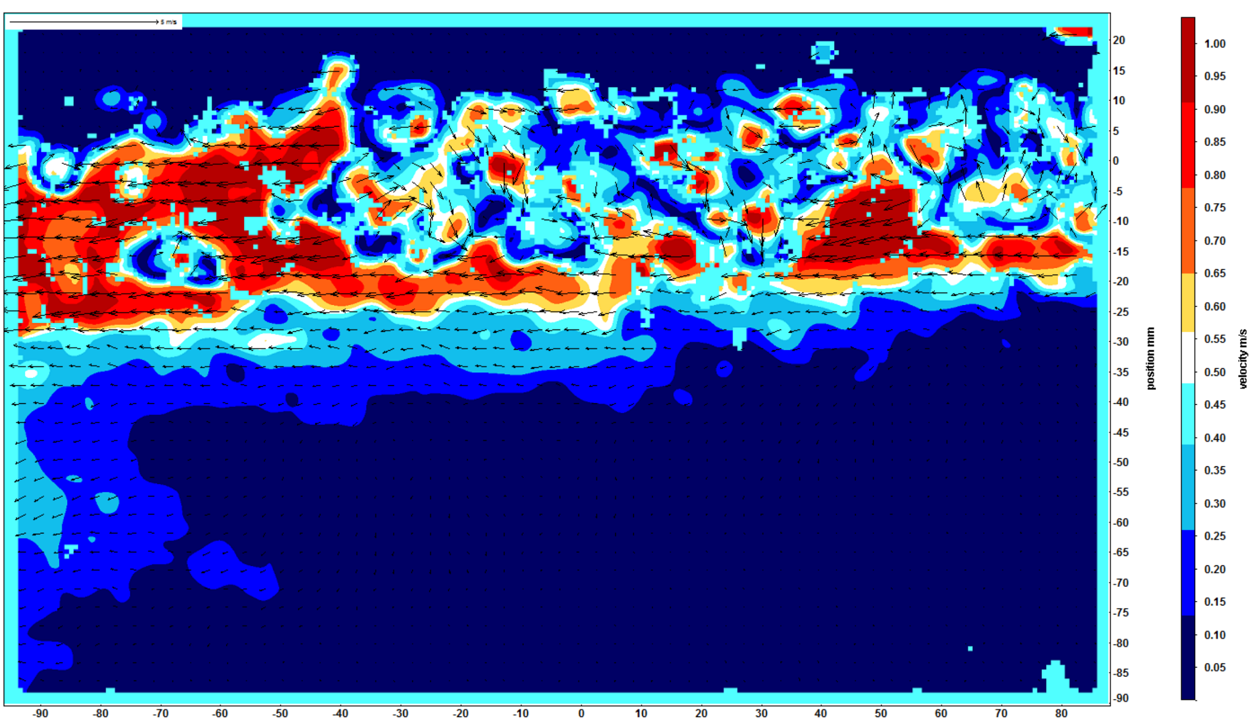

Figure 34 With solid and drill pipe rotation of 80 RPM

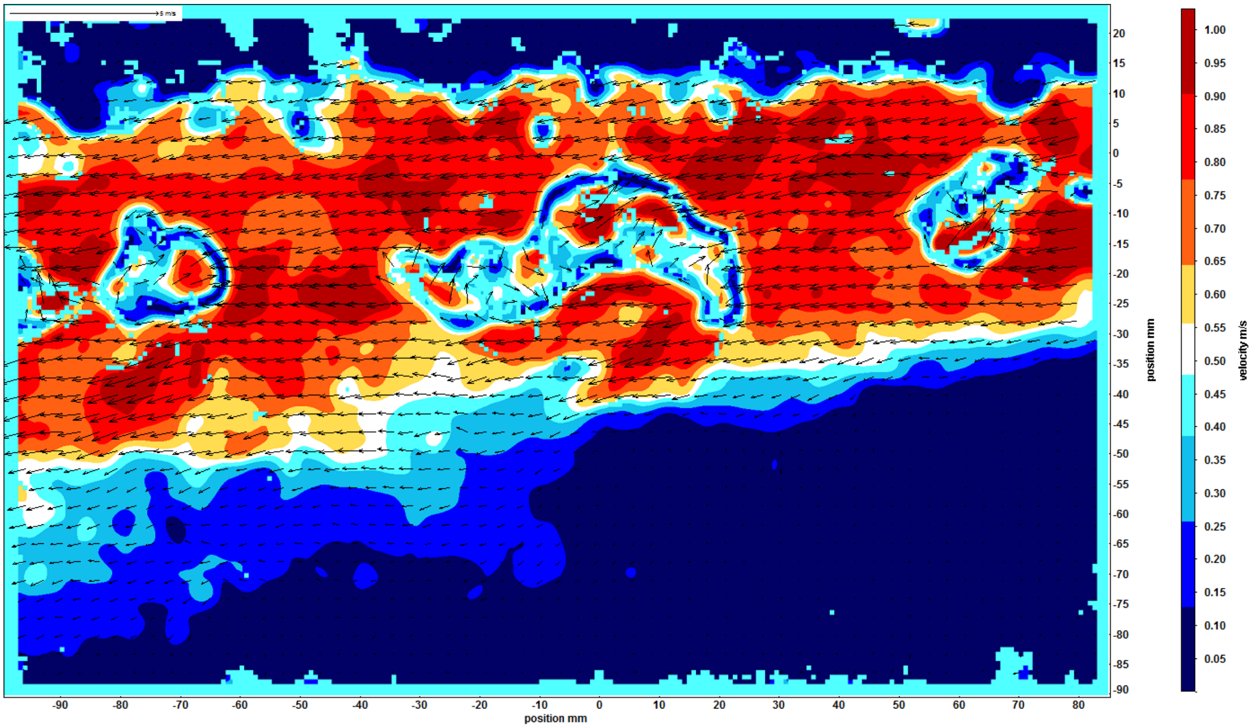

Figure 35 With solid, drill pipe rotation of 80 RPM and 0.5 eccentric condition of drill pipe

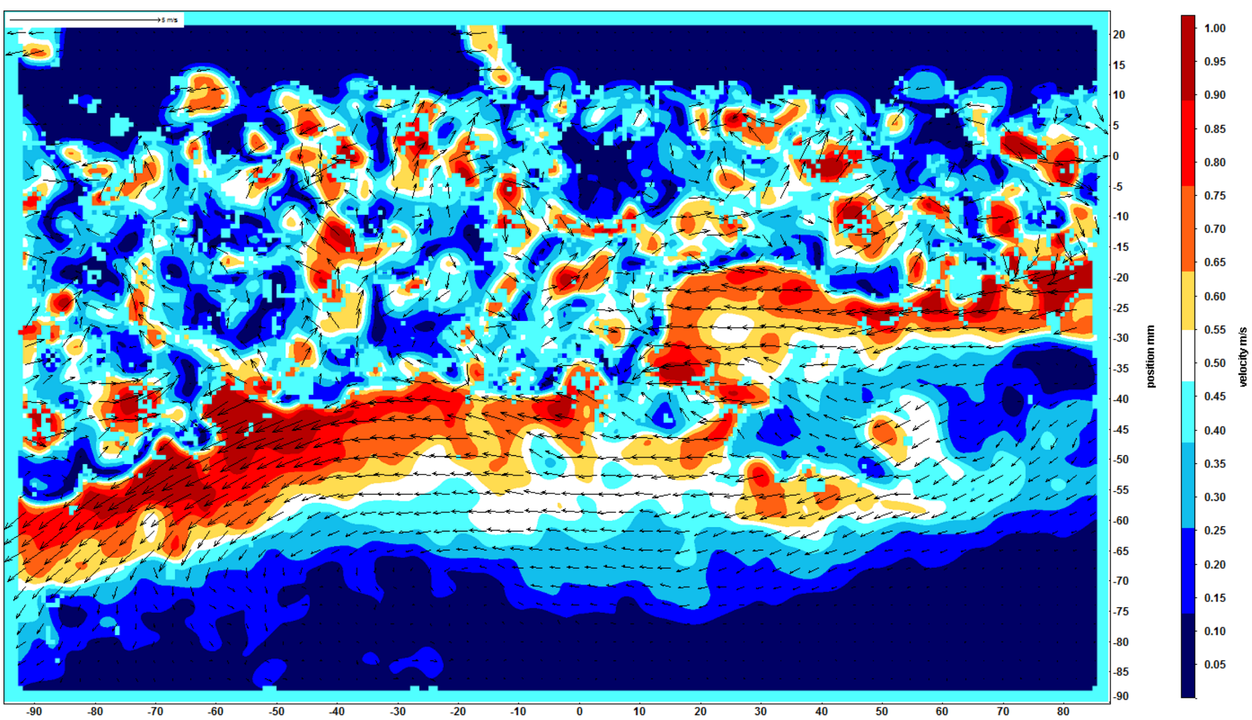

Figure 36 With solid and drill pipe rotation of 120 RPM

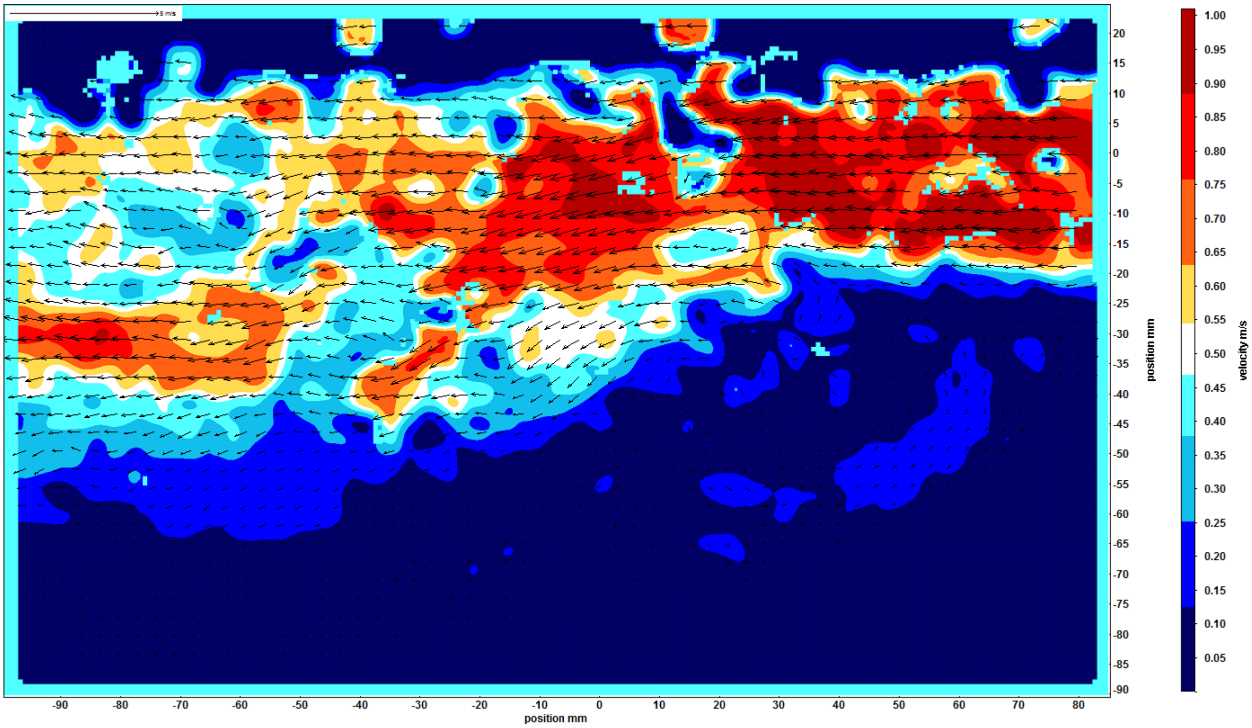

Figure 37 With solid, drill pipe rotation of 80 RPM and 0.5 eccentric condition of drill pipe

5.2.4 Mass flow rate 285 Kg/min @ Flowzan 0.05% w/w

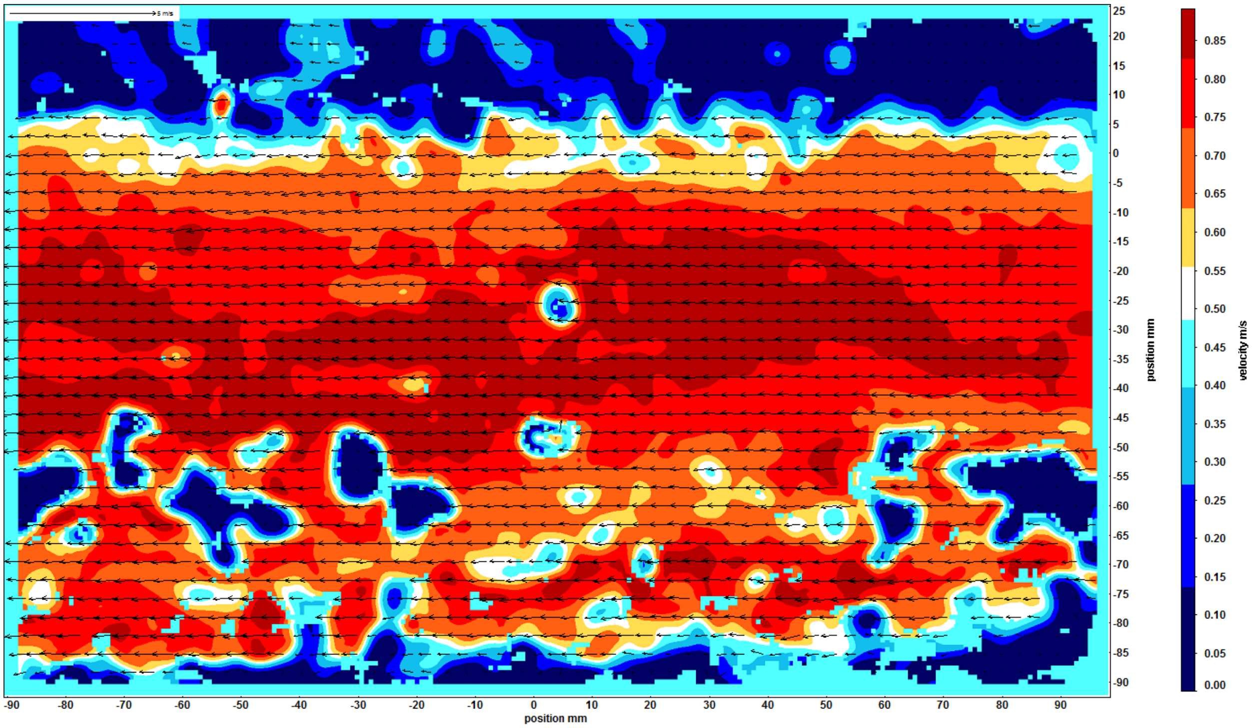

Figure 38 Without solid and drill pipe rotation

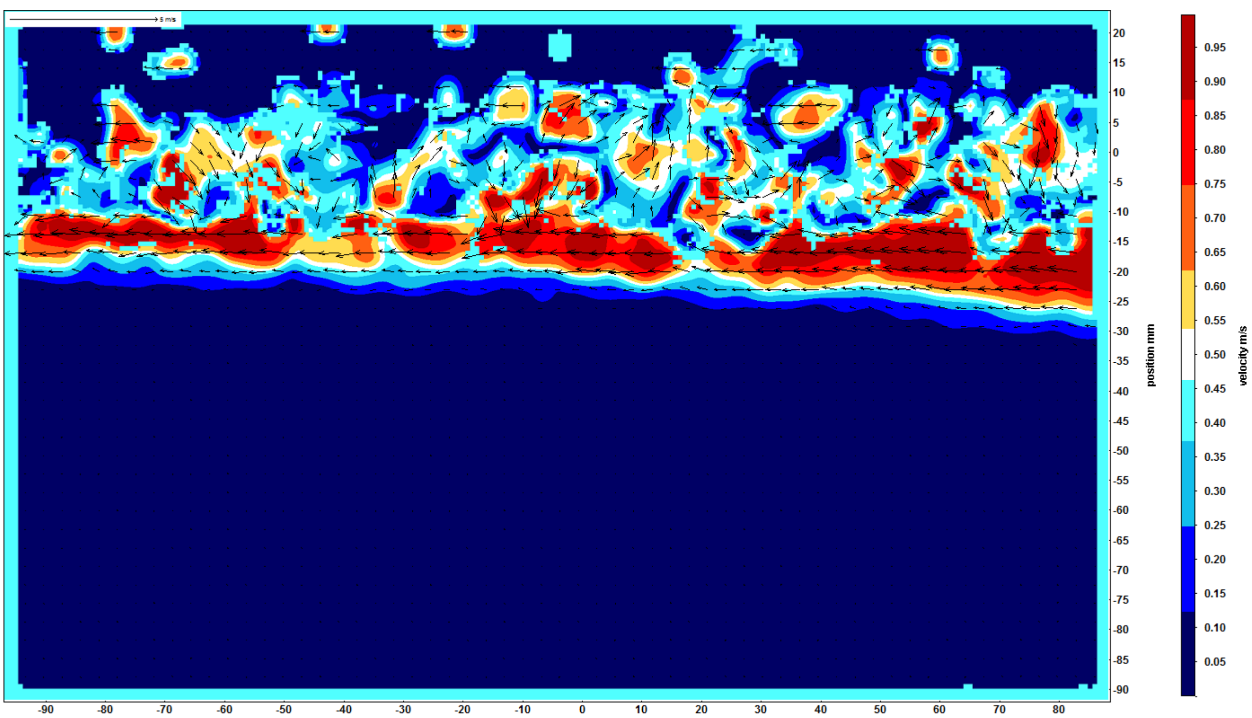

Figure 39 With solid and without drill pipe rotation

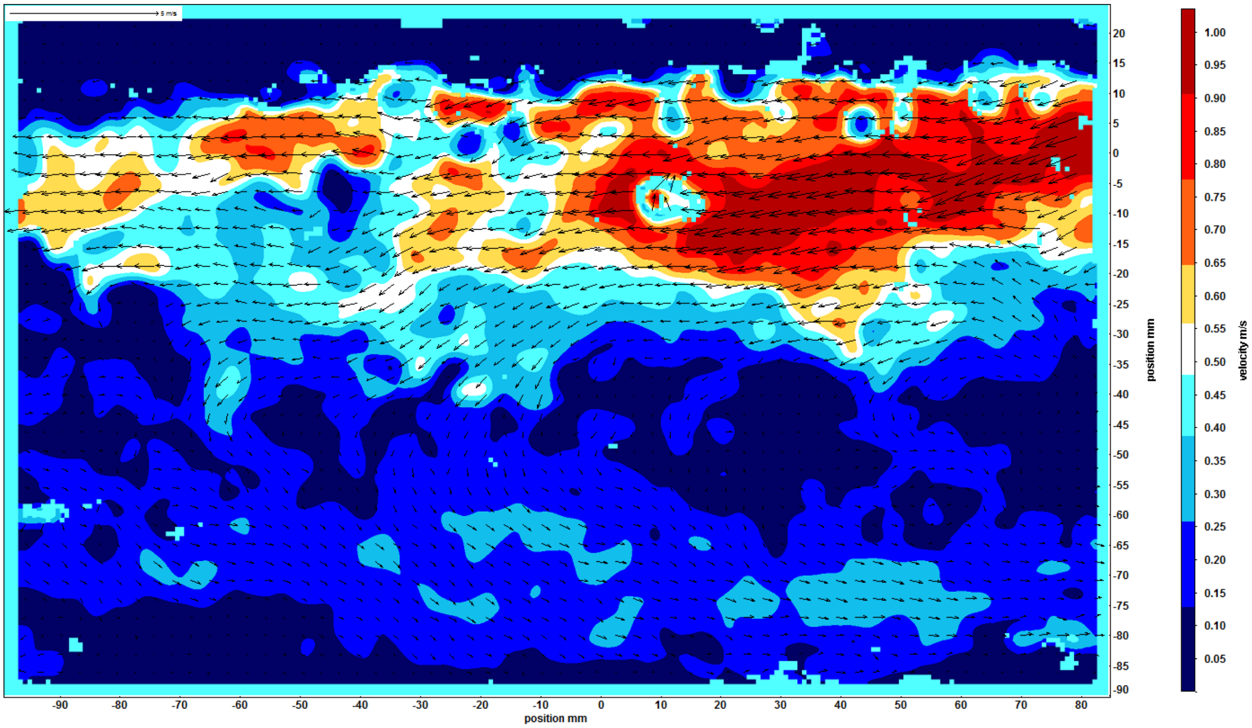

Figure 40 With solid, without drill pipe rotation and 0.5 eccentric condition of drill pipe

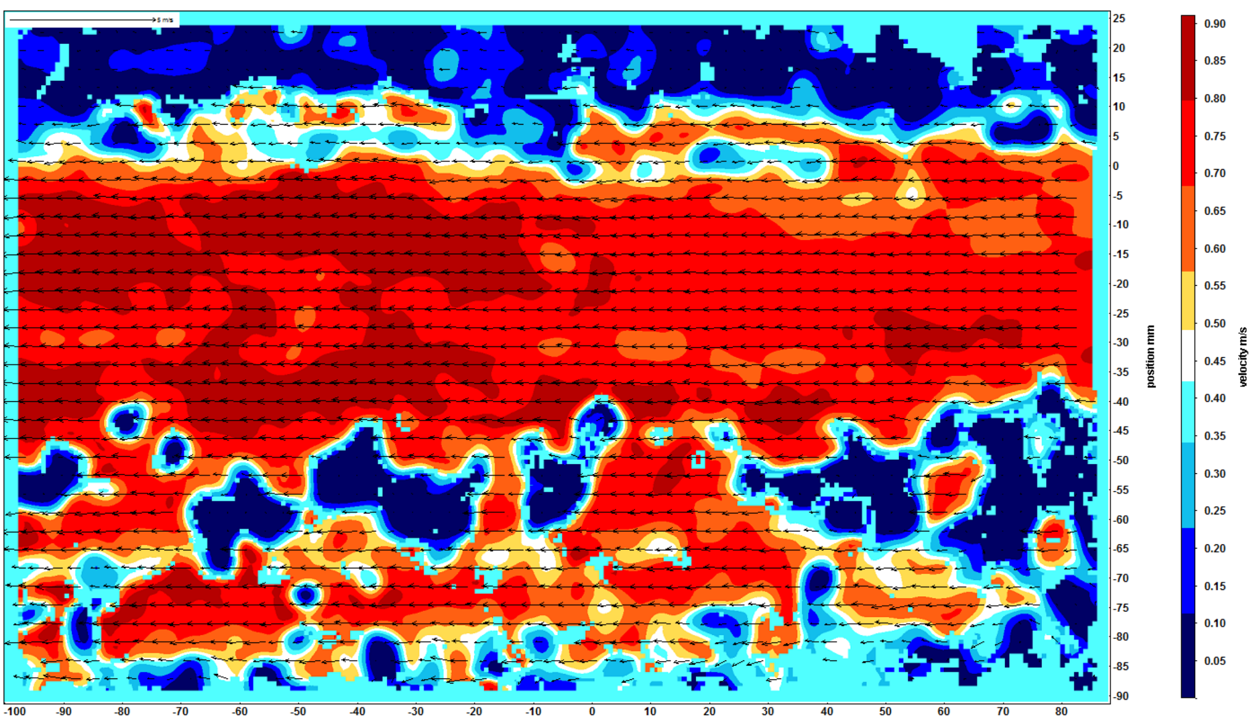

Figure 41 With solid and drill pipe rotation of 40 RPM

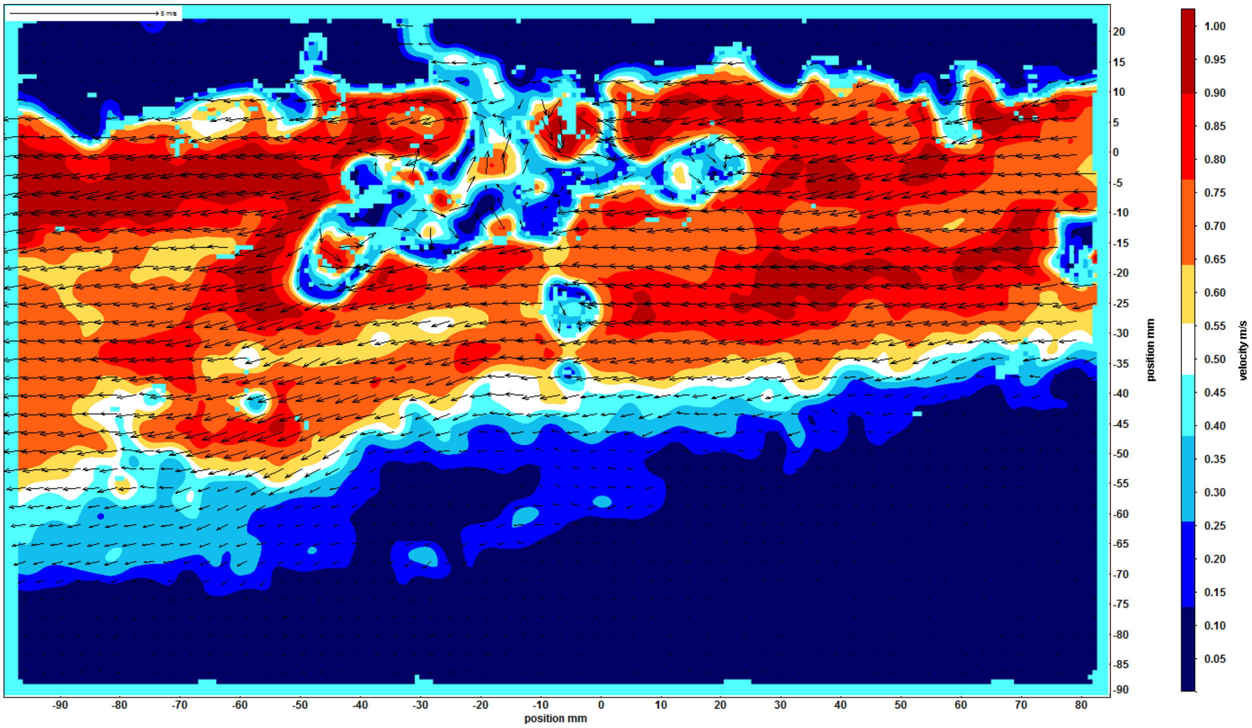

Figure 42 With solid, drill pipe rotation of 40 RPM and 0.5 eccentric condition of drill pipe

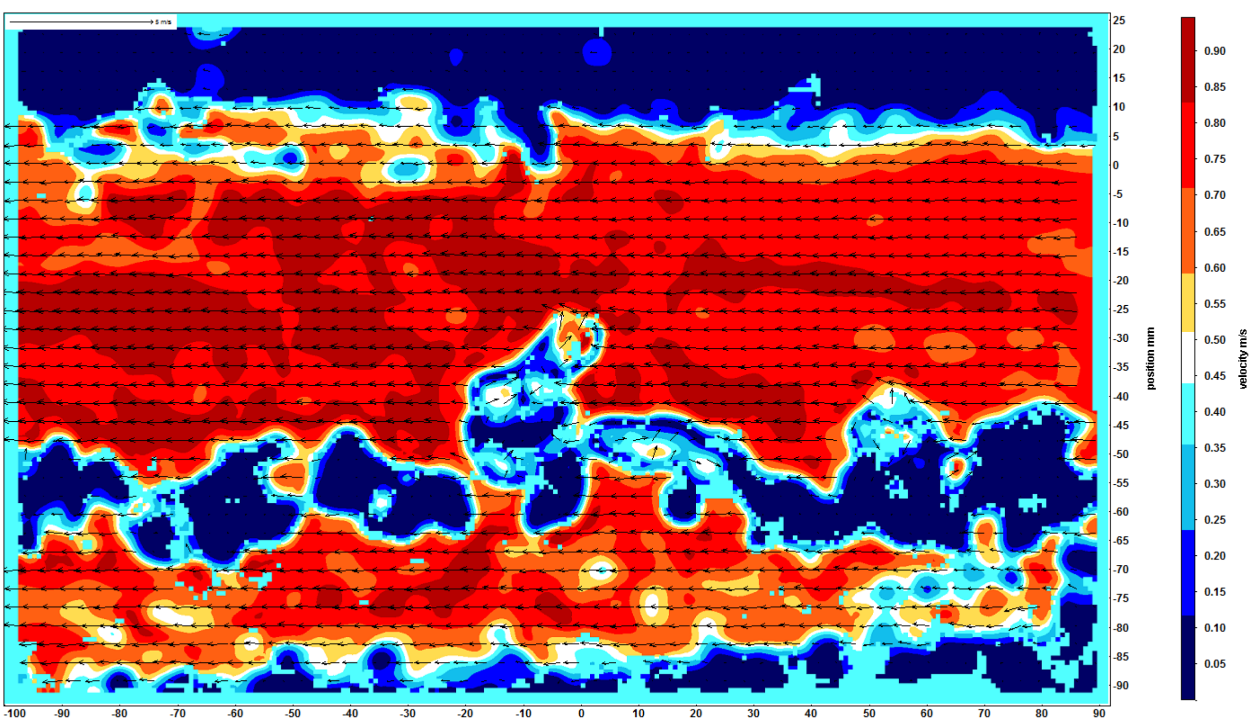

Figure 43 With solid and drill pipe rotation of 80 RPM

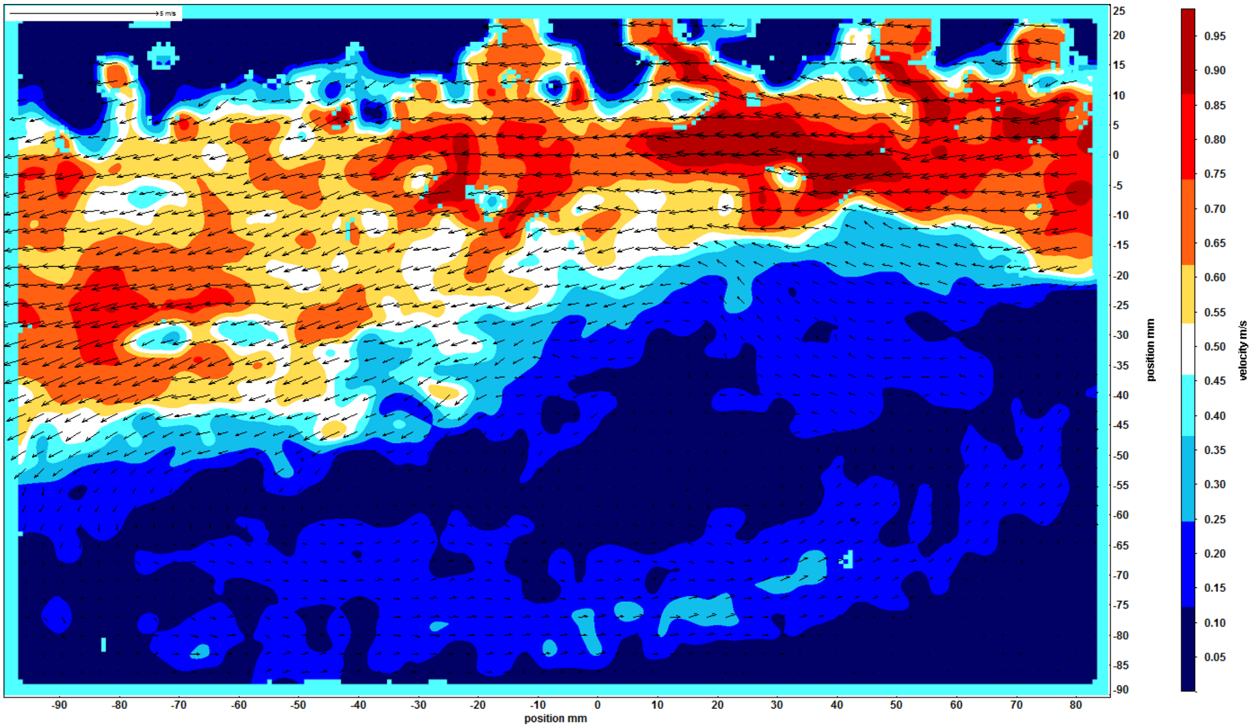

Figure 44 With solid, drill pipe rotation of 80 RPM and 0.5 eccentric condition of drill pipe

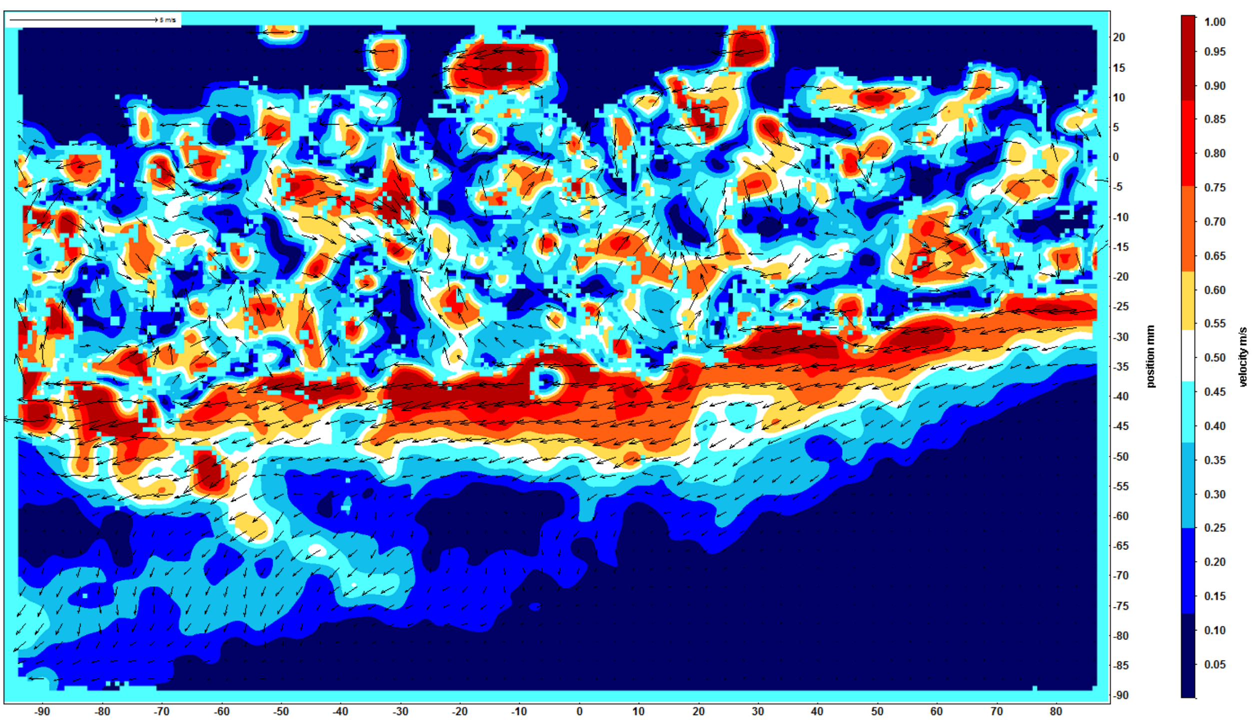

Figure 45 With solid and drill pipe rotation of 120 RPM

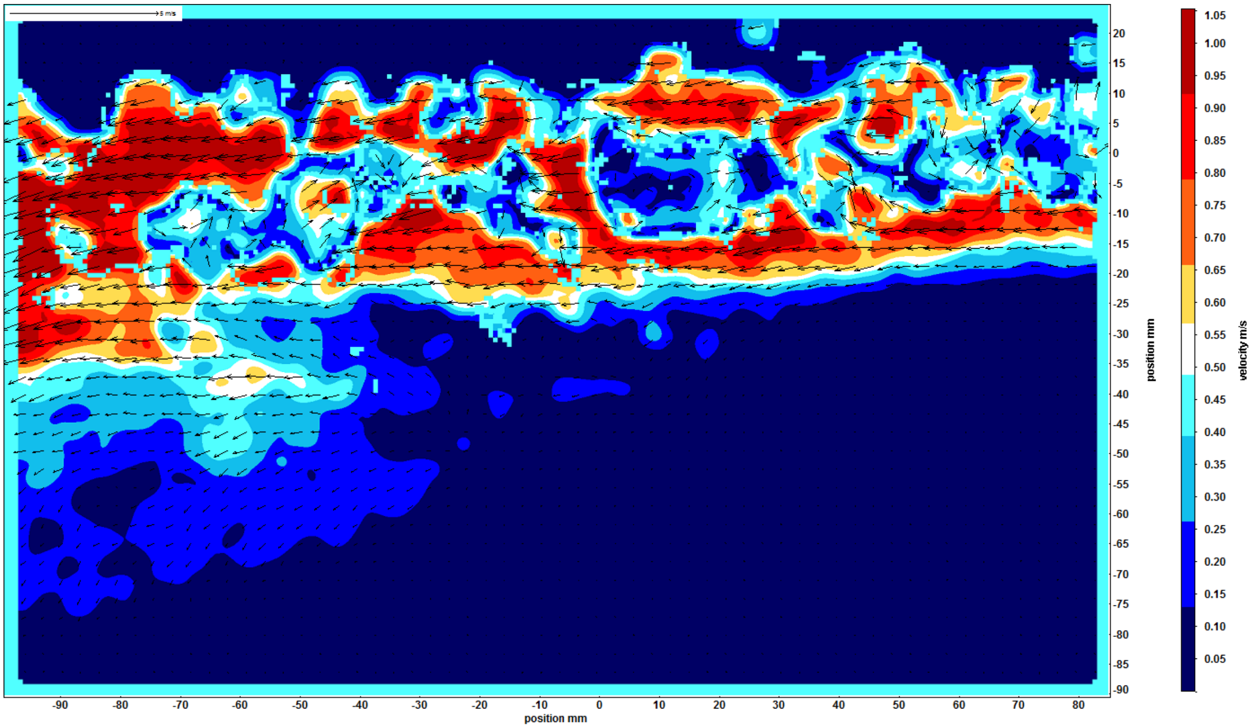

Figure 46 With solid, drill pipe rotation of 80 RPM and 0.5 eccentric condition of the drill pipe.

Velocity profiles

The PIV technique helped to obtain velocity profiles in both single and two-phase fluid flow. After the careful acquisition of PIV images and velocity vector field, the next finding is to analyze the velocity profiles to extract critical velocity for each dune movement at the given flow rate by using:

$$V\ \text{critical} = \frac{Re * \mu}{ID * \rho}$$

From the profiles, the fluctuations in the velocity profile at higher flow rates and in two-phase flow have shown turbulence characteristics in fluid dynamics. However, drill pipe rotations exhibited an effective hole cleaning operation. Drill pipe rotation distributed solid beads in the annular section due to centrifugal action where the pump flow rate provided momentum to distributed solid particles with increased velocity to transport through the annular section. In comparison, Eccentric condition (50%) of the drill pipe displayed less effective horizontal annular cleaning. The reason behind this is the reduction of the bottom annular area where solid dune accumulated. Due to the reduction in the area, solid deposited along the bedside of the pipe showing less effective solid dune movement and dune residence time was also increased. Even by providing drill pipe rotation, it did not shows effectiveness as compared to the concentric conditions. In eccentric conditions, at a low flow rate, i.e., at 700 RPM solid dune was unable to reach the investigation section and formed stationary solid beds in the pipe. The following are the velocity profiles obtained after processing PIV images at different flowrates, eccentricity, and the presence of solid glass beads.

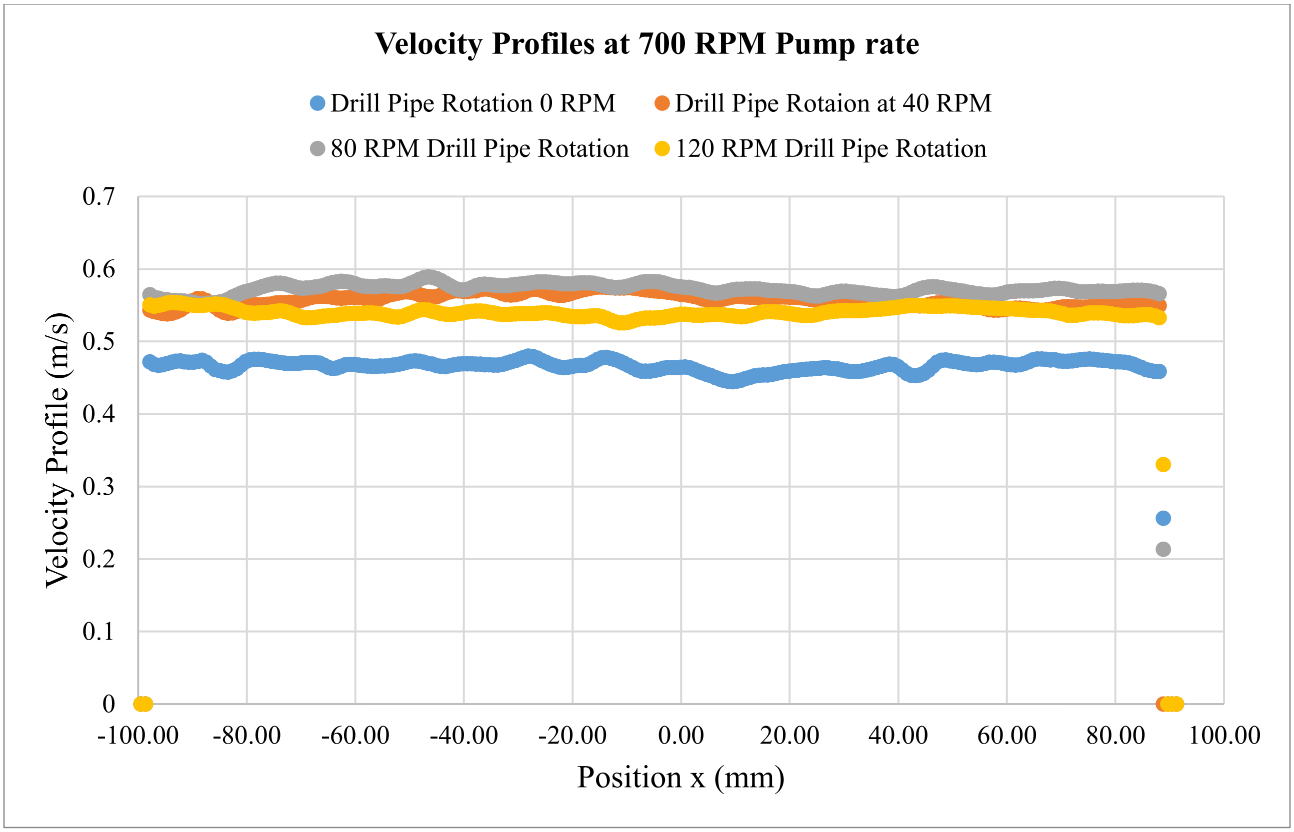
Velocity Profiles at 700 RPM Pump rate
Drill Pipe Rotation 0 RPM
Drill Pipe Rotaion at 40 RPM
80 RPM Drill Pipe Rotation
120 RPM Drill Pipe Rotation
0.7
0.6
0.5
0.4
0.3
0.2
0.1
0
Velocity Profile (m/s)
-100.00
-80.00
-60.00
-40.00
-20.00
0.00
20.00
40.00
60.00
80.00
100.00
Position x (mm)

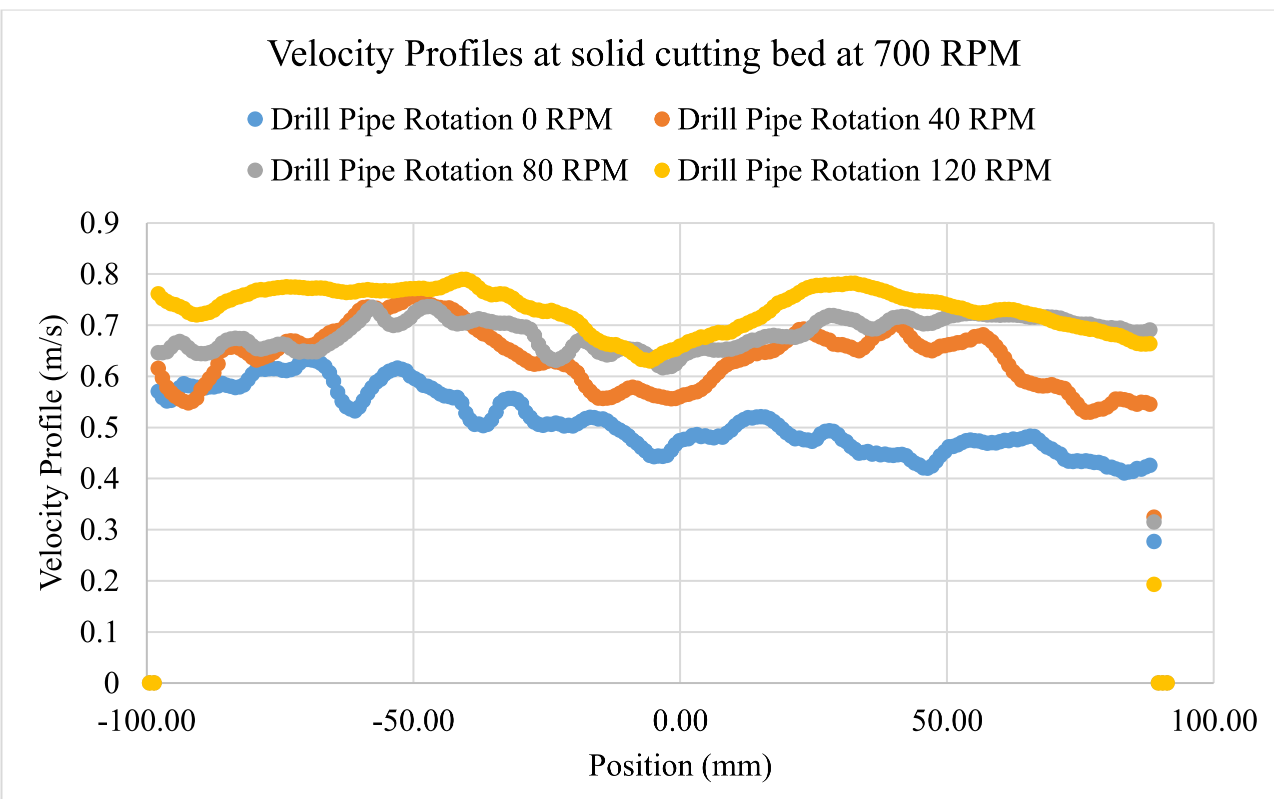
Velocity Profiles at solid cutting bed at 700 RPM
Drill Pipe Rotation 0 RPM
Drill Pipe Rotation 40 RPM
Drill Pipe Rotation 80 RPM
Drill Pipe Rotation 120 RPM
0.9
0.8
0.7
0.6
0.5
0.4
0.3
0.2
0.1
0
Velocity Profile (m/s)
-100.00
-50.00
0.00
50.00
100.00
Position (mm)

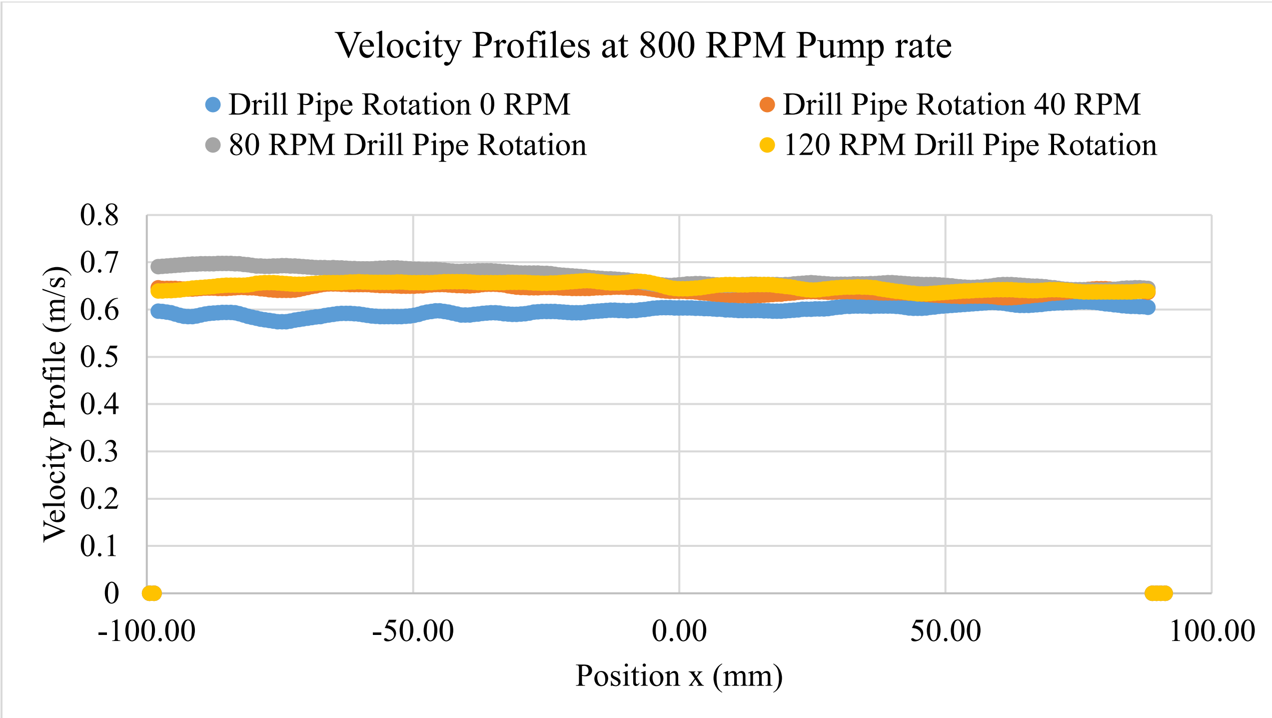
Velocity Profiles at 800 RPM Pump rate
Drill Pipe Rotation 0 RPM
Drill Pipe Rotation 40 RPM
80 RPM Drill Pipe Rotation
120 RPM Drill Pipe Rotation
Velocity Profile (m/s)
0.8
0.7
0.6
0.5
0.4
0.3
0.2
0.1
0
-100.00
-50.00
0.00
50.00
100.00
Position x (mm)

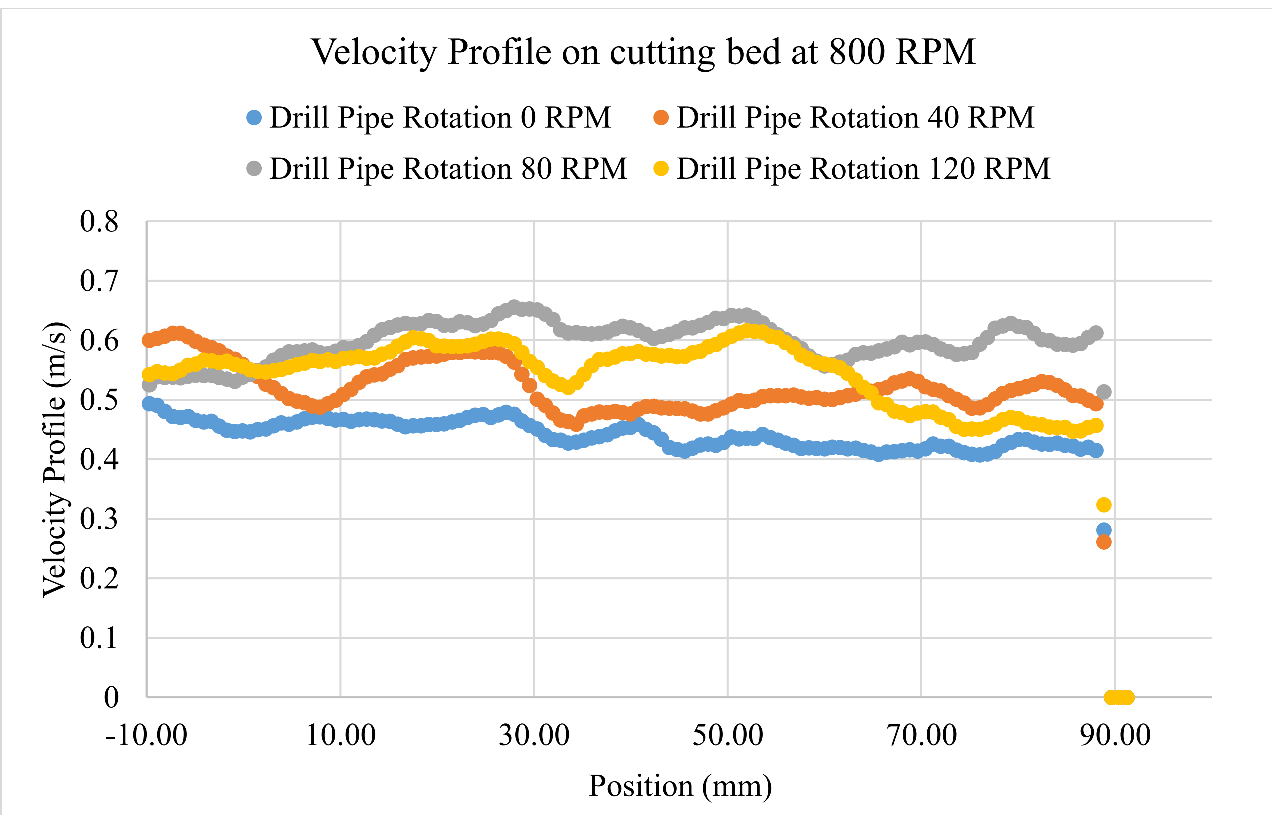
Velocity Profile on cutting bed at 800 RPM
Drill Pipe Rotation 0 RPM
Drill Pipe Rotation 40 RPM
Drill Pipe Rotation 80 RPM
Drill Pipe Rotation 120 RPM
Velocity Profile (m/s)
0.8
0.7
0.6
0.5
0.4
0.3
0.2
0.1
0
-10.00
10.00
30.00
50.00
70.00
90.00
Position (mm)

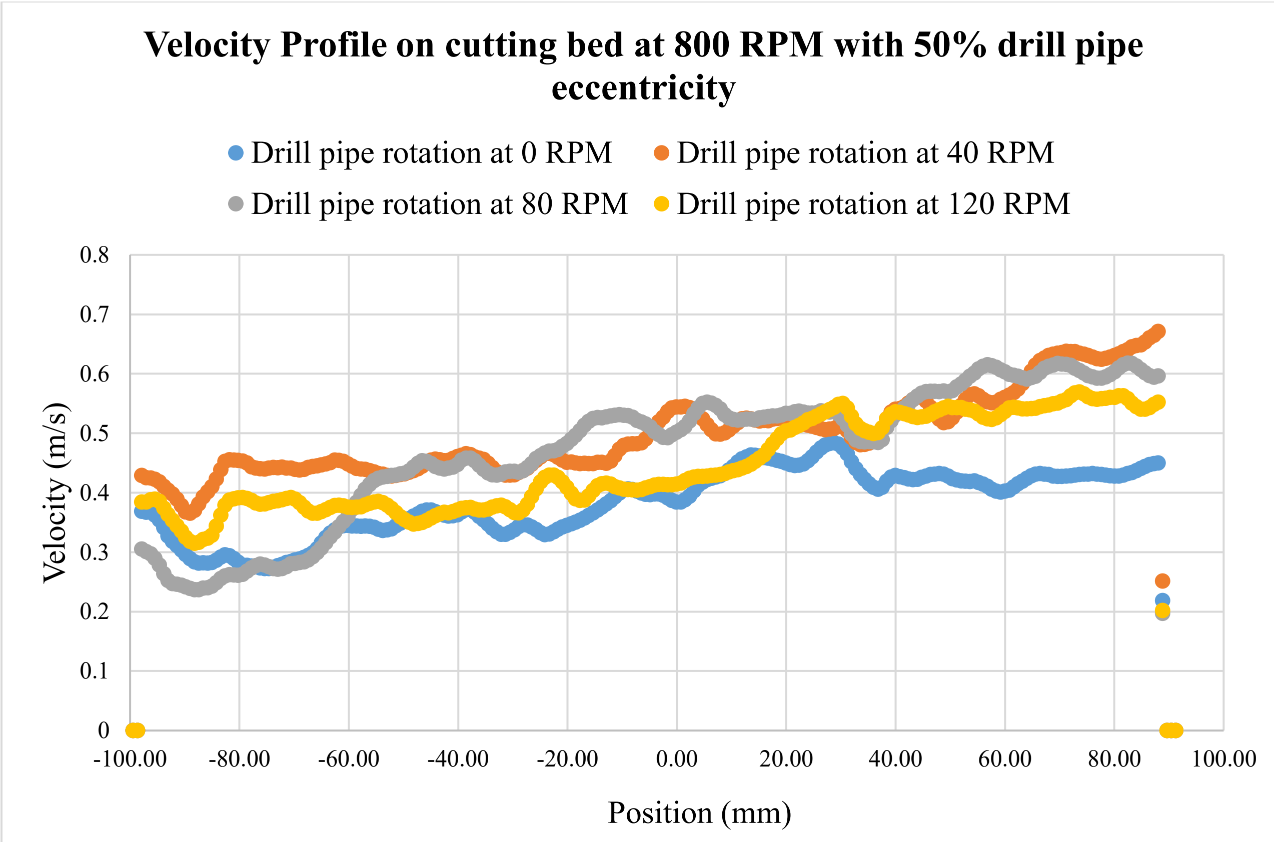

Velocity Profile on cutting bed at 800 RPM with 50% drill pipe eccentricity
Drill pipe rotation at 0 RPM
Drill pipe rotation at 40 RPM
Drill pipe rotation at 80 RPM
Drill pipe rotation at 120 RPM
Velocity (m/s)
0.8
0.7
0.6
0.5
0.4
0.3
0.2
0.1
0
-100.00
-80.00
-60.00
-40.00
-20.00
0.00
20.00
40.00
60.00
80.00
100.00
Position (mm)

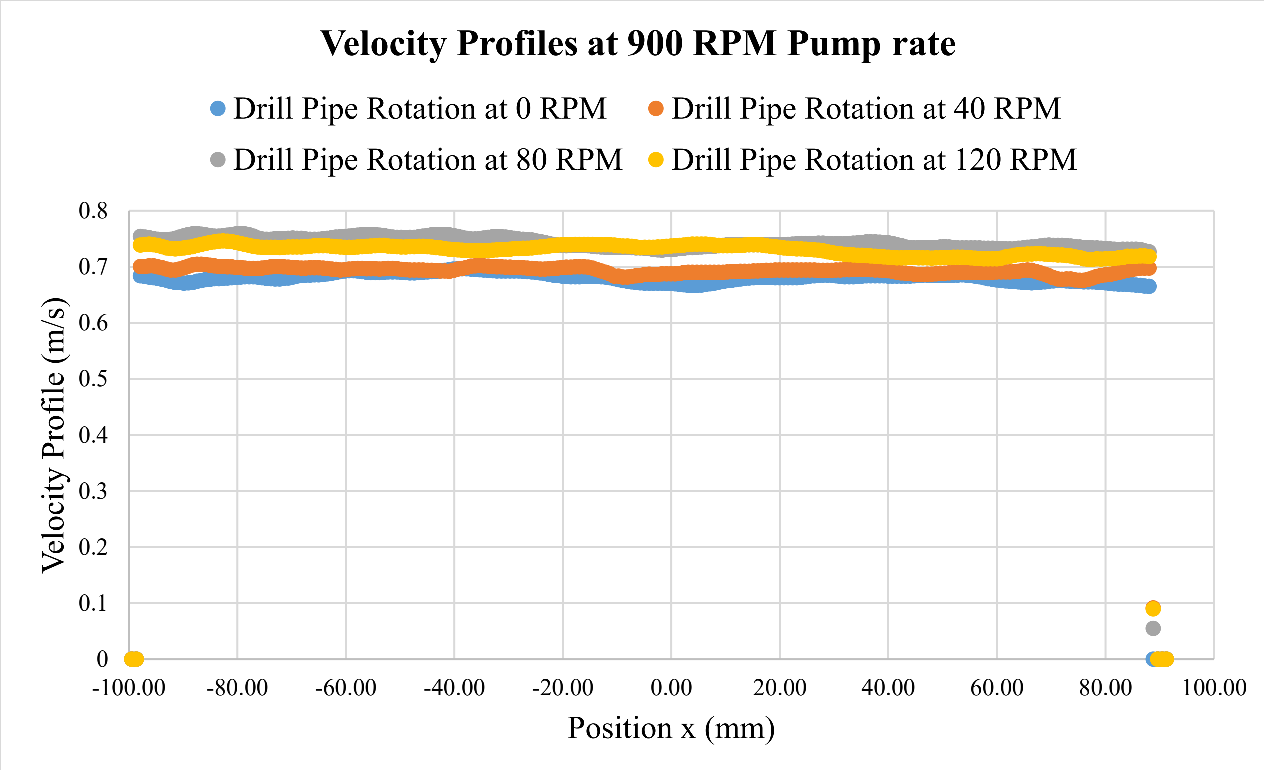
Velocity Profiles at 900 RPM Pump rate
Drill Pipe Rotation at 0 RPM
Drill Pipe Rotation at 40 RPM
Drill Pipe Rotation at 80 RPM
Drill Pipe Rotation at 120 RPM
Velocity Profile (m/s)
0.8
0.7
0.6
0.5
0.4
0.3
0.2
0.1
0
-100.00
-80.00
-60.00
-40.00
-20.00
0.00
20.00
40.00
60.00
80.00
100.00
Position x (mm)

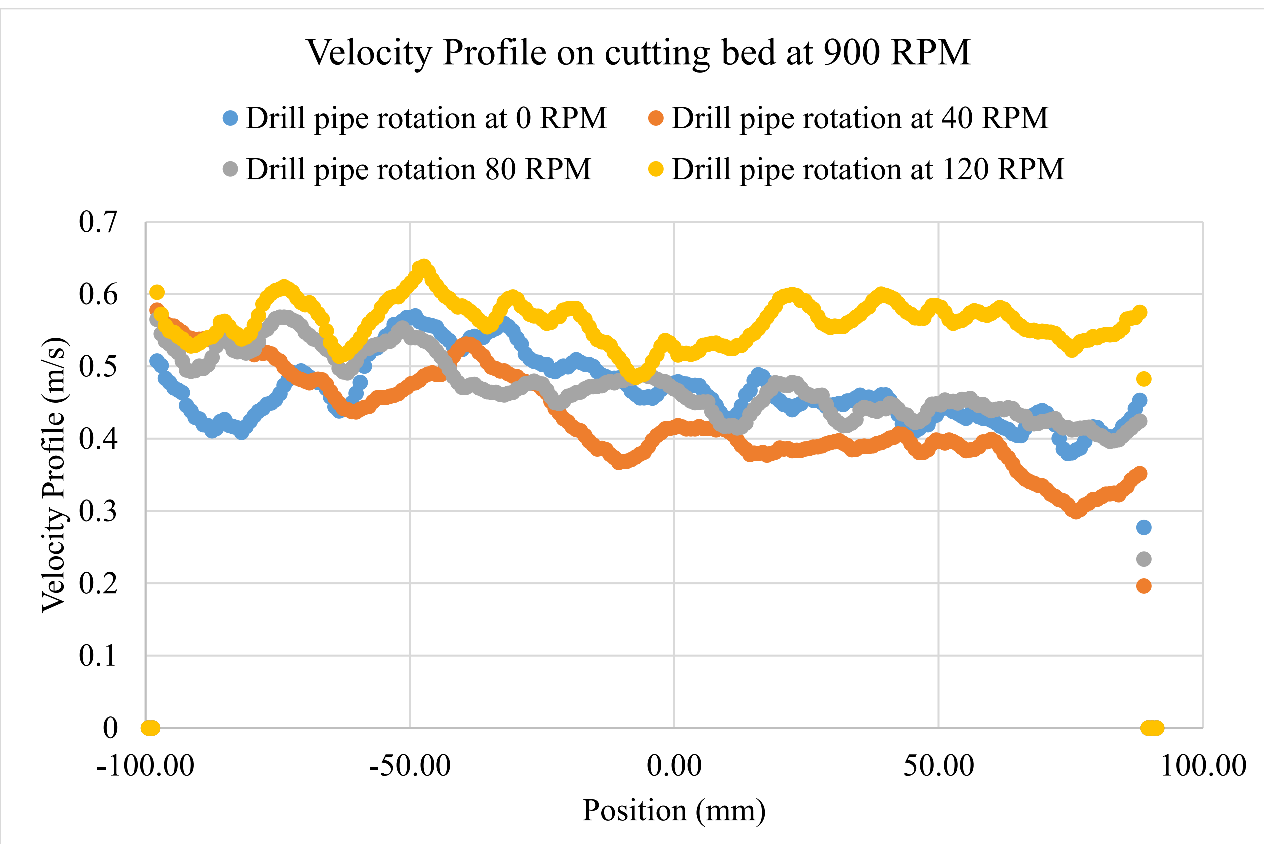
Velocity Profile on cutting bed at 900 RPM
Drill pipe rotation at 0 RPM
Drill pipe rotation at 40 RPM
Drill pipe rotation 80 RPM
Drill pipe rotation at 120 RPM
Velocity Profile (m/s)
0.7
0.6
0.5
0.4
0.3
0.2
0.1
0
-100.00
-50.00
0.00
50.00
100.00
Position (mm)

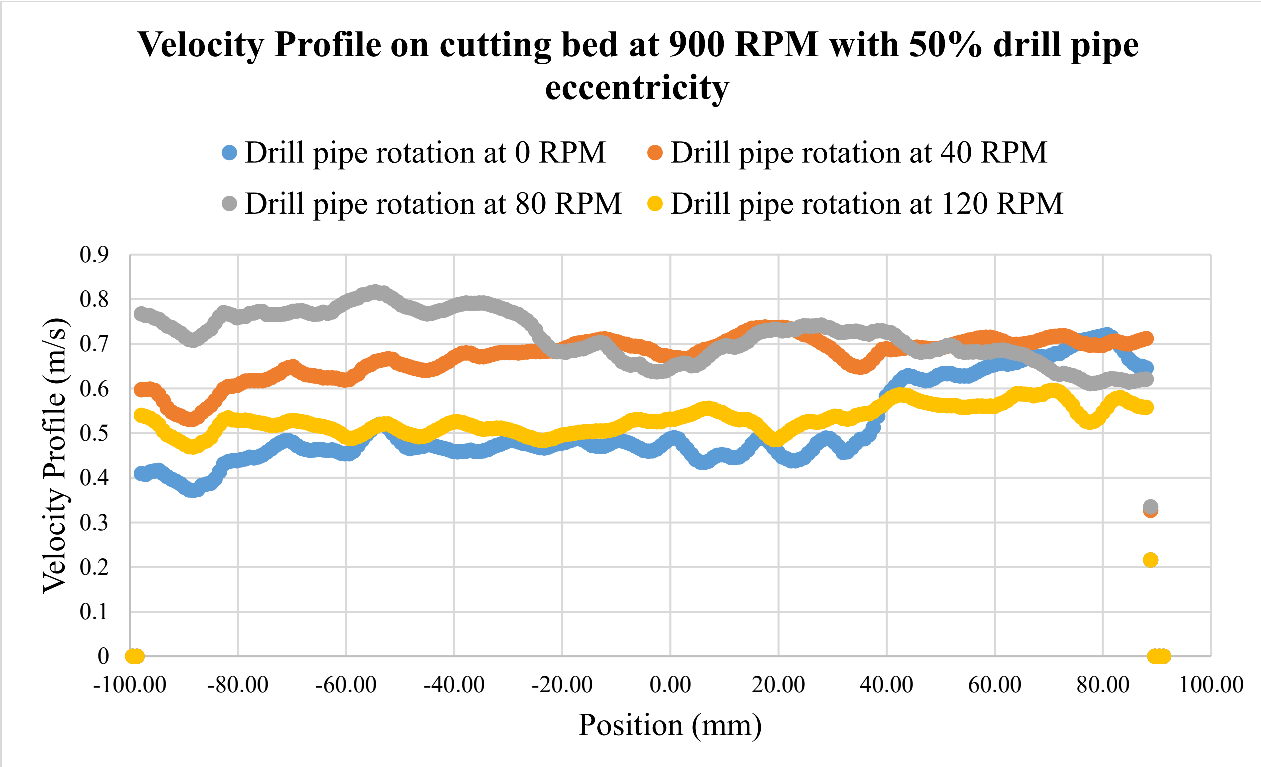
Velocity Profile on cutting bed at 900 RPM with 50% drill pipe eccentricity
Drill pipe rotation at 0 RPM
Drill pipe rotation at 40 RPM
Drill pipe rotation at 80 RPM
Drill pipe rotation at 120 RPM
Velocity Profile (m/s)
0.9
0.8
0.7
0.6
0.5
0.4
0.3
0.2
0.1
0
-100.00
-80.00
-60.00
-40.00
-20.00
0.00
20.00
40.00
60.00
80.00
100.00
Position (mm)

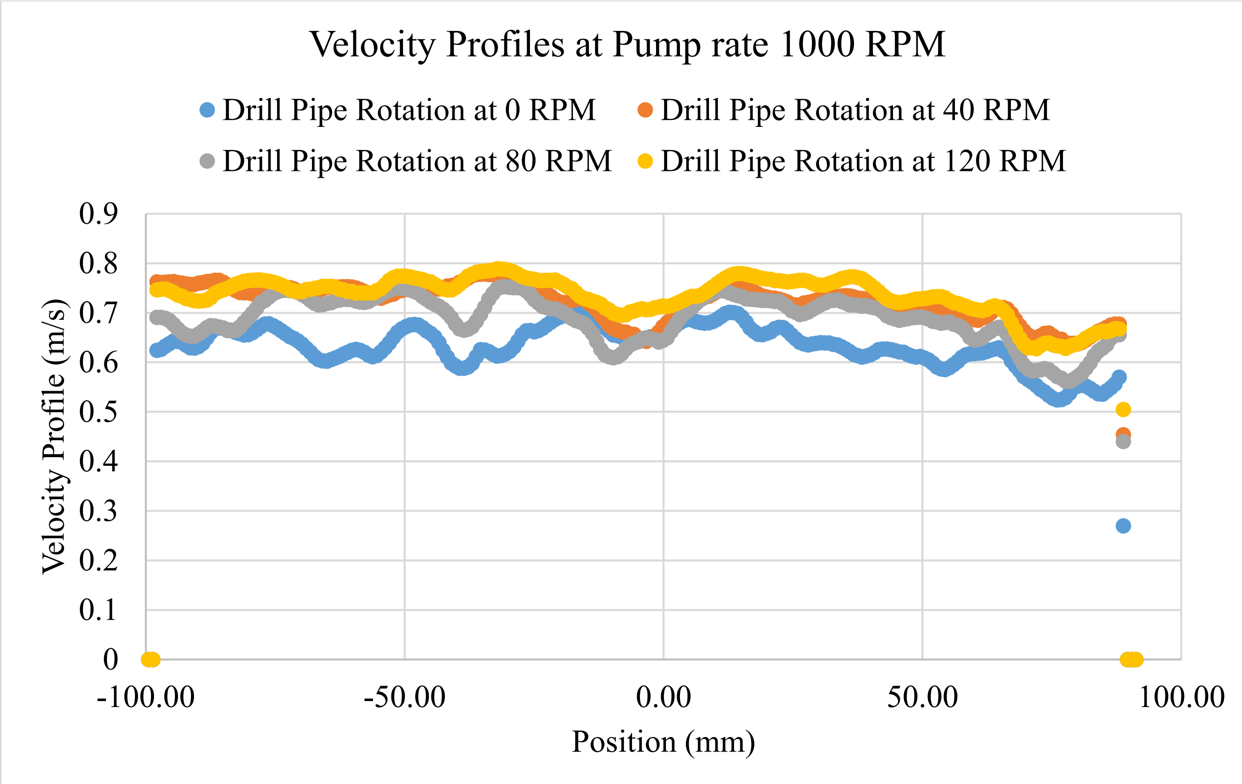

Velocity Profiles at Pump rate 1000 RPM
Drill Pipe Rotation at 0 RPM
Drill Pipe Rotation at 40 RPM
Drill Pipe Rotation at 80 RPM
Drill Pipe Rotation at 120 RPM
Velocity Profile (m/s)
0.9
0.8
0.7
0.6
0.5
0.4
0.3
0.2
0.1
0
-100.00
-50.00
0.00
50.00
100.00
Position (mm)

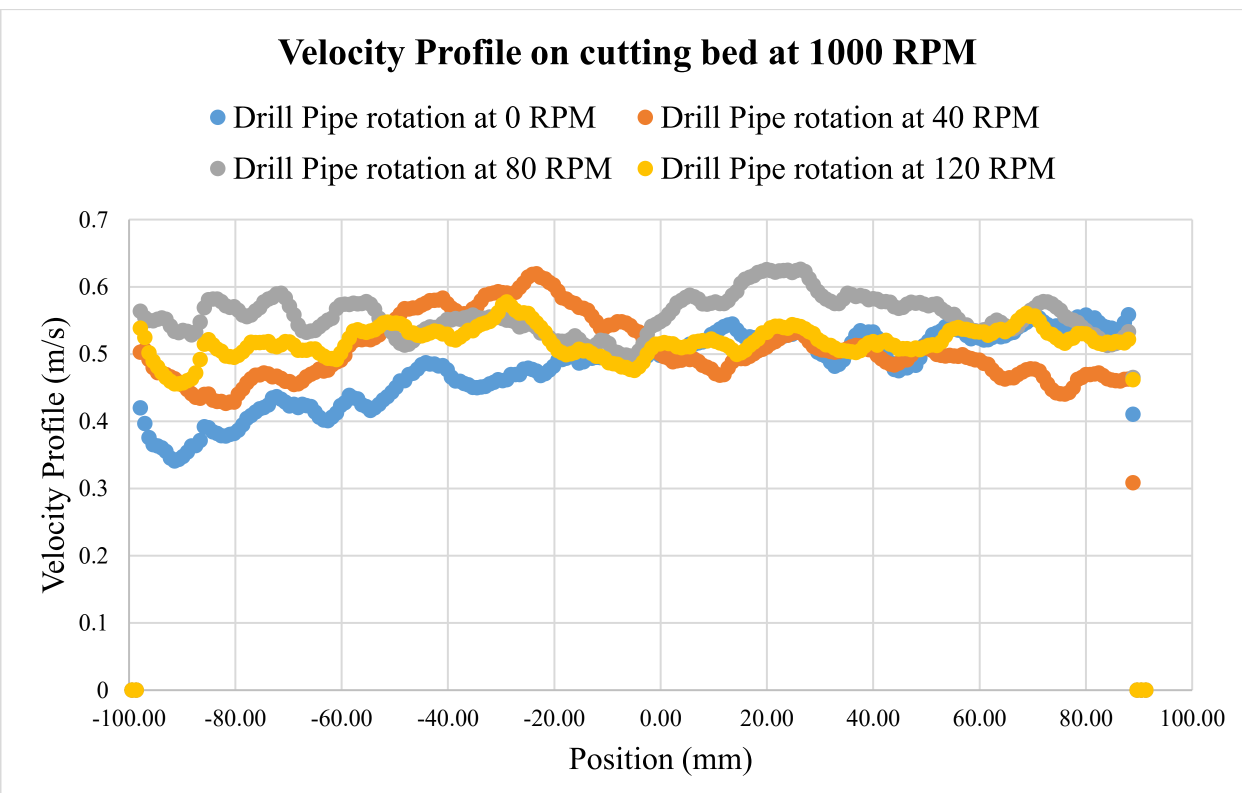

Velocity Profile on cutting bed at 1000 RPM
Drill Pipe rotation at 0 RPM
Drill Pipe rotation at 40 RPM
Drill Pipe rotation at 80 RPM
Drill Pipe rotation at 120 RPM
Velocity Profile (m/s)
0.7
0.6
0.5
0.4
0.3
0.2
0.1
0
-100.00
-80.00
-60.00
-40.00
-20.00
0.00
20.00
40.00
60.00
80.00
100.00
Position (mm)

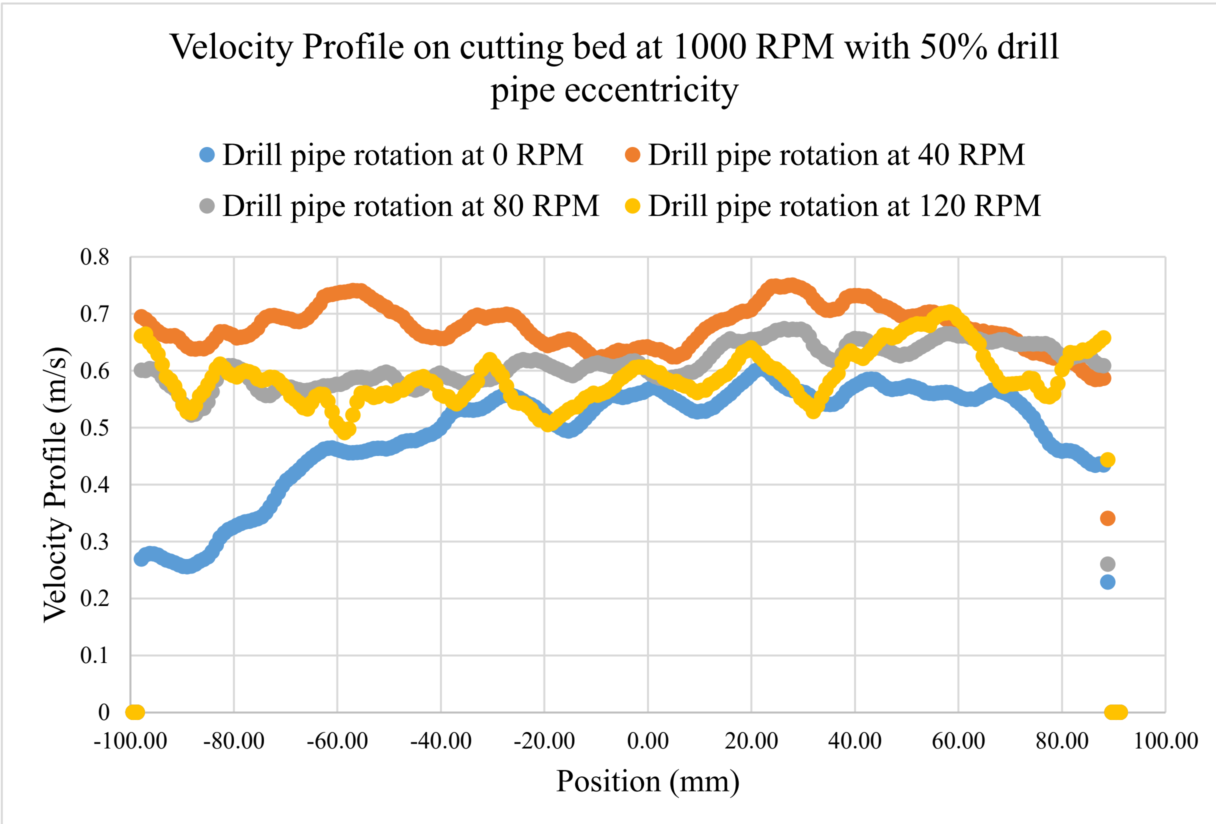
Velocity Profile on cutting bed at 1000 RPM with 50% drill pipe eccentricity
Drill pipe rotation at 0 RPM
Drill pipe rotation at 40 RPM
Drill pipe rotation at 80 RPM
Drill pipe rotation at 120 RPM
Velocity Profile (m/s)
0
0.1
0.2
0.3
0.4
0.5
0.6
0.7
0.8
-100.00
-80.00
-60.00
-40.00
-20.00
0.00
20.00
40.00
60.00
80.00
100.00
Position (mm)

Swirling strength

In pipe flow, turbulent fluid produces swirling effects with the interaction of pipe walls. This effect increases if two or more fluid phases are present. It is the measure of local fluid rotation and is denoted by $1/s^2$. In our experiments, the swirling strength is worth noted as the solid dune was advancing through the helical motion of individually solid particles. Vortices can be visualized by the velocity vector field, whereas swirling strength was quantified by using a built-in swirling strength calculation option from DaVis 8.4 software. The trends have generated to quantify the effects of drill pipe rotation on swirling strength in the presence of moving solid beds at different flow rates.

From the trends, it is evident that at all flow rates in the absence of solid, drill pipe rotation has not shown any significant impact on swirling strength. The reason behind is the centrifugal forces generated by the drill pipe to the fluid has canceled the formation of vortices in the absence of solid dune.

Swirling strength is significantly present during solid dune movement at all flow rates. The drill pipe rotation has an adverse impact on swirling strength. Without drill pipe rotation, swirling strength has been maximum at all respective flow rates and gradually decreases with an increase in drill pipe rotation. At no pipe rotation, solid transport is mainly due to the fluid shear, and solid particles moved in helical motion due to the fluid property of being pseudo-plastic.

At eccentric inner pipe (50%) condition, swirling strength was lesser in the presence of solids compared to concentric conditions. This is because of the reduced annular area at the bottom side of the pipe that does not provide enough strength to create potential vortices to move solid particles faster liken in non-eccentric case. Even in the rotating drill pipe scenario, swirling strength decreases due to the above mentioned reason but was greater at no rotation case.

However, from the visual analysis of cutting transport, low drill pipe rotation put a positive impact on cutting transport mechanisms. Graphically, the effect of swirling strength under observed parameters have reported below.

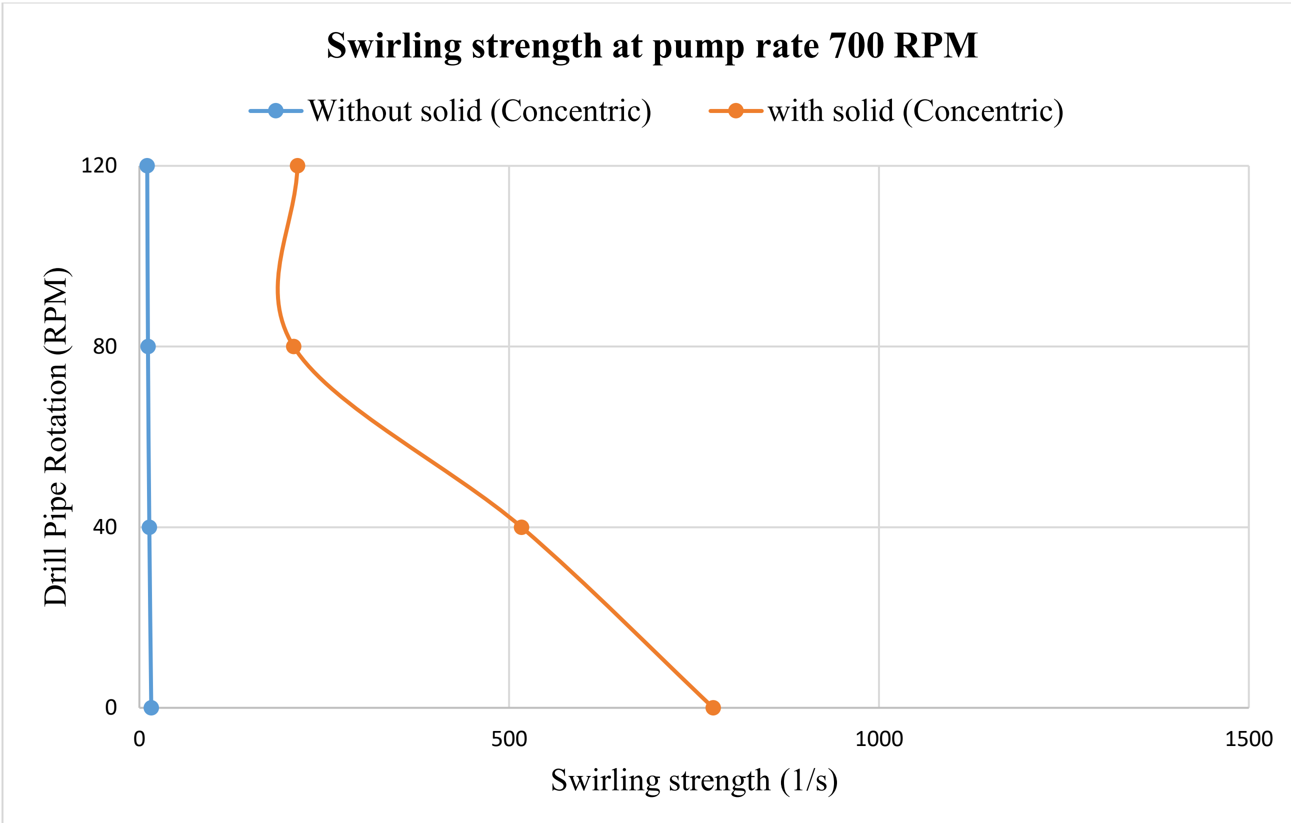
Swirling strength at pump rate 700 RPM
Without solid (Concentric)
with solid (Concentric)
Drill Pipe Rotation (RPM)
120
80
40
0
0
500
1000
1500
Swirling strength (1/s)

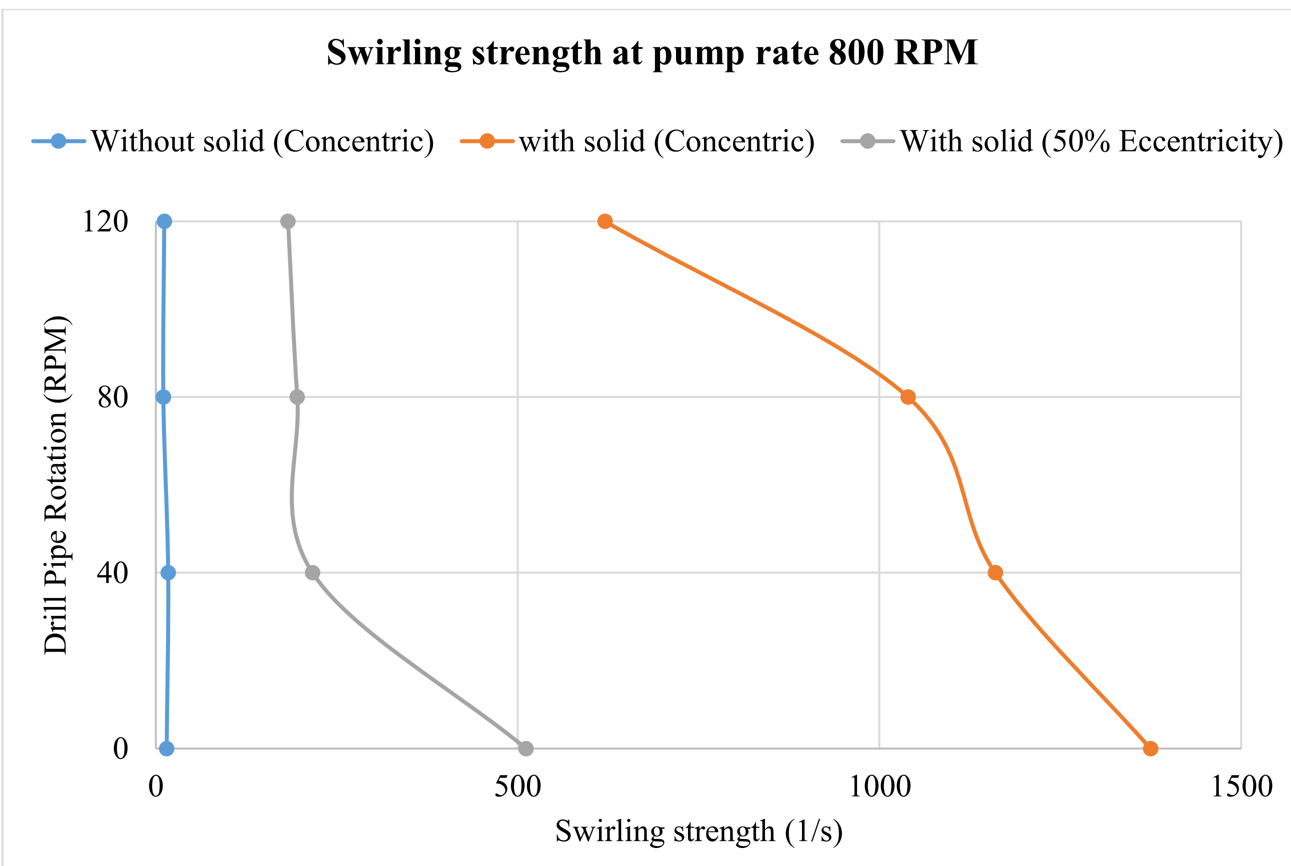
Swirling strength at pump rate 800 RPM
Without solid (Concentric)
with solid (Concentric)
With solid (50% Eccentricity)
Drill Pipe Rotation (RPM)
120
80
40
0
0
500
1000
1500
Swirling strength (1/s)

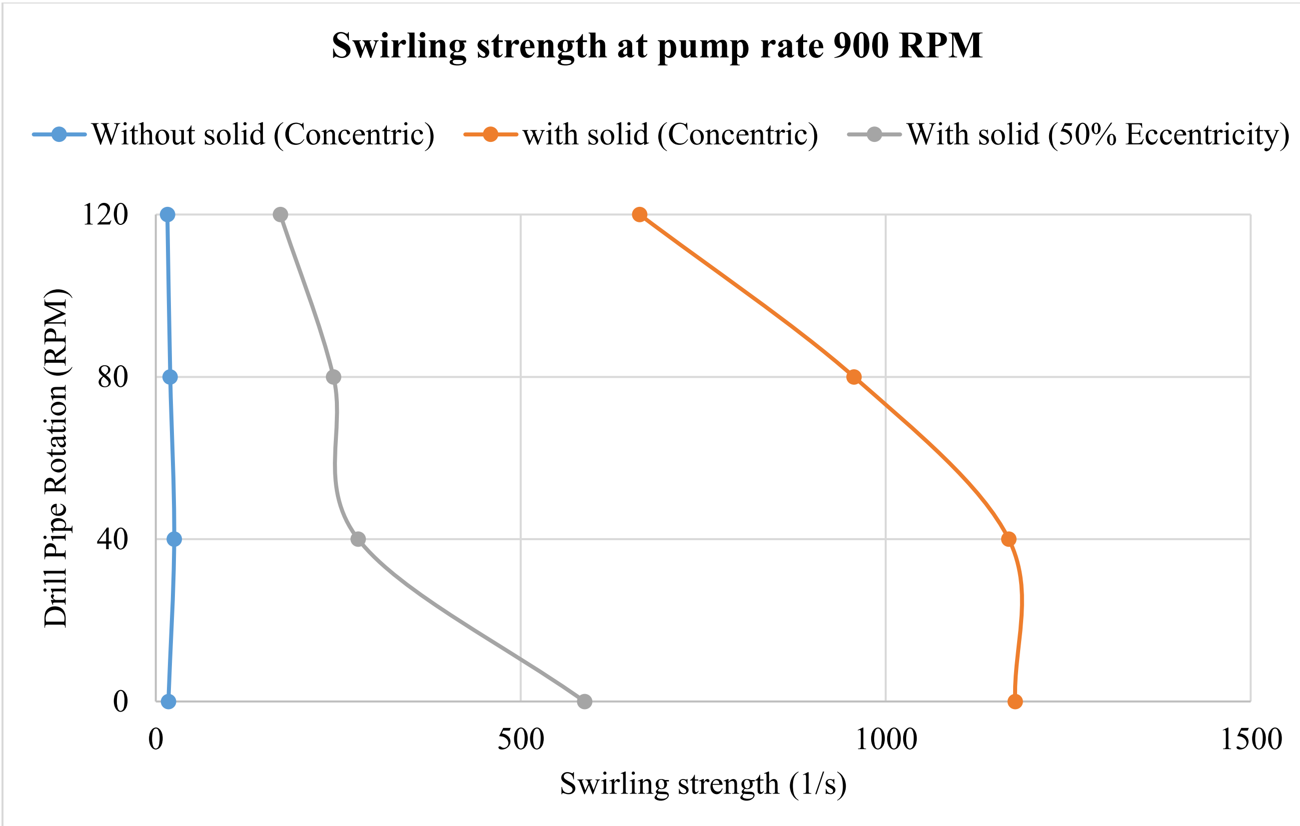
Swirling strength at pump rate 900 RPM
Without solid (Concentric)
with solid (Concentric)
With solid (50% Eccentricity)
Drill Pipe Rotation (RPM)
120
80
40
0
0
500
1000
1500
Swirling strength (1/s)

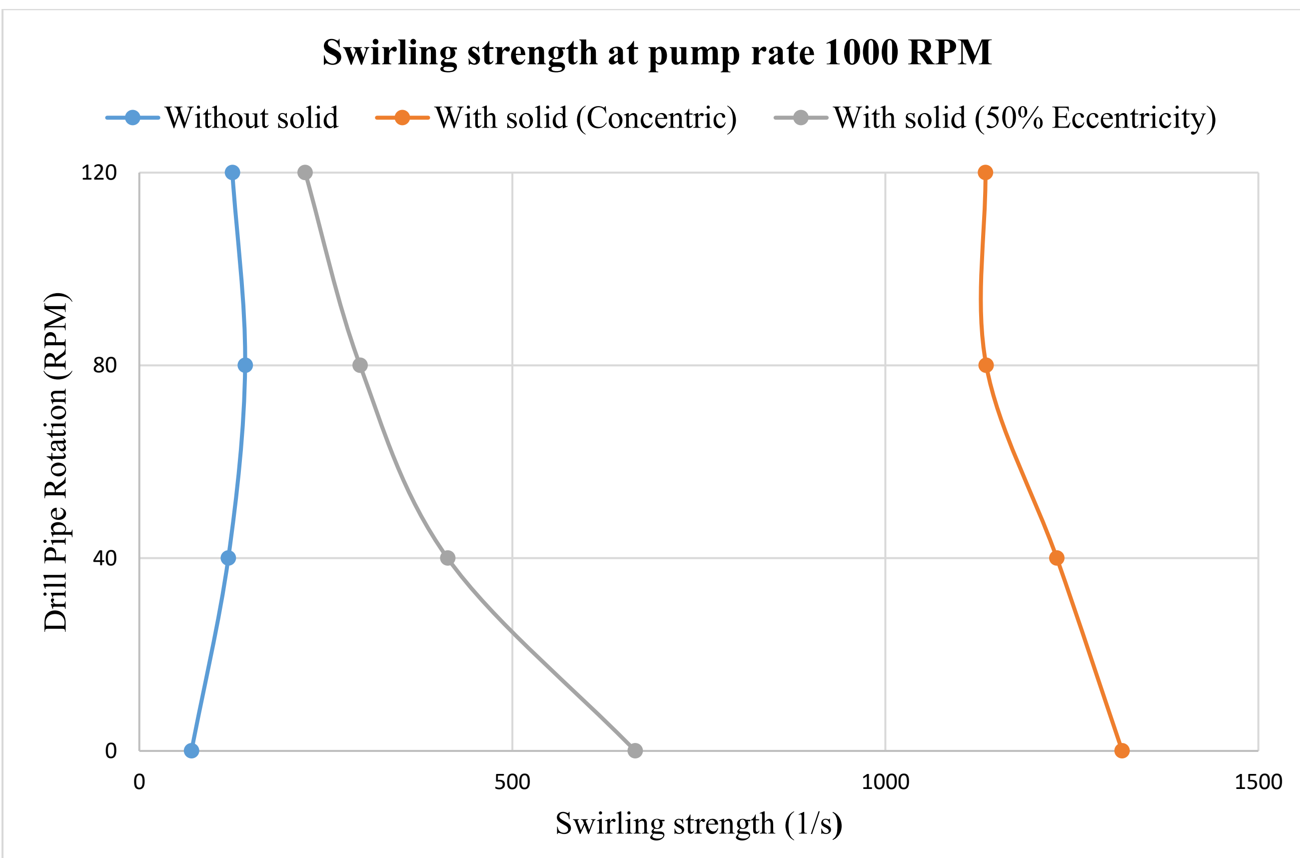
Swirling strength at pump rate 1000 RPM
Without solid
With solid (Concentric)
With solid (50% Eccentricity)
Drill Pipe Rotation (RPM)
120
80
40
0
0
500
1000
1500
Swirling strength (1/s)

Shear strength

Shear force is responsible for transporting solid in both annular and pipe flow (Chang and Lee 2010). Therefore, it is necessary to figure out the shear strength of fluid flow for an effective annular cleaning operation. Shear strength is obtained by the relative motion of adjacent flowing fluid layers. The velocity in pipe flow is maximum in the center and minimum at the walls. Therefore, shear is also maximum at the center of the pipe. In the annular flow, shear and shear strength is worth noting, especially in two-phase or multiphase flow. In Newtonian fluids, shear is a linear function of strain, while in Non-Newtonian fluids, its representation is complex.

In the experiments, shear strength was measured in the unit (sec^{-1}), and the magnitude of shear strength is determined from the velocity field by DaVis 8.4 in the desired conditions.

In single-phase flow, the magnitude of shear was low compared to two-phase flow; even the rotating drill pipe did not show a significant impact on shear strength. Although, shear strength was resulted higher in magnitude in the case of two-phase flow due to increased velocity over the solid bed. The increased velocity, along with the shear-thinning behavior of the fluid, helped in solid transport. The results obtained under the rotating drill pipe condition confirm the shear thinning behavior as the shear strength reduced with an increase in drill pipe rotation.

The shear strength was also reported less in two-phase flow at the eccentric condition as compare to concentric annular flow. The shearing phenomenon was reduced by the accumulation of solids due to the reduced cross-sectional area. The overall velocity in the investigation area was reduced, and hence the shear strength was also lowered. Graphically, the effect of shear strength under observed parameters have reported below.

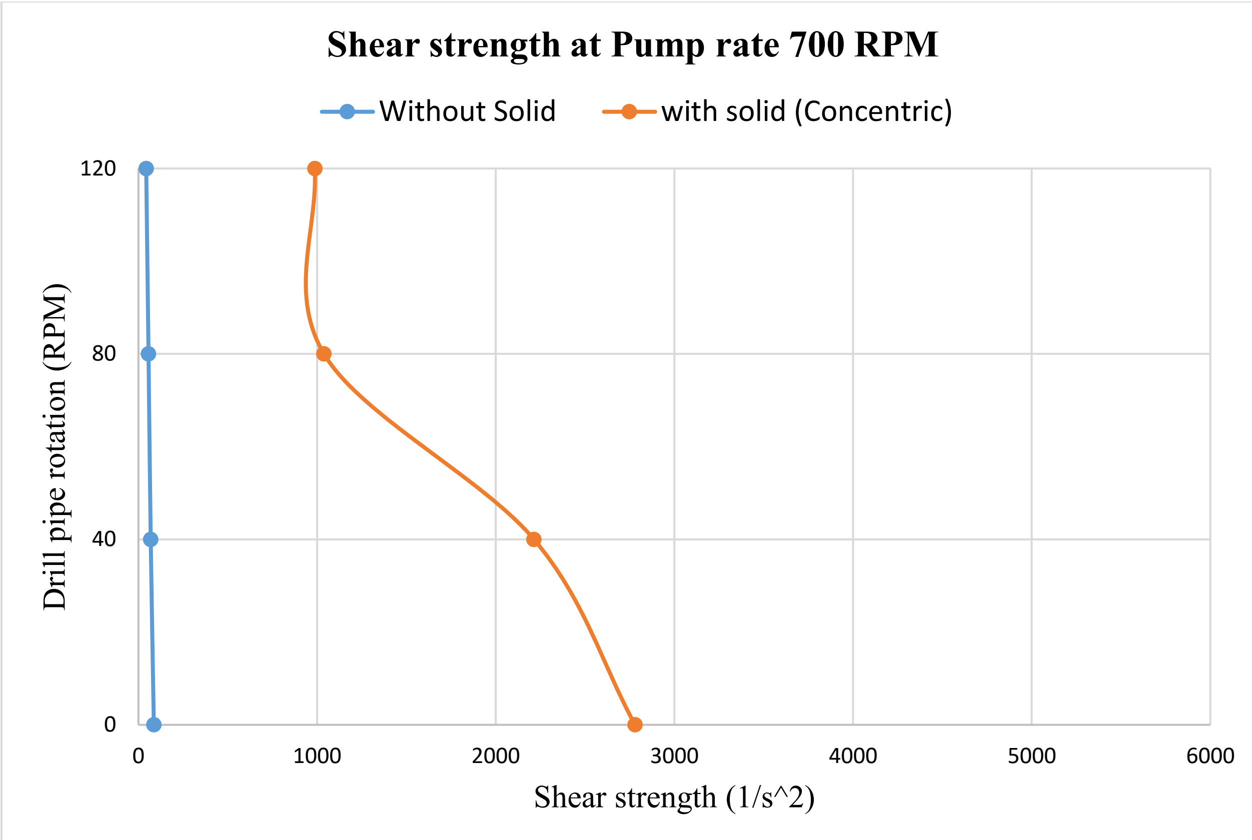
Shear strength at Pump rate 700 RPM
Without Solid
with solid (Concentric)
Drill pipe rotation (RPM)
120
80
40
0
0
1000
2000
3000
4000
5000
6000
Shear strength (1/s^2)

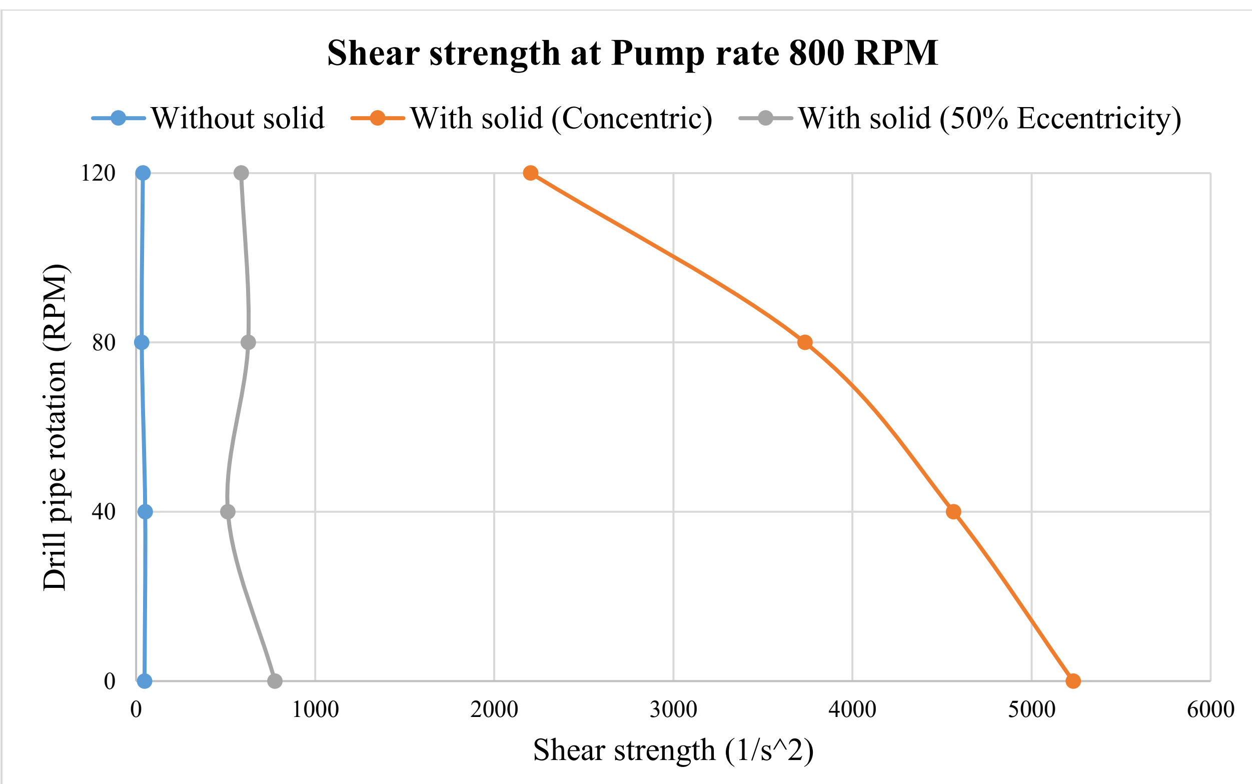
Shear strength at Pump rate 800 RPM
Without solid
With solid (Concentric)
With solid (50% Eccentricity)
Drill pipe rotation (RPM)
120
80
40
0
0
1000
2000
3000
4000
5000
6000
Shear strength (1/s^2)

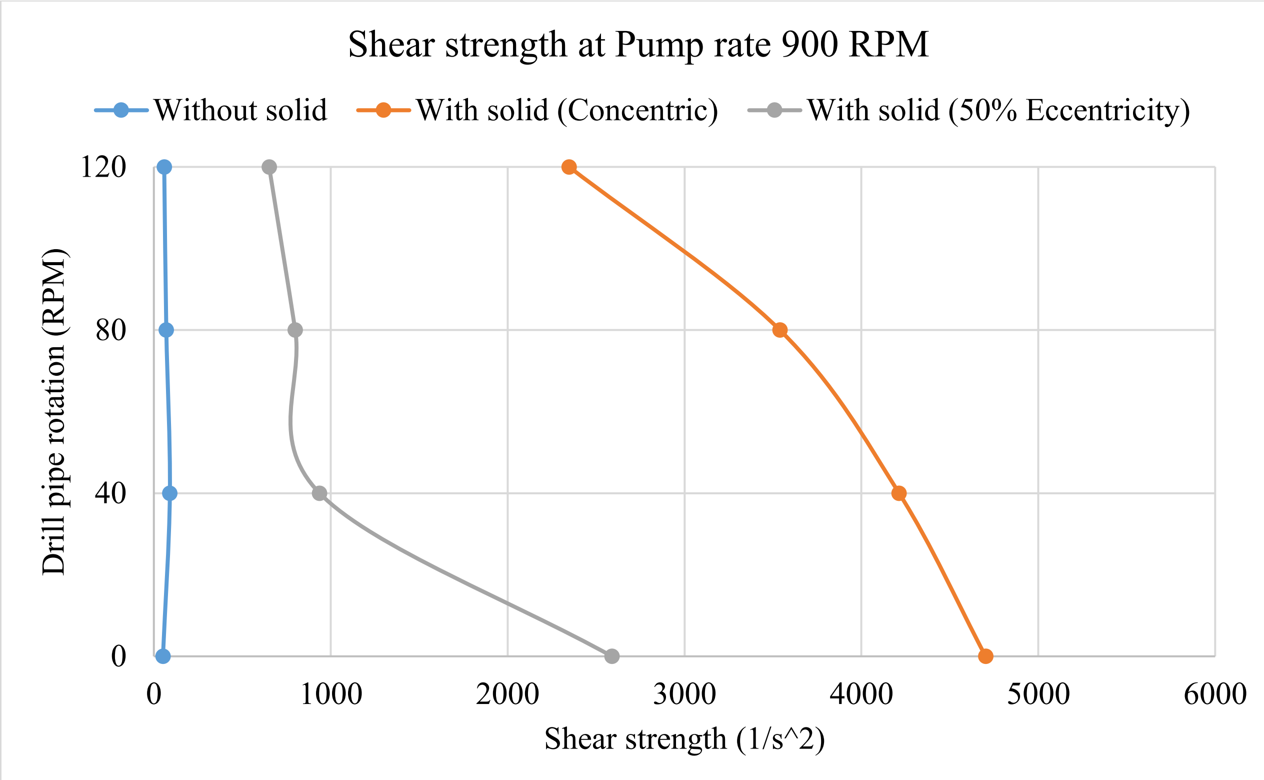
Shear strength at Pump rate 900 RPM
Without solid
With solid (Concentric)
With solid (50% Eccentricity)
Drill pipe rotation (RPM)
120
80
40
0
0
1000
2000
3000
4000
5000
6000
Shear strength (1/s^2)

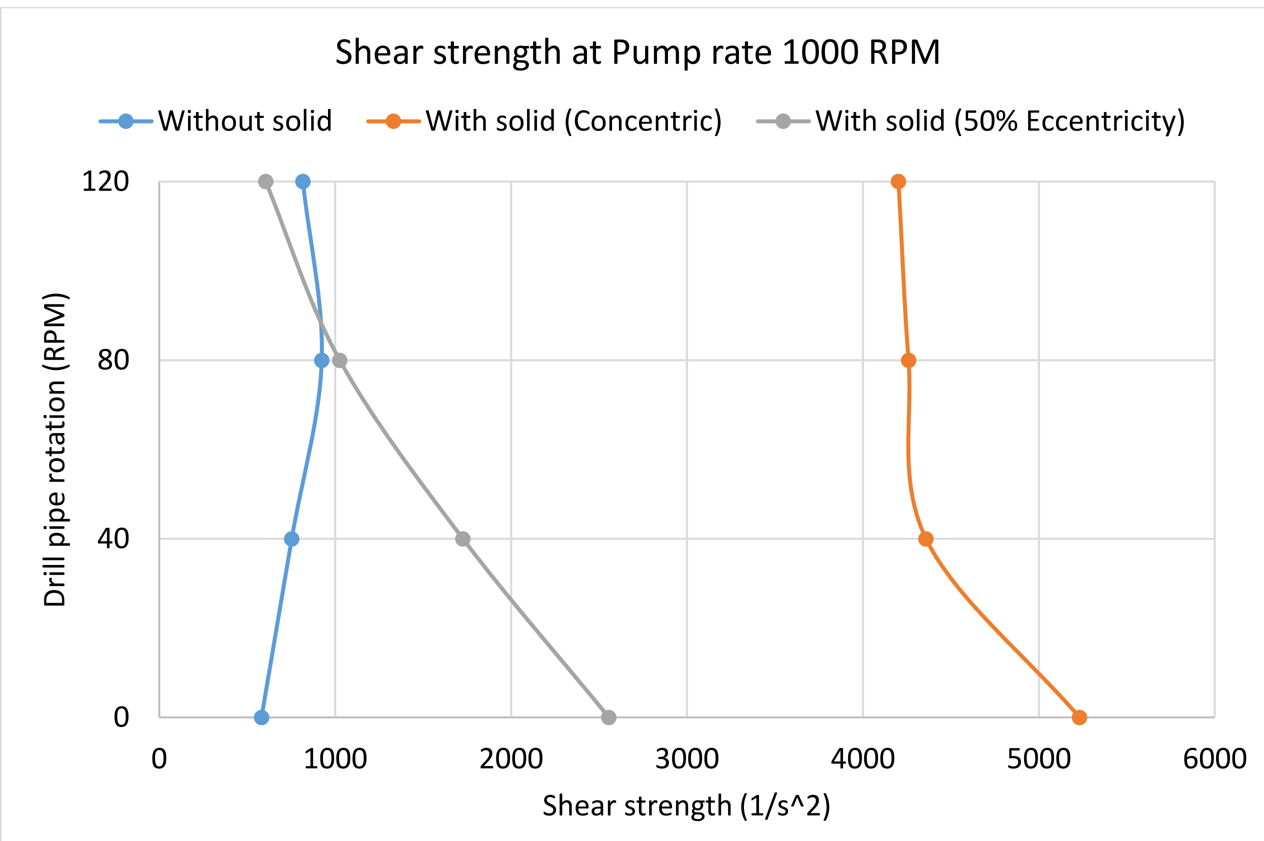
Shear strength at Pump rate 1000 RPM
Without solid
With solid (Concentric)
With solid (50% Eccentricity)
Drill pipe rotation (RPM)
120
80
40
0
0
1000
2000
3000
4000
5000
6000
Shear strength (1/s^2)

Chapter#6

Conclusion and recommendations

- Varying flow rate, drill pipe rotation and eccentricity, non-Newtonian fluid resulted considerable velocity change.
- Varying flow rate provides a higher velocity in the annulus, ultimately leads to an effective hole cleaning.
- Velocity profiles presented by the PIV gave information about the particle dynamics in annular flow and were used to describe the liquid-particle flow in a better way.
- At higher eccentricity of drill pipe (50%), Solid accumulated more at the bottom due to reduced annular area required to move the solid particles. The dune residence time increased, which was not desired phenomenon for horizontal drilling conditions.
- PIV provided good information about fluid flow in the annulus and a better option to describe the single-phase and dual-phase fluid flow in micro-scale.
- The flow patterns reported were on behalf of personal visualization and recorded images during the experiment.
- In this particular flow loop system, the critical velocity was found to be at 600 RPM in the absence of other parameters such as drill pipe rotation and eccentricity. This is the point at which the flowrate was not supporting the bed movement, and a stationary bed was forming.
- The optimal drilling conditions for best cutting transport from the experimental matrix were considered to be at a higher flow rate with moderate drill pipe rotation.

Future Directions:

- The study was performed purely experimental. It would be interesting to compare the results with parametric CFD modeling.
- The characteristics of glass particles, i.e., particle size, shape, and overall concentration used in this thesis, were not changing. Literature indicates that changing characteristics affect cuttings transport. Changes in size, shape, and concentration would give a good indication of how large this effect will be.

- In the future, research papers will be published by applying these parameters in non-dimensional functions such as non-dimensional swirling coefficient, shear and shear rate, turbulence intensity, etc.

Nomenclature

Greek symbols

$\Delta\overline{x}$	Particle displacement
Δt	Amount of time
μ	Fluid viscosity [kgm-1s-1]
λ	Ultrasonic wave length [ms-1Hz-1]
ρ	Fluid density [kgm-3]
τ	Shear stress [Nm-2]

Abbreviations

A	Area [m2]
dv/dy	Shear rate [s-1]
FFT	Fast Fourier Transform
ID	Inner diameter [mm]
LED	Light Emitting Diode
MB	Moving Bed
OD	Outer diameter [mm]
PIV	Particle Image Velocimetry
Re	Reynolds number
SB	Stationary Bed

References

Adrian, R J. 2005. "Twenty Years of Particle Image Velocimetry," 159–69. https://doi.org/10.1007/s00348-005-0991-7.

Allahvirdizadeh, Payam, Ergun Kuru, and Mahmut Parlaktuna. 2016. "Experimental Investigation of Solids Transport in Horizontal Concentric Annuli Using Water and Drag Reducing Polymer-Based Fluids." *Journal of Natural Gas Science and Engineering* 35: 1070–78. https://doi.org/10.1016/j.jngse.2016.09.052.

Ashwood, A. C., S. J. Vanden Hogen, M. A. Rodarte, C. R. Kopplin, D. J. Rodríguez, E. T. Hurlburt, and T. A. Shedd. 2015. "A Multiphase, Micro-Scale PIV Measurement Technique for Liquid Film Velocity Measurements in Annular Two-Phase Flow." *International Journal of Multiphase Flow* 68: 27–39. https://doi.org/10.1016/j.ijmultiphaseflow.2014.09.003.

Balamurugan, R, and B Jeeva. 2019. "Micron Size Particle Image Velocimetry by Fast Fourier Transform Micron Size Particle Image Velocimetry by Fast Fourier Transform" 020156 (October).

Bizhani, Majid, Ergun Kuru, and Sina Ghaemi. 2016. "Effect of near Wall Turbulence on the Particle Removal from Bed Deposits in Horizontal Wells." *Proceedings of the International Conference on Offshore Mechanics and Arctic Engineering - OMAE* 8: 1–10. https://doi.org/10.1115/OMAE2016-54051.

Boiten, Maren Louise. 2016. "Experimental Study on Cuttings Transportation in Turbulent Pipe Flow." University of Stavanger.

Brossard, C, J C Monnier, P Barricau, F X Vandernoot, Y Le Sant, G Le Besnerais, C Brossard, et al. 2015. "Principles and Applications of Particle Image Velocimetry." *Optical Diagnostics of Flows*, 19.

Busahmin, Bashir, Nawaf H Saeid, Gamal Alusta, and El-said M M Zahran. 2017. "REVIEW ON HOLE CLEANING FOR HORIZONTAL WELLS" 12 (16): 4697–4708.

CARLIER, JOHAN, and MICHEL STANISLAS. 2005. "Experimental Study of Eddy Structures in a Turbulent Boundary Layer Using Particle Image Velocimetry." *Journal of Fluid Mechanics*, 143–88. https://doi.org/doi:10.1017/S0022112005004751.

CHAKRABORTY, PINAKI, S. BALACHANDAR, and RONALD J. ADRIAN. 2005. "On the Relationships between Local Vortex Identification Schemes." *Journal of Fluid Mechanics* 535: 189–214. https://doi.org/doi:10.1017/S0022112005004726.

Chang, Tae Hyun, and Kwon Soo Lee. 2010. "An Experimental Study on Swirling Flow in a Cylindrical Annuli Using the PIV Technique." *Journal of Visualization* 13 (4): 293–301. https://doi.org/10.1007/s12650-010-0042-1.

Charogiannis, Alexandros, Jae Sik An, and Christos N. Markides. 2015. "A Simultaneous Planar Laser-Induced Fluorescence, Particle Image Velocimetry and Particle Tracking Velocimetry Technique for the Investigation of Thin Liquid-Film Flows." *Experimental Thermal and Fluid Science* 68: 516–36. https://doi.org/10.1016/j.expthermflusci.2015.06.008.

Corredor, Fabio Ernesto Rodriguez, Majid Bizhani, and Ergun Kuru. 2013. "An Experimental Investigation of Turbulent Drag Reduction in Concentric Annulus Using Particle Image Velocimetry Technique." *Proceedings of the International Conference on Offshore Mechanics and Arctic Engineering - OMAE* 7: 1–17. https://doi.org/10.1115/OMAE2013-11408.

GAO, Q., C. ORTIZ-DUEÑAS, and E. K. LONGMIRE. 2011. "Analysis of Vortex Populations in Turbulent Wall-Bounded Flows." *Journal of Fluid Mechanics* 678: 87–123. https://doi.org/doi:10.1017/jfm.2011.101.

Girmaa, and Belayneh. 2013. "Cutting Transport Models and Parametric Studies in Vertical and Deviated Wells." University of Stavanger.

Goharzadeh, A, and P Rodgers. 2009. "Experimental Characterization of Solid Particle Transport by Slug Flow Using Particle Image Velocimetry." *Journal of Physics: Conference Series* 147: 012069. https://doi.org/10.1088/1742-6596/147/1/012069.

Imaging, Focus O NPhantom v7.3, v9.1, V10. n.d. "Product - Manual."

Jahanmiri, Mohsen. 2011. "Particle Image Velocimetry : Fundamentals and Its Applications Particle Image Velocimetry : Fundamentals and Its Applications."

Kopplin, Charles R. 2003. "LOCAL LIQUID VELOCITIES IN HORIZONTAL, ANNULAR AIR/WATER FLOW." In *Ring Congress & Exposition Proceedings of IMECE'03 2003 ASME International Mechanical Engineering Congress*, 1–5.

"LaVision." n.d. https://www.lavision.de/en/applications/fluid-mechanics/piv-system-components/.

LaVision GmbH. n.d. "No Title." https://www.lavision.de/en/applications/fluid-mechanics/piv-system-components/seeding-particles/.

Lindken, Ralph, Massimiliano Rossi, Sebastian Große, and Jerry Westerweel. 2009. "Micro-Particle Image Velocimetry (m PIV): Recent Developments , Applications , and Guidelines †," 2551–67. https://doi.org/10.1039/b906558j.

Manual, Product. n.d. "Sheet Optics (Divergent) LaVision."

Messio, Laura, Cyprien Morize, Marc Rabaud, and Frédéric Moisy. 2008. “Experimental Observation Using Particle Image Velocimetry of Inertial Waves in a Rotating Fluid.” *Experiments in Fluids* 44 (4): 519–28. https://doi.org/10.1007/s00348-007-0410-3.

Nazari, T, G Hareland, and J J Azar. 2010. "SPE 132372 Review of Cuttings Transport in Directional Well Drilling : Systematic Approach."

Raffel, Markus, Christian E Willert, Steve T Wereley, and Jürgen Kompenhans. 2007. *Particle Image Velocimetry - A Practical Guide*. Second. Springer.

RATKOVSKÁ, Katarína. 2014. “Particle Image Velocimetry.” Bohemia, Czeck Republic.

Rodriguez-Corredor, F. E., Majid Bizhani, Mohammad Ashrafuzzaman, and Ergun Kuru. 2014. "An Experimental Investigation of Turbulent Water Flow in Concentric Annulus Using Particle Image Velocimetry Technique." *Journal of Fluids Engineering, Transactions of the ASME* 136 (5): 1–11. https://doi.org/10.1115/1.4026136.

Rodriguez Corredor, Fabio E., Majid Bizhani, and Ergun Kuru. 2015. "Experimental Investigation of Drag Reducing Fluid Flow in Annular Geometry Using Particle Image Velocimetry Technique." *Journal of Fluids Engineering, Transactions of the ASME* 137 (8): 1–16. https://doi.org/10.1115/1.4030287.

Santiago, J. G., S. T. Wereley, C. D. Meinhart, D. J. Beebe, and R. J. Adrian. 1998. "A Particle Image Velocimetry System for Microfluidics." *Experiments in Fluids* 25 (4): 316–19. https://doi.org/10.1007/s003480050235.

Shi, Baocheng, Jinjia Wei, and Mingjun Pang. 2015. "A Modified Cross-Correlation Algorithm for PIV Image Processing of Particle-Fluid Two-Phase Flow." *Flow Measurement and Instrumentation*. https://doi.org/10.1016/j.flowmeasinst.2015.06.010.

Sims, Karl. n.d. "No Title." https://www.karlsims.com/fluid-flow.html.

Taso, Chih-Hsiang. 2018. "Assembling and Testing of PIV System Master Thesis." Technical University of Liberec.

Webpage. n.d. "No Title." https://www.web-formulas.com/Math_Formulas/Linear_Algebra_Divergence_of_a_Vector_Field.aspx.

Wu, Qiong, Qian Ye, and Guoxiang Meng. 2013. "Particle Image Velocimetry Studies on the Swirling Flow Structure in the Vortex Gripper." *Proceedings of the Institution of Mechanical Engineers, Part C: Journal of Mechanical Engineering Science* 227 (9): 1927–37. https://doi.org/10.1177/0954406212469323.

List of tables

List of figures